ADAPTIVE GENERALIZED MULTISCALE MODEL REDUCTION TECHNIQUES FOR PROBLEMS IN PERFORATED DOMAINS

A Dissertation

by

YATING WANG

Submitted to the Office of Graduate and Professional Studies of
Texas A&M University
in partial fulfillment of the requirements for the degree of

DOCTOR OF PHILOSOPHY

Chair of Committee,	Yalchin Efendiev
Co-Chair of Committee,	Tsz Shun Eric Chung
Committee Members,	Eduardo Gildin
	Raytcho Lazarov
	Edriss Titi
Head of Department,	Emil Straube

August 2018

Major Subject: Mathematics

ABSTRACT

Multiscale modeling of complex physical phenomena in many areas, including hydrogeology, material science, chemistry and biology, consists of solving problems in highly heterogeneous porous media. In many of these applications, differential equations are formulated in perforated domains which can be considered as the region outside of inclusions or connected bodies of various sizes. Due to complicated geometries of these inclusions, solutions to these problems have multiscale features. Taking into account the uncertainties, one needs to solve these problems extensively many times. Model reduction techniques are significant for problems in perforated domains in order to improve the computational efficiency.

There are some existing approaches for model reduction in perforated domains including homogenization, heterogeneous multiscale methods and multiscale finite element methods. These techniques typically consider the case when there is a scale separation or the perforation distribution is periodic, and assume that the solution space can be approximated by the solutions of directional cell problems and the effective equations contain a limited number of effective parameters.

For more complicated problems where the effective properties may be richer, we are interested in developing systematic local multiscale model reduction techniques to obtain accurate macroscale representations of the underlying fine-scale problem in highly heterogeneous perforated domains. In this dissertation, based on the framework of Generalized Multiscale Finite Element Method, we develop novel methods and algorithms including (1) development of systematic local model reduction techniques for computig multiscale basis in perforated domains, (2) numerical analysis and exhaustive simulation utilizing the proposed basis functions, (3) design of different applicable global coupling frameworks

and (4) applications to various problems with challenging engineering backgrounds. Our proposed methods can significantly advance the computational efficiency and accuracy for multiscale problemss in perforated media.

ACKNOWLEDGMENTS

Firstly, I want to express my sincere gratitude to my advisor Dr. Yalchin Efendiev for his support on my graduate research. Dr. Efendiev provides me with precious opportunities to attend workshops, conferences, and professional internship, which allow me to exchange ideas with researchers from different areas and build up my own professional network. He has always been patient and gives me inspiring directions when I am facing difficulties, which helps me in all the time of research and writing of this thesis.

Secondly, I am very grateful to my co-advisor Dr. Eric Chung for his professional suggestions and great help on my research. His insightful comments and encouragement throughout my graduate studies are very beneficial to me in the pursuit of the degree. He always explains concepts clearly with great patience when we discuss research topics.

I would also thank Dr. Eduardo Gildin, Dr. Raytcho Lazarov and Dr. Edriss Titi for taking precious their time serving as my committee. I also appreciate the help from Dr. Yuhe Wang at Texas A& M University at Qatar. Dr. Wang was very generous for supporting me to visit Qatar for a semester. During the visit in Qatar, Dr. Wang also provided me great opportunities to attend international conferences to communicating with people having different areas of expertise.

I am also thankful to my colleagues and friends, especially Dr.Wing Tat Leung at University of Texas at Austin, Dr. Maria Vaselyeva at Texas A& M Univeristy.

I appreciate all the help from the the Department of Mathematics, Texas A&M University. It will be difficult for me to pursue my doctorate degree without the support of the department. The Department of Mathematics gives me many opportunities to attend different seminars, conferences and workshops. It helps me to explore future development

of my research. It also allows me to make connection which potentially lead to interesting collaborative work.

Finally, thanks to my family for their encouragement, patience and love. Without them at my back, I was not able to fully focous on my study and research.

CONTRIBUTORS AND FUNDING SOURCES

Contributors

This work was supervised by a dissertation committee consisting of Professor Yalchin Efendiev and Professor Eric Chung of the Department of Mathematics.

Funding Sources

Graduate study was partially supported by the Department of Mathematics from Texas A& M University. This work was made possible in part by partial support from NSF 1620318, the U.S. Department of Energy Office of Science, Office of Advanced Scientific Computing Research, Applied Mathematics program under Award Number DE-FG02-13ER26165 and National Priorities Research Program grant NPRP grant 7-1482-1278 from the Qatar National Research Fund.

NOMENCLATURE

GMsFEM	Generalized Multiscale Finite Element Method
Ω^ϵ	Perforated domain
$\mathcal{B}^\epsilon$	Perforated domain
$\mathcal{T}^h$	A partition of Ω^ϵ into fine elements
$\mathcal{T}^H$	A partition of Ω into coarse elements
h	The fine mesh size
H	The coarse mesh size
x_i	A coarse grid node
E_i	A coarse grid edge
ω_i^ϵ	A coarse neighborhood of coarse node x_i
$\omega_i^{+,\epsilon}$	An oversampled subdomain for ω_i^ϵ
K_i^ϵ	a coarse grid element
$K_i^{+,\epsilon}$	a oversampled subdomain for K_i
χ_i	The partition of unity

TABLE OF CONTENTS

Page

LIST OF FIGURES

FIGURE Page

LIST OF TABLES

TABLE Page

1. INTRODUCTION

1.1 Motivation

Scale disparity exists in many practical engineering problems. The microscale features of the problem are believed to affect the large scale formation and continues to challenge the charaterization of the system in many applications. Multiscale modeling of complex physical phenomena has been a popular research topic in many areas, including climate dynamics, material science, chemistry and biology, which consists of solving problems in heterogeneous porous media.

In many of these applications, differential equations are formulated in perforated domains (see Figure 1.1 for an illustration). Perforated domains can be considered as the region outside of inclusions or connected bodies of various sizes. Because of the variable sizes and geometries of these inclusions, solutions to such problems have multiscale properties. Solving these problems at all scales directly can be extremely expensive even with today's computing capacity. In combination with extremely sparse data sampling, missing information and the associated uncertainty requires thousands of simulations which exerbates the computing difficulty. In order to reduce the computational cost, we are interested in formulating methods that avoid global fine scale calculations. Model reduction techniques have shown their great neccessity for problems in perforated domains.

One approach for model reduction is homogenization. For a given PDE, it can have differernt natural scales, for instance, a macroscale of order 1 and microsale of order $0 < \epsilon < 1$. Homogenization learns the limiting behavior of the solution u^ϵ as the microscopic length ϵ goes to zero [1, 2]. There have been many homogenization results in perforated domains where perforations can have distinctly different properties, e.g. [3, 4, 5, 6, 7, 8, 9, 10, 11, 12]. Homogenization approaches average microscale proper-

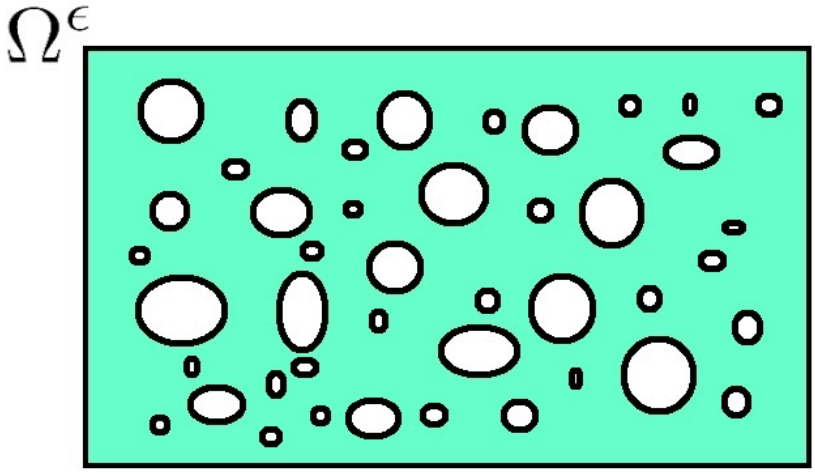

Figure 1.1: Illustration of a perforated domain.

tites, resulting in macroscale equations in the domain without perforations using effective properties, and the macroscale equations can differ from microscale equations. In [3], the author studied the homogenization of Stokes or Navier-Stokes equations in domain containing many periodically distributed tiny obstacles with the no-slip boundary condition. In the paper, it is proved that for perforations with critical size, the limit problem follows Brinkman type of law; for smaller obstacles, the limit problem converges to the solution of Stokes equation; and for larger holes, the problem reduces to the Darcy's law. However, typical assumptions on periodicity or scale separation are needed to formulate the cell problems in the homogenization theory.

In the numerical homogenization procedure, the local cell problems which account for the microscale interaction are solved on a fine grid. Using the solutions of the local problems, the effective properties can be computed. The resulting homogenized equations can be solved on the coarse grid with the mesh size independent of the size of the perforations for different boundary conditions and right hand sides.

One of the numerical homogenization method is the heterogeneous multiscale methods. The heterogeneous multiscale method was proposed in [13]. In this approach, one first selects an incomplete macroscale model, and then estimates the needed data for the macroscale scheme from the micorscale simulations. Due to the absence of the knowledge of overall microscale properties, the local problem are only solved around some quadrature points. The locally constructed basis are used in the numerical integration to form the stiffness matrix of the coarse scale global problem. The work based on heterogeneous multiscale finite element method was adapt to elliptic homogenization problem in perforated domain in [14] using local representative volume concepts. Under the assumption of periodicity, the authors reformulate the HMM into a two-scale problem to get a posterior estimates. The method proposed in this work does not depend on the fine sacle parameter ϵ and exhibits applicability for heterogeneous problems numerically. To apply this mehod, one assumes that the information of the media can be described by the representative volumes, and the effective equations contain a limited number of effective parameters.

There are some generalization to problems with random statistically homogeneous pore-space geometries [15]. A multiscale finite element (MsFEM) approach for perforated domains was proposed in a recent work [16], which studied an MsFEM type method in the manner of Crouzeix-Raviart finite element method on a perforated domain. MsFEM methods were first introduced in [17] and further developed in [18, 19, 20, 21, 22, 23] etc. The main ingredients of MsFEMs are the global formulation and the basis construction. Instead of using standard finite element basis such as piecewise polynomials, MsFEM employs basis functions which are constructed by solving local problems with some boundary conditions. The multiscale basis will then carry the local information of the microscale heterogeneity and outperforms the standard finite element on a coarse grid. In MsFEM approaches, the boudary condition used in the local problem play a critical role for the accuracy of the method. In [16], the authors employ Crouzeix-Raviart elements,

where only the weak continuity of the multiscale basis across the edges of the coarse mesh is enforced, thus leading to some natural boundary conditions for the basis functions. The authors also enrich the multiscale finite element space using some bubble functions. However, for general heterogeneities, the effective properties may be richer, we are interested in a more systematic way to enrich the coarse space accurately and efficiently.

Generalized Multiscale Finite Element Method(GMsFEM) [24, 25, 26] was proposed to generalize the MsFEM by identifying enriched local multiscale space and obtains more accurate numerical macroscopic systems. The main idea of the GMsFEM is to use local snapshot vectors to represent the solution space and then identify local multiscale spaces by performing appropriate local spectral problem. The GMsFEM framework usually contains two stages: the offline stage and the online stage. In the offline computation, snapshot spaces are first constructed. Using snapshot spaces is essential in problems with perforations, because the snapshots contain necessary geometry information. Next, some local spectral decomposition is performed to identify dominate modes in the snapshot space. The local multiscale basis functions obtained as a result represent the necessary degrees of freedom and will be used in the macroscale solver. This is in contrast to some other approaches, where one apriori selects the number of cell problems. The online stage of the GMsFEM is to solve a globbal problem for a given source term or boundary condition. One can accelerate the convergence by computing multiscale basis functions using a residual at the online stage [27, 28, 29]. Online basis functions are computed adaptively and only added in regions with largest residuals.

This thesis concentrates on developing systematic local multiscale model reduction techniques under the framework of GMsFEM to obtain accurate macroscale representations of the underlying fine-scale problem in highly heterogeneous perforated domains.

1.2 Outline of the dissertation

In this section, we show a general picture of this dissertation.

In chapter 3, the adaptive online generalized finite element methods for problems in perforated domain was studied. The physical problem we are interested include the Laplace problem, the elasticity problem and the Stokes problem. We present the analysis of the proposed method and focus on analyzing Stokes equations, since similar techniques can be easily extended to the elliptic and the elasticity equations. We note that in previous work [30], the offline simulations for heterogeneous problems in perforated domains was studied. The main improvements in my work are (1) more accurate and efficient way of constructing offline basis (2) the development of the online algorithm and their analysis (3) the development of adaptive strategies.

In GMsFEM, the offline multiscale basis function construction is local and needs to solve local snapshot problems and local spectral problems to get the multiscale basis functions. A modified version of offline multiscale basis functions for Stokes equation are introduced such that the velocity basis functions have constant divergence. This is because we want the range of the divergence to be a polynomial space of the same order as the discrete pressure space, which consists of piecewise constant in our approximation scheme. Another thing worth mentioning is that the offline computations might be heavy if the contrast between the coarse grid size and fine grid size is too large. In this chapter, we discuss the use of randomized snapshots[31] to reduce the offline cost associated with the snapshot space computations. The randomized snapshot strategy is an efficient calculation of the snapshot space based on the randomized SVD theory. The main idea is that a smaller number of snapshots can be calculated instead of the whole snapshot space for a given accuracy. One can also use local oversampling techniques [18, 32] to reduce the boundary effect introduced by the randomized boundary condition to improve accu-

racy. However, the global effects are still not used. In order to accelerate the convergence, one can compute multiscale basis functions at the online stage [27, 28, 29]. This is done by designing new multiscale basis functions, which solve local problems using the global residual information.

Online basis functions are computed adaptively and only added in regions with largest residuals. In chapter 3, we design online basis functions according to an analysis of the problem [33]. It is worth emphasizing that the adaptivity and online basis construction are important for the success of multiscale methods. Actually, one may need only a few basis functions in many regions, while more degrees of freedom may be required in some other regions in order to approximate the solution space accurately. The online basis functions allow a fast convergence and it is important that adding online basis function in one online iteration can decrease the error substantially. We reveal the relationship between the number of offline multiscale basis functions chosen initially and the decreasing rate of online solution error. This can help us to get an estimate of the error reduction apriori, which is important in practical simulations. The analysis starts with the proof of the inf-sup condition, which shows the well-posedness of the proposed scheme. A posteriori error bound for the algorithm is then discussed. Extensive numerical tests are performed to validate the theoretical results.

We mention that in the previous approach, the global system is coupled using a continuous Galerkin (CG) method. The computational domain are partitioned into a union of overlapping coarse neighborhoods, and local multiscale basis functions are constructed in each coarse neighborhood for the CG coupling. Thus there is a need to multiply each eigen basis by a partition of unity function, which may modify the local basis properties and need some extra modification after the multiplication.

In chapter 4, a new GMsFEM for problems in perforated domains using a discontinuous Galerkin (DG) approach is introduced [34]. The use of the DG approach in GMsFEM

has been successfully developed for many problems, such as the elliptic equations and the wave equations with heterogeneous coefficients ([35, 36, 37, 38]). One of the main features of the DG approach is that the basis functions are constructed locally for each non-overlapping coarse region. This fact provides more flexibility in designing the coarse mesh and in constructing the local multiscale space. In addtition, there is no need to construct and use any partition of unity functions in the DG approach. Furthermore, it is important to note that the mass conservation is a crucial property for the Stokes flow. Our multiscale basis functions was obtained by solving the local Stokes problems with some suitable boundary conditions. By the construction of the basis functions, the multiscale solution satisfies some local mass conservation property within coarse regions. However, mass conservation does not in general hold globally in the coarse grid level. To tackle this issue, we construct a hybridized scheme and introduce additional pressure variables on the coarse grid edges. This additional pressure variable serves as a Lagrange multiplier to enforce the mass conservation property in the coarse grid level. To investigate the performance of the proposed method, we will numerically study the Stokes problem in various perforated domains with various choices of boundary conditions and forcing terms. We present the construction of the snapshot space using both the standard and the oversampling approaches. Local spectral decompositions are also proposed for various approaches of snapshots correspondingly. Moreover, when constructing multiscale basis, we will test the use of different shapes of coarse blocks for different types of perforated domains. Numerical results are presented and convergence of the method is analyzed. Furthermore, we will numerically show that the local mass conservation property is satisfied by the multiscale solution.

In chapter 5, we study the convection-dominated transport phenomena which is broadly applicable in many research areas such as kinetic theory and fluid dynamics. In these physical processes, the transport velocity is often a solution of a heterogeneous flow problem.

We consider coupled flow (Stokes problem) and transport (unsteady convection-diffusion problem) in perforated domains. We use a mixed formulation and appropriate multiscale basis functions for both flow and transport to guarantee a mass conservation. Due to the non-symmetric property of convection operator, Petrov-Galerkin mixed formulations are used for the transport problem, which provide stability. We consider two different approaches. As a first approach, the flow equation is solved on a coarse grid using the GMsFEM and, furthermore, the approximate velocity solution is used in constructing offline spaces for the transport equations (both trial and test spaces). We call this approach, de-coupled GMsFEM. In the second approach, the multiscale basis functions for flow and transport are constructed jointly. i.e., we do not solve global flow equation in this case. This is challenging because one does not know the global flow information and the basis functions for the transport depend nonlinearly on the coarse-grid components of the flow equations. The novelty of this approach is to construct coupled multiscale basis functions. Moreover, with the aim of further improving accuracy, we also present multiscale interior basis construction for the concentration and online basis construction for the flux in transport equation. Numerical results are presented to show the accuracy of our proposed method[39].

2. PRELIMINARIES

In this chapter, we present an overview of the problems in heterogeneous perforated domains, as well as some common definitions for discretization. In the section 2.1, we present a general form of the physical problems we are interested in. We consider commonly used model problems including the Laplace equation, the elasticity equation, the Stokes equation, and the coupled transport and flow system in perforated regions. Some definitions of the coarse and fine grid discretization are given in section 2.2. A general idea of the GMsFEM is discussed in section 2.3.

2.1 Problem setting

In this section, we present the underlying problem. Let $\Omega \subset \mathbb{R}^d$ $(d = 2, 3)$ be a bounded domain covered by perforations $\mathcal{B}^\varepsilon$. In this dissertation, we will consider the case when $d = 2$. Define $\Omega^\varepsilon := \Omega \backslash \mathcal{B}^\varepsilon$, assume it is polygonally bounded. See Figure 1.1 in chapter 1 for an illustration of the perforated domain. We consider the following problem defined in a perforated domain Ω^ε

$$\mathcal{L}^\varepsilon(w) = f, \quad \text{in} \quad \Omega^\varepsilon, \tag{2.1}$$

$$w = 0 \text{ or } \frac{\partial w}{\partial n} = 0, \text{ on } \partial\Omega^\varepsilon \cap \partial\mathcal{B}^\varepsilon, \tag{2.2}$$

$$w = g, \text{ on } \partial\Omega \cap \partial\Omega^\varepsilon, \tag{2.3}$$

where $\mathcal{L}^\varepsilon$ denotes a linear differential operator, n is the unit outward normal to the boundary, f and g denote given functions with sufficient regularity.

Denote by $V(\Omega^\varepsilon)$ the appropriate solution space, and

$$V_0(\Omega^\varepsilon) = \{v \in V(\Omega^\varepsilon), v = 0 \text{ on } \partial\Omega^\varepsilon\}.$$

The variational formulation of Problem (2.1)-(2.3) is to find $w \in V(\Omega^\varepsilon)$ such that

$$\langle \mathcal{L}^\varepsilon(w), v\rangle_{\Omega^\varepsilon} = (f, v)_{\Omega^\varepsilon} \qquad \text{for all } v \in V_0(\Omega^\varepsilon),$$

where $\langle \cdot, \cdot \rangle_{\Omega^\varepsilon}$ denotes a specific inner product over Ω^ε for either scalar functions or vector functions, and and $(f, v)_{\Omega^\varepsilon}$ is the L^2 inner product. Some specific examples for the above abstract notations are given below.

Laplace: For the Laplace operator with homogeneous Dirichlet boundary conditions on $\partial\Omega^\varepsilon$, we have

$$\mathcal{L}^\varepsilon(u) = -\Delta u, \tag{2.4}$$

and $V(\Omega^\varepsilon) = H_0^1(\Omega^\varepsilon)$, and

$$\langle \mathcal{L}^\varepsilon(u), v\rangle_{\Omega^\varepsilon} = (\nabla u, \nabla v)_{\Omega^\varepsilon}$$

.

Elasticity: For the elasticity operator with a homogeneous Dirichlet boundary condition on $\partial\Omega^\varepsilon$, we assume the medium is isotropic. Let $u \in (H^1(\Omega^\varepsilon))^2$ be the displacement field. The strain tensor $\boldsymbol{\varepsilon}(u) \in (L^2(\Omega^\varepsilon))^{2\times 2}$ is defined by

$$\boldsymbol{\varepsilon}(u) = \frac{1}{2}(\nabla u + \nabla u^T).$$

Thus, the stress tensor $\sigma(u) \in (L^2(\Omega^\varepsilon))^{2\times 2}$ relates to the strain tensor $\boldsymbol{\varepsilon}(u)$ such that

$$\sigma(u) = 2\mu\boldsymbol{\varepsilon} + \xi\nabla \cdot u\, I,$$

where $\xi > 0$ and $\mu > 0$ are the Lamé coefficients. We have

$$\mathcal{L}^{\varepsilon}(u) = -\nabla \cdot \sigma, \tag{2.5}$$

where $V(\Omega^{\varepsilon}) = (H_0^1(\Omega^{\varepsilon}))^2$ and

$$\langle \mathcal{L}^{\varepsilon}(u), v \rangle_{\Omega^{\varepsilon}} = 2\mu(\boldsymbol{\varepsilon}(u), \boldsymbol{\varepsilon}(v))_{\Omega^{\varepsilon}} + \xi(\nabla \cdot u, \nabla \cdot v)_{\Omega^{\varepsilon}}$$

.

Stokes: For the Stokes equation, we have

$$\mathcal{L}^{\varepsilon}(u\ , p) = \begin{pmatrix} \nabla p - \mu \Delta u \\ \nabla \cdot u \end{pmatrix}, \tag{2.6}$$

where μ is the viscosity, p is the fluid pressure, u represents the velocity, $V(\Omega^{\varepsilon}) = (H_0^1(\Omega^{\varepsilon}))^2 \times L_0^2(\Omega^{\varepsilon})$, and

$$\langle \mathcal{L}^{\varepsilon}(u\ , p), (v\ , q) \rangle_{\Omega^{\varepsilon}} = \begin{pmatrix} (\nabla u, \nabla v)_{\Omega^{\varepsilon}} & -(\nabla \cdot v, p)_{\Omega^{\varepsilon}} \\ (\nabla \cdot u, q)_{\Omega^{\varepsilon}} & 0 \end{pmatrix}. \tag{2.7}$$

We note that $L_0^2(\Omega^{\varepsilon})$ contains functions in $L^2(\Omega^{\varepsilon})$ with zero average in Ω^{ε}.

Besides the above models, we are also interested in the coupled flow and transport equation. **Transport:** For the unsteady state transport equation, we have

$$\frac{\partial c}{\partial t} - D\Delta c + u \cdot \nabla c = f, \quad \text{in } \Omega^{\varepsilon}, \tag{2.8}$$

where c is the concentration, D is the diffusion conefficient, and u is the velocity that driving the flow. We are interested in the mixed formulation of the transport equation. The

details of the different mixed formulations are presented in chapter 5.

2.2 Coarse and fine grid notations

For the numerical approximation of the above problems, we first introduce the notations of fine and coarse grids. Let $\mathcal{T}^H$ be a coarse-grid partition of the domain Ω^ε with mesh size H. Here, we assume that the perforations will not split the coarse triangular element, as in this case, the coarse block will have two disconnected regions. In general, the proposed concept can be applied to this disconnected case; however, for simplicity, we avoid it and assume that every coarse-grid block is path-connected (i.e., any two points can be connected within the coarse block). Notice that, the edges of the coarse elements do not necessarily have straight edges because of the perforations (see Figure 2.1). By conducting a conforming refinement of the coarse mesh $\mathcal{T}^H$, we can obtain a fine mesh $\mathcal{T}^h$ of Ω^ε with mesh size h. Typically, we assume that $0 < h \ll H < 1$, and that the fine-scale mesh $\mathcal{T}^h$ is sufficiently fine to fully resolve the small-scale information of the domain, and $\mathcal{T}^H$ is a coarse mesh containing many fine-scale features. The j-th coarse element is denoted by K_j^ϵ. See an illustration of the coarse element in Figure 2.1.

Let N_v and N_e be the number of nodes and edges in coarse grid respectively. We denote by $\{x_i | 1 \leq i \leq N_v\}$ the set of coarse nodes, and $\{E_j | 1 \leq j \leq N_e\}$ the set of coarse edges.

We define two kinds of coarse neighborhood, i.e, the nodal-based and the edge-based coarse neighborhood. The nodal-based coarse neighborhood ω_i^ε is defined for each coarse node x_i by

$$\omega_i^\varepsilon = \cup\{K_j^\varepsilon \in \mathcal{T}^H;\ \ x_i \in \bar{K}_j^\varepsilon\}, \tag{2.9}$$

which is the union of all coarse elements having the node x_i. The edge-based coarse

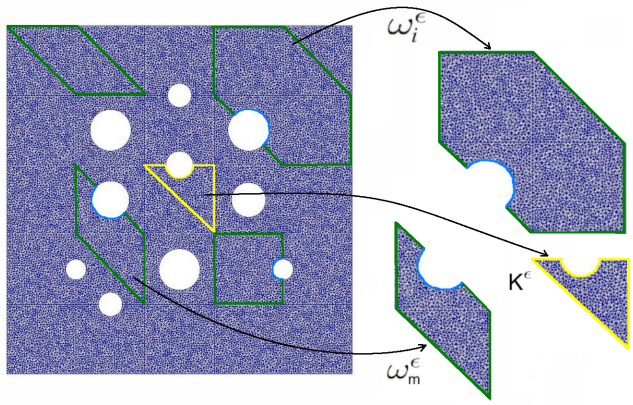

Figure 2.1: Illustration of coarse elements and coarse neighborhoods.

neighborhood ω_m^ε for each coarse edge E_m by

$$\omega_m^\varepsilon = \cup\{K_j^\varepsilon \in \mathcal{T}^H;\ \ E_m \in \bar{K}_j^\varepsilon\}, \tag{2.10}$$

which is the union of all coarse elements having the edge E_m. See Figure 2.1 for an illustration of the coarse neighborhoods.

We remark that we use the subscript $+$ to denote the oversampling region of a coarse region. For example, $K^{+,\varepsilon}$ is an oversampled coarse block obtaining by adding a few fine grid layers to the coarse block K^ε. Similarly, $\omega^{+,\varepsilon}$ is an oversampled coarse neighborhood of ω^ε.

On the triangulation $\mathcal{T}^h$, we introduce the finite element spaces V_h, we will then obtain the fine-scale solution $u \in V_h$ by solving some variational problems. For example, we can solve

$$\langle \mathcal{L}^\varepsilon(u), v\rangle_{\Omega^\varepsilon} = (f, v)_{\Omega^\varepsilon}, \qquad \text{for all } v \in V_h \tag{2.11}$$

for Laplace and elasticity, and obtain the fine-scale solution $(u, p) \in V_h \times Q_h$ by solving

the following variational problem

$$\langle \mathcal{L}^{\varepsilon}(u,p),(v,q)\rangle_{\Omega^{\varepsilon}} = ((f,0),(v,q))_{\Omega^{\varepsilon}}, \qquad \text{for all } (v,q)\in V_h\times Q_h \tag{2.12}$$

for the Stokes system. These solutions are used as reference solutions to test the performance of our schemes.

As for the discretization scheme on $\mathcal{T}^h$, we will first give an introduction of GMsFEM and show details in the chapters later on.

2.3 General idea of GMsFEM

In this section, we will briefly discuss the idea of GMsFEM [24, 17, 27]. In GMsFEM, one can divide the computations into offline and online stages.

Offline stage. The construction of offline space usually contains two steps:

- Construction of a snapshot space that will be used to compute an offline space.
- Construction of a small dimensional offline space by performing a dimension reduction in the snapshot space.

From the above process, we will get a set of basis functions $\{\Psi_i^{\text{off}}\}$ such that each Ψ_i^{off} is supported in some coarse neighborhood ω_l^{ε} or some coarse element K_j^{ε}, depending on the global coupling method. If the resulting basis are supported in an overlapping region, we will ensure that the basis functions satisfy a partition of unity property.

Once the bases are constructed, we define the coarse function space as

$$V_{\text{off}} := \text{span}\{\Psi_i^{\text{off}}\}_{i=1}^{M},$$

where M is the number of coarse basis functions.

In the offline stage of GMsFEM, we seek an approximation $u_{\text{ms}} = \sum_{i=1}^{M} c_i \Psi_i^{\text{off}}$ in V_{off}, which satisfies the coarse-scale offline formulation,

Online stage. At the enrichment level m, denote by V_{ms}^m and u_{ms}^m the corresponding GMsFEM space and solution, respectively. The online basis functions are constructed based on the residuals of the current multiscale solution u_{ms}^m. To be specific, one can compute the local residual $R_i = (f, v)_{\omega_i^\varepsilon} - \langle \mathcal{L}^\varepsilon(u_{\text{ms}}^m), v \rangle_{\omega_i^\varepsilon}$ in each coarse neighborhood ω_i^ε. For the coarse neighborhoods where the residuals are large, we can add one or more basis functions by solving

$$\mathcal{L}^\varepsilon(\phi_i^{\text{on}}) = R_i.$$

$$\langle \mathcal{L}^\varepsilon(u_{\text{ms}}), v \rangle_{\Omega^\varepsilon} = (f, v)_{\Omega^\varepsilon}, \qquad \text{for all } v \in V_{\text{off}}. \tag{2.13}$$

Adding the online basis in the solution space, we will get a new coarse function space V_{ms}^{m+1}. The new solution u_{ms}^{m+1} will be found in this new approximation space. This iterative process is terminated when some error tolerance is achieved. The accuracy of the GMsFEM relies on the coarse basis functions. We shall present the construction of suitable basis functions in both offline and online stages for the differential operators in the following chapters.

3. ADAPTIVE ONLINE LOCAL MULTISCALE MODEL REDUCTION*

In this chapter , we develop and analyze an adaptive multiscale approach for problems in heterogeneous perforated domains. We consider commonly used model problems including the Laplace equation, the elasticity equation, and the Stokes system in perforated regions. We note that the continuous Galerkin coupling method is considered in this chapter, and the multiscale basis are constructed in some overlapping coarse regions. We discuss the construction of offline and online basis functions in Section 3.1. Section 3.2 is devoted to numerical examples. In Section 3.3, the convergence analysis for proposed methods is shown. In this chapter, we will show the results for elasticity and Stokes equations. The results for Laplace have similar convergence analysis and computational results as those for elasticity equations, so we will omit them here.

3.1 The construction of offline and online basis functions

We first introduce the following finite element spaces

$$V_h := \{v \in V(\Omega^\varepsilon) : \quad v|_K \in (P^k(K))^l \text{ for all } K \in \mathcal{T}^h\},$$

where P^k denotes the polynomial of degree $k(\ k = 0,\ 1,\ 2)$, and $l(\ l = 1,\ 2)$ indicates either a scalar or a vector. Note that for the Laplace and elasticity operators, we choose $k = 1$, i.e., piecewise linear function space as our fine-scale approximation space; for Stokes problem, we use $(P^2(K))^2$ for fine-scale velocity approximation and $P^0(K)$ for fine-scale pressure approximation. We use Q_h to denote the space for pressure. Now we illustrate the construction of multiscale basis for the above problems.

We remark that, we only describe the construction of offline and online basis for elas-

*This is an Accepted Manuscript of an article published by Taylor & Francis in Applicable Analysis on 07/06/2016, available online https://www.tandfonline.com/doi/full/10.1080/00036811.2016.1199799.

ticity problem and Stokes problem.

In the offline computation, we first construct a snapshot space V^i_{snap} for each coarse neighborhood ω^ε_i. Construction of the snapshot space involves solving the local problems with a set of boundary conditions. The offline space V_{off} is then constructed via a dimension reduction in the snapshot space using an auxiliary spectral decomposition. The main objective is to seek a subspace of the snapshot space such that it can approximate any functions of the snapshot space in an appropriate sense defined via auxiliary bilinear forms. Based on the residual of the current solution, we enrich the solution space by adding some online functions to enhance the accuracy of the solution. The precise construction of offline and online basis will be presented for different applications.

3.1.1 Elasticity problem

In this section, we will consider the elasticity problem (2.5) with a homogeneous Dirichlet boundary condition.

3.1.1.1 Snapshot space

The snapshot space for elasticity problem consists of extensions of the fine-grid functions δ^h_k in ω^ε_i. Here $\delta^h_k = 1$ at the fine node $x_k \in \partial\omega^\varepsilon_i \backslash \partial\mathcal{B}^\varepsilon$, $\delta^h_k = 0$ at other fine nodes $x_j \in \partial\omega^\varepsilon_i \backslash \partial\mathcal{B}^\varepsilon$, and $\delta^h_k = 0$ in $\partial\mathcal{B}^\varepsilon$. Let V^i_h be the restriction of the fine grid space V_h in ω^ε_i and $V^i_{h,0} \subset V^i_h$ be the set of functions that vanish on $\partial\omega^\varepsilon_i$. We will find $u^i_k \in V^i_h$ with $supp(u^i_k) \subset \omega^\varepsilon_i$ by solving the following problems on a fine grid

$$\int_{\omega^\varepsilon_i} \Big(2\mu\boldsymbol{\varepsilon}(u^i_k) : \boldsymbol{\varepsilon}(v) + \xi\nabla\cdot u^i_k \nabla\cdot v\Big)dx = 0, \quad \forall v \in V^i_{h,0}, \tag{3.1}$$

with boundary conditions

$$u^i_k = 0 \text{ on } \partial\omega^\varepsilon_i \cap \partial\mathcal{B}^\varepsilon, \quad u^i_k = (\delta^i_j, 0) \text{ or } (0, \delta^i_j) \text{ on } \partial\omega^\varepsilon_i.$$

We will collect the solutions of the above local problems to generate the snapshot space. Let $\psi_k^{i,\text{snap}} := u_k^i$ and define the snapshot space by

$$V_{\text{snap}} = \text{span}\{\psi_k^{i,\text{snap}} : \ \ 1 \leq k \leq J_i,\, 1 \leq i \leq N_v\},$$

where J_i is the number of snapshot basis in ω_i^ε, and N_v is the number of nodes. To simplify notations, let $M_{\text{snap}} = \sum_{i=1}^N J_i$ and write

$$V_{\text{snap}} = \text{span}\{\psi_i^{\text{snap}} : \ \ 1 \leq i \leq M_{\text{snap}}\}.$$

3.1.1.2 Offline space

This section is devoted to the construction of the offline space via a spectral decomposition. We will consider the following eigenvalue problems in the space of snapshots:

$$A^{i,\text{off}}\Psi_k^{i,\text{off}} = \lambda_k^{i,\text{off}} S^{i,\text{off}}\Psi_k^{i,\text{off}}, \tag{3.2}$$

where

$$\begin{aligned} A^{i,\text{off}} &= a_i(\psi_m^{i,\text{snap}}, \psi_n^{i,\text{snap}}) = \int_{\omega_i^\varepsilon} \left(2\mu\boldsymbol{\varepsilon}(\psi_m^{i,\text{snap}}) : \boldsymbol{\varepsilon}(\psi_n^{i,\text{snap}}) + \xi\nabla\cdot\psi_m^{i,\text{snap}}\,\nabla\cdot\psi_n^{i,\text{snap}}\right), \\ S^{i,\text{off}} &= s_i(\psi_m^{i,\text{snap}}, \psi_n^{i,\text{snap}}) = \int_{\omega_i^\varepsilon} (\xi + 2\mu)\psi_m^{i,\text{snap}}\cdot\psi_n^{i,\text{snap}}. \end{aligned} \tag{3.3}$$

We assume that the eigenvalues are arranged in the increasing order. To simplify notations, we write $\lambda_k^i = \lambda_k^{i,\text{off}}$.

To generate the offline space, we choose the smallest M_i eigenvalues from Equation (3.2) and form the corresponding eigenfunctions in the respective snapshot spaces by setting $\Phi_k^{i,\text{off}} = \sum_j \Psi_{kj}^{i,\text{off}}\psi_j^{i,\text{snap}}$, for $k = 1, \ldots, M_i$, where $\Psi_{kj}^{i,\text{off}}$ are the coordinates of

the vector $\Psi_k^{i,\text{off}}$. The offline space is defined as the span of $\chi_i \Phi_k^{i,\text{off}}$, namely,

$$V_{\text{off}} = \text{span}\{\chi_i \Phi_l^{i,\text{off}} : \ \ 1 \leq l \leq l_i,\, 1 \leq i \leq N_v\},$$

where l_i is the number of snapshot basis in ω_i^ε, and $\{\chi_i\}$ is a set of partition of unity functions for the coarse grid. One can take $\{\chi_i\}$ as the standard hat functions or standard multiscale basis functions. To simplify notations further, let $M = \sum_{i=1}^N l_i$ and write

$$V_{\text{off}} = \text{span}\{\chi_i \Phi_i^{\text{off}} : \ \ 1 \leq i \leq M\}.$$

3.1.1.3 Online adaptive method

By the offline computation, we construct multiscale basis functions that can be used for any input parameters to solve the problem on the coarse grid. In the earlier works [27], the online method for the diffusion equation with heterogeneous coefficients has been proposed. In this section, we consider the construction of the online basis functions for elasticity problem in perforated domains and present an adaptive enrichment algorithm. We use the index $m \geq 1$ to represent the enrichment level. The online basis functions are computed based on some local residuals for the current multiscale solution $u_{\text{ms}}^m \in V_{\text{ms}}^m$, where we use V_{ms}^m to denote the corresponding space that can contain both offline and online basis functions.

Let $V_{\text{ms}}^{m+1} = V_{\text{ms}}^m + \text{span}\{\phi^{\text{on}}\}$ be the new approximate space that constructed by adding online basis $\phi^{\text{on}} \in V_{h,0}^i$ on the i-th coarse neighborhood ω_i^ε. For each coarse grid neighborhood ω_i^ε, we define the residual R_i as a linear functional on $V_{h,0}^i$ such that

$$R_i(v) = \int_{\omega_i^\varepsilon} f v dx - \int_{\omega_i^\varepsilon} \Big(2\mu \boldsymbol{\varepsilon}(u_{\text{ms}}^m) : \boldsymbol{\varepsilon}(v) + \xi \nabla \cdot u_{\text{ms}}^m \nabla \cdot v \Big) dx, \quad \forall v \in V_{h,0}^i.$$

The norm of R_i is defined as

$$||R_i||_{(V_h^i)^*} = \sup_{v \in V_{h,0}^i} \frac{|R_i(v)|}{a_i(v,v)^{\frac{1}{2}}},$$

where $a_i(v,v) = \int_{\omega_i^\varepsilon} \Big(2\mu\boldsymbol{\varepsilon}(v) : \boldsymbol{\varepsilon}(v) + \xi \nabla \cdot v \nabla \cdot v\Big) dx$.

For the computation of this norm, according to the Riesz representation theorem, we can first compute ϕ^{on} as the solution of following problem

$$\begin{aligned} &\int_{\omega_i^\varepsilon} \Big(2\mu\boldsymbol{\varepsilon}(\phi^{\text{on}}) : \boldsymbol{\varepsilon}(v) + \xi \nabla \cdot \phi^{\text{on}} \nabla \cdot v\Big) dx \\ = &\int_{\omega_i^\varepsilon} f v \, dx - \int_{\omega_i^\varepsilon} \Big(2\mu\boldsymbol{\varepsilon}(u_{\text{ms}}^m) : \boldsymbol{\varepsilon}(v) + \xi \nabla \cdot u_{\text{ms}}^m \nabla \cdot v\Big) dx, \\ &\forall v \in V_{h,0}^i \end{aligned} \tag{3.4}$$

and take $||R_i||_{(V_h^i)^*} = a_i(\phi^{\text{on}}, \phi^{\text{on}})^{\frac{1}{2}}$.

For the construction of the adaptive online basis functions, we use the following error indicators to access the quality of the solution. In those non-overlapping coarse grid neighborhoods ω_i^ε with large residuals, we enrich the space by finding online basis $\phi^{\text{on}} \in V_{h,0}^i$ using equation (3.4).

- *Indicator 1.* The error indicator based on local residual

$$\eta_i = ||R_i||^2_{(V_h^i)^*} \tag{3.5}$$

- *Indicator 2.* The error indicator based on local residual and eigenvalue

$$\eta_i = \left(\lambda_{l_i+1}^{\omega_i}\right)^{-1} ||R_i||^2_{(V_h^i)^*} \tag{3.6}$$

Now we present the adaptive online algorithm. We start with enrichment iteration

number $m = 0$ and choose $\theta \in (0, 1)$. Suppose the initial number of offline basis functions is $l_i^m(m = 1)$ for each coarse grid neighborhood ω_i^ε, and the multiscale space is $V_{\text{ms}}^m(m = 1)$. For $m = 1, 2, ...$

- *Step 1.* Find u_{ms}^m in V_{ms}^m such that

$$\int_{\omega_i^\varepsilon} \Big(2\mu\boldsymbol{\varepsilon}(u_{\text{ms}}^m) : \boldsymbol{\varepsilon}(v) + \xi\nabla \cdot u_{\text{ms}}^m \nabla \cdot v\Big)dx = \int_{\omega_i^\varepsilon} fv, \quad \forall v \in V_{\text{ms}}^m.$$

- *Step 2.* Compute error indicators (η_i) for every coarse grid neighborhoods ω_i^ε and sort them in decreasing order $\eta_1 \geq \eta_2 \geq ... \geq \eta_N$.

- *Step 3.* Select coarse grid neighborhoods ω_i^ε, where enrichment is needed. We take smallest k such that

$$\theta \sum_{i=1}^{N_v} \eta_i \leq \sum_{i=1}^{k} \eta_i.$$

- *Step 4.* Enrich the space by adding online basis functions. For each ω_i^ε, where $i = 1, 2, ..., k$, we find $\phi^{\text{on}} \in V_{h,0}^i$ by solving (3.4). The resulting space is denoted by V_{ms}^{m+1}.

We repeat the above procedure until the global error indicator is small or we have certain number of basis functions.

3.1.2 Stokes problem

In the above section, we presented the online procedure for the elasticity equations. In this section, we present the constructions of snapshot, offline and online basis functions for the Stokes problem.

3.1.2.1 Snapshot space

Snapshot space is a space which contains an extensive set of basis functions that are solutions of local problems with all possible boundary conditions up to fine-grid resolution.

To get snapshot functions, we solve the following problem on the coarse neighborhood ω_i^ε: find (u_l^i, p_l^i) (on a fine grid) such that

$$\begin{aligned} \int_{\omega_i^\varepsilon} \nabla u_l^i : \nabla v dx - \int_{\omega_i^\varepsilon} p_l^i \text{div}(v) dx = 0, \quad \forall v \in V_{h,0}^i, \\ \int_{\omega_i^\varepsilon} q \text{div}(u_l^i) dx = \int_{\omega_i^\varepsilon} cq dx, \quad \forall q \in Q_h^i, \end{aligned} \tag{3.7}$$

with boundary conditions

$$u_l^i = (0,0), \text{ on } \partial\mathcal{B}^\varepsilon, \quad u_l^i = (\delta_l^i, 0) \text{ or } (0, \delta_l^i), \text{ on } \partial\omega_i^\varepsilon \backslash \partial\mathcal{B}^\varepsilon,$$

where function δ_l^i is a piecewise constant function such that it has value 1 on e_l and value 0 on other fine-grid edges. Notice that $\omega_i^\varepsilon \backslash \partial\mathcal{B}^\varepsilon = \cup_{l=1}^{S_i} e_l$, where e_l are the fine-grid edges and S_i is the number of these fine grid edges on $\omega_i^\varepsilon \backslash \partial\mathcal{B}^\varepsilon$. In (3.7), we define V_h^i and Q_h^i as the restrictions of the fine grid space in ω_i^ε and $V_{h,0}^i \subset V_h^i$ be functions that vanish on $\partial\omega_i^\varepsilon$. Notice that u_l^i and p_l^i are supported in ω_i^ε. We remark that the constant c in (3.7) is chosen by compatibility condition, $c = \frac{1}{|\omega_i^\varepsilon|} \int_{\partial\omega_i^\varepsilon \backslash \partial\mathcal{B}^\varepsilon} u_l^i \cdot n_i \, ds$. We emphasize that, for the Stokes problem, we will solve (3.7) in both node-based coarse neighborhoods (2.9) and edge-based coarse neighborhoods (2.10).

The collection of the solutions of above local problems generates the snapshot space, $\psi_l^{i,\text{snap}} = u_l^i$ in ω_i^ε:

$$V_{\text{snap}} = \{\psi_l^{i,\text{snap}} : 1 \leq l \leq 2S_i, \, 1 \leq i \leq (N_e + N_v)\},$$

where we recall that N_e is the number of coarse-grid edges and N_v is the number of coarse-grid nodes.

3.1.2.2 *Offline space*

We perform a space reduction in the snapshot space through the use of a local spectral problem in ω_i^ε. The purpose of this is to determine the dominant modes in the snapshot space and to obtain a small dimension space for the approximation the solution.

We consider the following local eigenvalue problem in the snapshot space

$$A^{i,\text{off}}\Psi_k = \lambda_k^{i,\text{off}} S^{i,\text{off}}\Psi_k^{i,\text{off}}, \tag{3.8}$$

where

$$A^{i,\text{off}} = a_i(\psi_m^{i,\text{snap}}, \psi_n^{i,\text{snap}})$$

$$S^{i,\text{off}} = s_i(\psi_m^{i,\text{snap}}, \psi_n^{i,\text{snap}})$$

and

$$a_i(u,v) = \int_{\omega_i^\varepsilon} \nabla u : \nabla v dx, \quad \text{and} \quad s_i(u,v) = \int_{\omega_i^\varepsilon} |\nabla \chi_i|^2 u \cdot v \, dx$$

and χ_i will be specified later. Note that the above spectral problem is solved in the local snapshot space corresponding to the neighborhood domain ω_i^ε. We arrange the eigenvalues in the increasing order, and choose the first M_i eigenvalues and take the corresponding eigenvectors $\Psi_k^{i,\text{off}}$, for $k = 1, 2, ..., M_i$, to form the basis functions, i.e., $\widetilde{\Phi}_k^{i,\text{off}} = \sum_j \Psi_{kj}^{i,\text{off}} \psi_j^{i,\text{snap}}$, where $\Psi_{kj}^{i,\text{off}}$ are the coordinates of the vector $\Psi_k^{i,\text{off}}$. We define

$$\widetilde{V}_{\text{off}}^i = \text{span}\{\widetilde{\Phi}_k^{i,\text{off}}, \quad k = 1, 2, ..., 2S_i\}. \tag{3.9}$$

For construction of conforming offline space, we need to multiply the functions $\widetilde{\Phi}_k^{i,\text{off}} = (\widetilde{\Phi}_{x_1,k}^{i,\text{off}}, \widetilde{\Phi}_{x_2,k}^{i,\text{off}})$ by a partition of unity function χ_i. We remark that the partition of unity functions $\{\chi_i\}$ are defined with respect to the coarse nodes and the mid-points of coarse edges. One can choose $\{\chi_i\}$ as the standard multiscale finite element basis. However,

upon multiplying by partition of unity functions, the resulting basis functions do not have constant divergence any more, which affects the stability of the scheme. To resolve this problem, we solve two local optimization problems in every coarse element $K_j^i \subset \omega_i^\varepsilon$:

$$\min \left\| \nabla \Phi_{x_1,k}^{i,\text{off}} \right\|_{L^2(K_j^i)} \text{ such that } \operatorname{div}(\Phi_{x_1,k}^{i,\text{off}}) = \frac{1}{|K_j^i|} \int_{\partial K_j^i} (\chi_i \widetilde{\Phi}_{x_1,k}^{i,\text{off}}, 0) \cdot n_i \, ds, \quad \text{in } K_j^i \tag{3.10}$$

with $\Phi_{x_1,k}^{i,\text{off}} = (\chi_i \widetilde{\Phi}_{x_1,k}^{i,\text{off}}, 0), \text{ on } \partial K_j^i$, and

$$\min \left\| \nabla \Phi_{x_2,k}^{i,\text{off}} \right\|_{L^2(K_j^i)} \text{ such that } \operatorname{div}(\Phi_{x_2,k}^{i,\text{off}}) = \frac{1}{|K_j^i|} \int_{\partial K_j^i} (0, \chi_i \widetilde{\Phi}_{x_2,k}^{i,\text{off}}) \cdot n_i \, ds \quad \text{in } K_j^i, \tag{3.11}$$

with $\Phi_{x_2,k}^{i,\text{off}} = (0, \chi_i \widetilde{\Phi}_{x_2,k}^{i,\text{off}}), \text{ on } \partial K_j^i$. We write that $\Phi_{x_1,k}^{i,\text{off}} = \mathcal{H}(\chi_i \widetilde{\Phi}_{x_1,k}^{i,\text{off}})$ and $\Phi_{x_2,k}^{i,\text{off}} = \mathcal{H}(\chi_i \widetilde{\Phi}_{x_2,k}^{i,\text{off}})$, where $\mathcal{H}(v)$ is the *Stokes extension* of the function v.

Combining them, we obtain the global offline space:

$$V_{\text{off}} = \text{span}\{\Phi_{x_1,k}^{i,\text{off}} \text{ and } \Phi_{x_2,k}^{i,\text{off}} : \quad 1 \le i \le (N_e + N_v) \text{ and } 1 \le k \le M_i\}.$$

Using a single index notation, we can write

$$V_{\text{off}} = \text{span}\{\Phi_i^{\text{off}}\}_{i=1}^{N_u},$$

where $N_u = \sum_{i=1}^{N_e+N_v} M_i$. This space will be used as the approximation space for the velocity. For coarse approximation of pressure, we will take Q_{off} to be the space of piecewise constant functions on the coarse mesh.

3.1.2.3 Online adaptive method

Similar to Section 3.1.1.3, we will define the online velocity basis for Stokes problem. For each coarse grid neighborhood ω_i^ε, we define the residual R_i as a linear functional on

V^i such that

$$R_i(v) = \int_{\omega_i^\varepsilon} f \cdot v \, dx - \int_{\omega_i^\varepsilon} \nabla u_{\text{ms}}^m : \nabla v dx + \int_{\omega_i^\varepsilon} p_{\text{ms}}^m \text{div}(v) dx, \quad \forall v \in V^i \tag{3.12}$$

where $(u_{\text{ms}}^m, p_{\text{ms}}^m)$ is the multiscale solution at the enrichment level m, and $V^i = (H_0^1(\omega_i^\varepsilon))^2$. The norm of R_i is defined as

$$||R_i||_{(V^i)^*} = \sup_{v \in V^i} \frac{|R_i(v)|}{\|v\|_{H^1(\omega_i^\varepsilon)}}. \tag{3.13}$$

We will then use indicators (3.5) and (3.6) for our adaptive enrichment method. For the computation of online basis $\phi_i^{\text{on}} \in V_{h,0}^i$, we solve the following problem

$$\begin{aligned} \int_{\omega_i^\varepsilon} \nabla \phi_i^{\text{on}} : \nabla v dx - \int_{\omega_i^\varepsilon} p^{\text{on}} \text{div}(v) dx &= R_i(v), \quad \forall v \in V_{h,0}^i, \\ \int_{\omega_i^\varepsilon} \text{div}(\phi_i^{\text{on}}) \, q \, dx &= 0, \quad \forall q \in Q_{\text{off}}. \end{aligned} \tag{3.14}$$

The adaptivity procedure follows the one presented in Section 3.1.1.3.

3.1.3 Randomized snapshots

In the above construction, the local problems are solved for every bounday node. This procedure is expensive and may not be practical. However, one can use the idea of randomized snapshots (as in [31]) and reduce the cost substantially. In randomized snapshots, one computes a few more snapshots compared to the required number of multiscale basis functions. e.g., we compute $n + 4$ snapshots for n multiscale basis functions. To be more specific, we first generate inexpensive snapshots using random boundary conditions. Instead of solving the local problem (3.1) and (3.7) for each fine boundary degree of free-

dom, we solve a small number of local problems with boundary conditions:

$$u_k^{+,i} = (r_l^i, 0) \quad \text{or} \quad (0, r_l^i) \quad \text{on} \quad \partial\omega_i^{+,\varepsilon} \backslash \partial\mathcal{B}^\varepsilon,$$
$$u_k^{+,i} = (0,0) \quad \text{on} \quad \partial\mathcal{B}^\varepsilon.$$

Here r_l^i are independent identically distributed (i.i.d.) standard Gaussian random vectors defined on the fine degree freedom of the boundary. Notice that we will solve for $u_k^{+,i}$ in a larger domain, the oversampling domian $\omega_i^{+,\varepsilon}$. The oversampling technique is used avoid the effects of randomized boundaries. After removing dependence, we finally get our snapshot basis by taking the restriction of $u_k^{+,i}$ in ω_i^ε, i.e, $u_k^i = u_k^{+,i}|_{\omega_i^\varepsilon}$.

In Section 3.2, we will take the Stokes problem as an example and show the numerical results for randomized sanpshots.

3.2 Numerical results

In this section, we show simulation results using the framework of online adaptive GMsFEM presented in Section 2.3 for elasticity equations and Stokes equations. We note that the code is based on the FEniCS project [40] and DOLFIN libary [41].

We set $\Omega = [0,1] \times [0,1]$ and use two types of perforated domains as illustrated in Figure 3.1, where the perforated regions $\mathcal{B}^\varepsilon$ are circular. We have also used perforated regions of other shapes instead and obtained similar results. The computational domain is discretized coarsely using uniform triangulation, where the coarse mesh size $H = \frac{1}{10}$ for elasticity problem and $H = \frac{1}{5}$ for Stokes problem. Furthermore, nonuniform triangulation is used inside each coarse triangular element to obtain a finer discretization. Examples of this triangulation are displayed also in Figure 3.1.

First we will choose a fixed number of offline basis (initial basis) for every coarse neighborhood, and obtain corresponding offline space V_{off}, which is also denoted by V_{ms}^1.

Then, we perform the online iterations on non-overlapping coarse neighborhoods to obtain enriched space V_{ms}^m, $m \geq 1$. We will add online basis both with adaptivity and without adaptivity and compare the results. All the errors are in percentage. We note that our approaches are designed to explore the sparsity and the adaptivity in the solution space and our main emphasis is on the construction of coarse spaces. Our numerical results will show the approximation of the fine-scale solution for different dimensional coarse spaces.

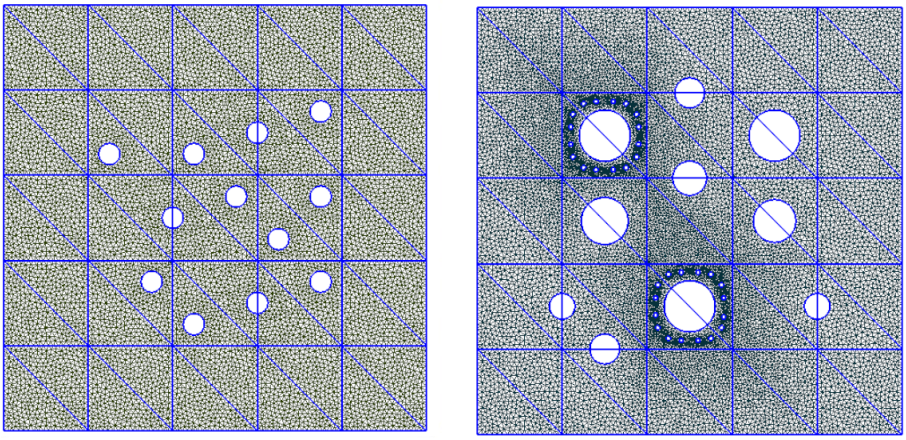

Figure 3.1: Two heterogeneous perforated media used in the simulations.

3.2.1 Elasticity equations in perforated domain

We consider the elasticity operator (2.5). We use zero displacements $u = 0$ on the inclusions, $u_1 = 0, \sigma_2 = 0$ on the left boundary, $\sigma_1 = 0, u_2 = 0$ on the bottom boundary and $\sigma_1 = 0, \sigma_2 = 0$ on the right and top boundaries. Here, $u = (u_1, u_2)$ and $\sigma = (\sigma_1, \sigma_2)$. The source term is defined by $f = (10^7, 10^7)$, the elastic modulus is given by $E = 10^9$, Poisson's ratio is $\nu = 0.22$, where

$$\mu = \frac{E}{2(1+\nu)}, \quad \xi = \frac{E\nu}{(1+\nu)(1-2\nu)}.$$

We use the following error quantities to measure the performance of the online adaptive GMsFEM

$$||e||_{L^2} = \|e_u\|_{L^2(\Omega^\varepsilon)} = \frac{\|(\xi + 2\mu)(u - u_{\text{ms}})\|_{L^2(\Omega^\varepsilon)}}{\|(\xi + 2\mu)u\|_{L^2(\Omega^\varepsilon)}}$$

$$||e||_{H^1} = \|e_u\|_{H^1(\Omega^\varepsilon)} = \sqrt{\frac{\langle \mathcal{L}^\varepsilon(u - u_{\text{ms}}), u - u_{\text{ms}} \rangle_{\Omega^\varepsilon}}{\langle \mathcal{L}^\varepsilon(u), u \rangle_{\Omega^\varepsilon}}}$$

where u and u_{ms} are the fine and coarse solutions, respectively, and

$$\langle \mathcal{L}^\varepsilon(u), v \rangle_{\Omega^\varepsilon} = 2\mu \langle \boldsymbol{\varepsilon}(u), \boldsymbol{\varepsilon}(v) \rangle_{\Omega^\varepsilon} + \xi \langle \nabla \cdot u, \nabla \cdot v \rangle_{\Omega^\varepsilon}$$

. Note that the reference solution u needs a full fine scale computation. The fine grid DOF is 13262 for the domain with small perforations(Figure 3.1 (a)) and 21986 for the domain with big perforations (Figure 3.1 (b)).

The fine-scale solution and coarse-scale solution corresponding to the two different perforated domains in Figure 3.1 are presented in Figures 3.2 and 3.3. Fine solutions are shown on the left of the figure, coarse offline solutions are in the middle and online solutions are on the right. In Tables 3.1 and 3.2, we present the convergence history when the problem is solved in two different perforated domain with one, two and four initial bases in the left, middle and right column, respectively. Each column shows the error behavior when the online method is applied without adaptivity, with adaptivity using Indicator 1 (see (3.5)) and with adaptivity using Indicator 2 (see (3.6)).

Numerical results for the first perforated domain are displayed in Figure 3.2. We observe that the offline solution is close to the fine-scale solution; however, there are some missing features in the offline solution. For example, the low values of the solution for a connected regions around circular inclusions, while this is not the case for the fine-scale solution. Also, we observe that the offline solution does not capture the low values of the solution near the inclusions. On the other hand, the solution using the online procedure

with approximately the same number of degrees of freedom as the offline solution has very good accuracy. From Table 3.1, we observe that when using one initial basis, the L^2 and energy error reduce to 1.3% and 5.82% respectively after one online iteration in the case without adaptivity. However, if we select two initial bases, the the L^2 and energy error can be reduced to 0.567% and 2.92% respectively after one online iteration, which is almost half of the errors for one initial basis situation. When the number of basis is fixed, it shows that adding online basis can reduce the error more effectively than adding offline basis. For example, when we use two offline basis and two online basis, the energy error is 0.369%; while when we select four offline basis, the energy error is 26.703%. Comparison of the error behavior between solving with and without adaptivity in this table shows that, error is smaller under the similar DOF when adaptive online method is applied. For example, if we start with one initial basis, the energy error is 5.482% with DOF 500 when online method is applied without adaptivity, but the energy error becomes 2.589% with DOF 536 when online adaptive method is applied. When we solve with the adaptivity, we observe that the first indicator (see (3.5)) is more effective when one initial basis is selected. However, if we start with two or four initial bases, the second indicator (see (3.6)) gives us slightly better results. The smallest eigenvalues are $\Lambda_{min} = 31.4, 79.9, 204.8$ when one, two and four initial basis are used.

In Figure 3.3, we test with a different perforated domain where the circular inclusions are larger compared to the domain in Figure 3.2 and extremely small inclusions are set around some big ones. Comparing the offline and fine solution, we notice that some features of solution in the interior of the domain are missing, and the errors around the boundary are large. However, the online solution fix these problems well and show much better accuracy. Looking at Table 3.2, we observe that as we select more initial basis, the error decreases faster after one online iteration. For example, when one online iteration is applied without adaptivity, the H^1 error reduces 8.5 times if we use one initial basis,

yet it reduces around 12 times if we use two initial basis. Considering the convergence behavior of online method with adaptivity against the online method without adaptivity, we see that the adaptivity is important. For instance, in a similar DOF of 1300 in the case of four initial basis used, the H^1 error 10^{-5} without adaptivity, while it is only 10^{-6} with adaptivity.

DOF (# iter)	$\|\|e\|\|_{L^2}$	$\|\|e\|\|_{H^1}$
without adaptivity		
338	29.3	53.7
500 (1)	1.3	5.5
662 (2)	0.08	0.45
824 (3)	0.01	0.07
986 (4)	0.001	0.007
with adaptivity, $\eta_i^2 = r_i^2$		
338	29.3	53.7
510 (3)	0.57	3.12
654 (6)	0.04	0.31
852 (10)	0.001	0.01
1014 (13)	0.0001	0.0008
with adaptivity, $\eta_i^2 = r_i^2 \lambda_{i+1}^{-1}$		
338	29.3	53.7
536 (4)	0.47	2.6
684 (7)	0.04	0.3
846 (10)	0.003	0.02
1002 (13)	0.0002	0.001

DOF (# iter)	$\|\|e\|\|_{L^2}$	$\|\|e\|\|_{H^1}$
without adaptivity		
412	10.7	32.9
574 (1)	0.57	2.92
736 (2)	0.05	0.37
898 (3)	0.005	0.05
1060 (4)	0.0005	0.004
with adaptivity, $\eta_i^2 = r_i^2$		
412	10.7	32.9
584 (3)	0.4	2.3
740 (6)	0.029	0.24
932 (10)	0.001	0.009
1190 (15)	1.685e-05	0.0001
with adaptivity, $\eta_i^2 = r_i^2 \lambda_{i+1}^{-1}$		
412	10.7	32.9
570 (3)	0.43	2.5
730 (6)	0.03	0.25
924 (10)	0.001	0.009
1072 (13)	8.772e-05	0.0006

DOF (# iter)	$\|\|e\|\|_{L^2}$	$\|\|e\|\|_{H^1}$
without adaptivity		
648	7.4	26.7
810 (1)	0.48	2.5
972 (2)	0.046	0.37
1134 (3)	0.004	0.04
1296 (4)	0.0005	0.004
with adaptivity, $\eta_i^2 = r_i^2$		
648	7.4	26.7
808 (3)	0.3	2.0
980 (6)	0.02	0.2
1144 (9)	0.001	0.016
1302 (12)	0.0001	0.001
with adaptivity, $\eta_i^2 = r_i^2 \lambda_{i+1}^{-1}$		
648	7.4	26.7
808 (3)	0.3	1.8
976 (6)	0.02	0.17
1174 (10)	0.0006	0.005
1338 (13)	3.492e-05	0.0002

Table 3.1: Elasticity problem in the perforated domain with small inclusions (Figure 3.1 (a)). One (Left), Two (Middle) and Four (Right) offline basis functions ($\theta = 0.7$).

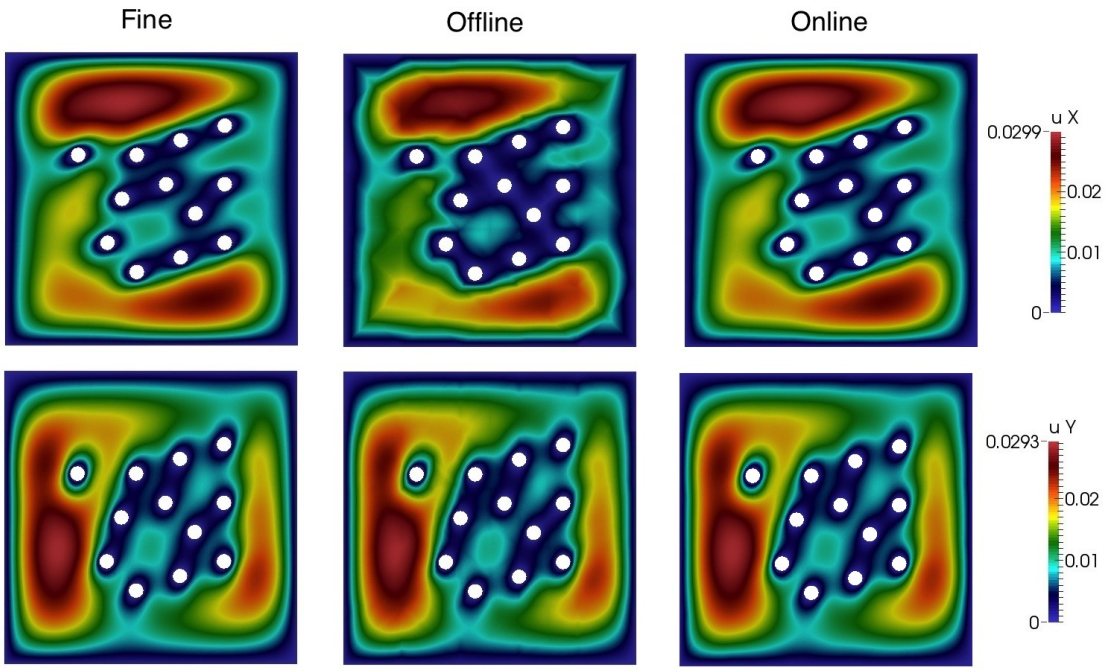

Figure 3.2: Elasticity problem in the perforated domain with small inclusions (Figure 3.1 (a)). Comparison of solutions in: fine scale (left) $DOF = 13262$, coarse-scale offline, $DOF = 412$ (middle), coarse-scale online without adaptivity, $DOF = 574$ (right). Top: u_1. Bottom: u_2.

3.2.2 Stokes equations in perforated domain

In our final example, we consider the Stokes equation with zero velocity $u = (0, 0)$ on $\partial\Omega^\varepsilon \cap \partial\mathcal{B}^\varepsilon$ and $\frac{\partial u}{\partial n} = (0, 0)$ on $\partial\Omega$, and source term $f = (1, 1) \in \Omega^\varepsilon$. For the fine-scale approximation of the Stokes problem, we use P_2 elements for velocity and piecewise constants for pressure. To improve the accuracy of multiscale solutions, we have enriched velocity spaces by adding online velocity basis.

The errors will be measured in relative L^2 and H^1norms for velocity and L^2 norm for

DOF (# iter)	$\|\|e\|\|_{L^2}$	$\|\|e\|\|_{H^1}$
without adaptivity		
278	38.1	61.2
440 (1)	2.1	7.2
602 (2)	0.17	0.67
764 (3)	0.02	0.11
926 (4)	0.001	0.010
with adaptivity, $\eta_i^2 = r_i^2$		
278	38.1	61.2
436 (3)	1.1	4.5
628 (7)	0.03	0.18
760 (10)	0.002	0.01
950 (14)	5.339e-05	0.0003
with adaptivity, $\eta_i^2 = r_i^2\lambda_{i+1}^{-1}$		
278	38.1	61.2
436 (3)	1.7	7.1
614 (7)	0.07	0.4
748 (10)	0.005	0.04
940 (14)	0.0002	0.001

DOF (# iter)	$\|\|e\|\|_{L^2}$	$\|\|e\|\|_{H^1}$
without adaptivity		
382	15.6	38.4
544 (1)	0.8	3.2
706 (2)	0.07	0.4
868 (3)	0.008	0.05
1030 (4)	0.0006	0.003
with adaptivity, $\eta_i^2 = r_i^2$		
382	15.6	38.4
556 (3)	0.5	2.1
704 (6)	0.03	0.2
892 (10)	0.001	0.007
1038 (13)	8.760e-05	0.0005
with adaptivity, $\eta_i^2 = r_i^2\lambda_{i+1}^{-1}$		
382	15.6	38.4
548 (3)	0.5	2.5
740 (7)	0.02	0.1
878 (10)	0.001	0.01
1064 (14)	4.710e-05	0.0003

DOF (# iter)	$\|\|e\|\|_{L^2}$	$\|\|e\|\|_{H^1}$
without adaptivity		
648	8.9	27.3
810 (1)	0.6	2.4
972 (2)	0.06	0.4
1134 (3)	0.006	0.04
1296 (4)	0.0005	0.003
with adaptivity, $\eta_i^2 = r_i^2$		
648	8.9	27.3
820 (3)	0.3	1.4
972 (6)	0.02	0.14
1154 (10)	0.0006	0.004
1300 (13)	3.784e-05	0.0002
with adaptivity, $\eta_i^2 = r_i^2\lambda_{i+1}^{-1}$		
648	8.9	27.3
810 (3)	0.4	1.5
996 (7)	0.008	0.07
1138 (10)	0.0006	0.005
1314 (14)	1.659e-05	0.0001

Table 3.2: Elasticity problem in the perforated domain with various sizes of inclusions (Figure 3.1 (b)). one (Left), two (Middle) and four (Right) offline basis functions ($\theta = 0.7$).

pressure

$$||e_u||_{L^2} = \|e_u\|_{L^2(\Omega^\epsilon)} = \frac{\|u - u_{\text{ms}}\|_{L^2(\Omega^\epsilon)}}{\|u\|_{L^2(\Omega^\epsilon)}}, \quad ||e_u||_{H^1} = \|e_u\|_{H^1(\Omega^\epsilon)} = \frac{\|u - u_{\text{ms}}\|_{H^1(\Omega^\epsilon)}}{\|u\|_{H^1(\Omega^\epsilon)}},$$
$$||e_p||_{L^2(\Omega^\epsilon)} = \frac{\|\bar{p} - p_{\text{ms}}\|_{L^2(\Omega^\epsilon)}}{\|\bar{p}\|_{L^2(\Omega^\epsilon)}},$$

where (u, p) and $(u_{\text{ms}}, p_{\text{ms}})$ are fine-scale and coarse-scale solutions, respectively for velocity and pressure, and $\bar{p}$ is the cell average of the fine scale pressure, that is, $\bar{p} = \frac{1}{|K_i^\epsilon|}\int_{K_i^\epsilon} p$ for all $K_i^\epsilon \in \mathcal{T}^H$. Notice that we solve the reference solution (u, p) on a full fine grid. The fine grid DOF is 77524 for the domain with small perforations(Figure 3.1 (a)) and 101386 for the domain with big perforations (Figure 3.1 (b)).

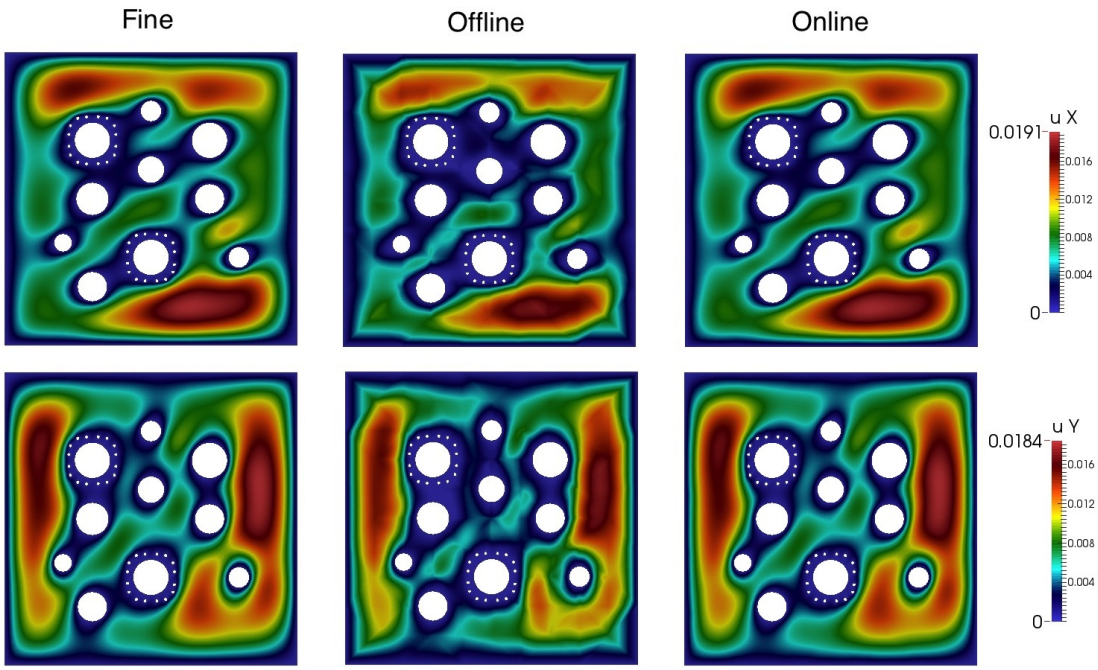

Figure 3.3: Elasticity problem in the perforated domain with various sizes of inclusions (Figure 3.1 (b)). Comparison of solutions in: fine scale (left) $DOF = 21986$, coarse scale offline, $DOF = 382$ (middle), coarse scale online without adaptivity, $DOF = 544$ (right). Top: u_1. Bottom: u_2.

3.2.2.1 Randomized snapshots

As mentioned in Section 3.1.3, we will show the numerical results of Stokes problem for the offline GMsFEM using randomized snapshots. The convergence behaviors are shown in Tables 3.3 and 3.4 for perforated domain with small inclusions (Figure 3.1 (a)) and various sizes of inclusions (Figure 3.1 (b)), respectively, where the notation $\omega^{+,\varepsilon} = \omega^{\varepsilon} + 4$ means that the oversampled region $\omega^{+,\varepsilon}$ is obtained by enlarging the region ω^{ε} by 4 fine grid cells. From these tables, we observe that the approach using randomized snapshots is more efficient since much fewer snapshot functions are used to achieve comparable accuracy. In particular, we get similar errors when the number of randomized snapshots is only around 20% of the number of standard snapshots. Notice that in

the randomized snapshot construction, we need to add the constant basis, i.e, the constant function in each $\omega^{+,\varepsilon}$. Note that, we do not have the constant basis in domain with inclusions when calculating snapshot basis in the standard way. This additional constant basis function makes the errors smaller for low degrees of freedom. For example, in the domain with small inclusions, when $DOF = 534$, the velocity L^2 error is 12.49% when we use standard snapshots, while the error is only 4.54% when the dimension of the randomized snapshots is 24.1% of the dimension of the whole snapshot space (see Table 3.3). However, when the DOF becomes larger, the errors for randomized snapshots are similar to that for standard snapshots. For instance, the velocity L^2 error is 0.07% when $DOF = 1986$ in domain with various sized of inclusions for both standard snapshots and randomized snapshots (see Table 3.4), where the dimension of the randomized snapshot is 13.8% of the dimension of the whole snapshots. We remark that, by balancing the computational cost and accuracy, we find the results are satisfactory when 24.1% randomized snapshots for domain with small inclusions(Figure 3.1 (a)) and 20.7% randomized snapshots for domain with various sized of inclusions(Figure 3.1 (b)) are used.

3.2.2.2 Adaptive online results

In this section, we present adaptive online results for Stokes problem for two perforated domains depicted in Figure 3.1. The solutions are shown in Figure 3.4 and Figure 3.5. In these figures, the x_1-component and x_2-component of the velocity solution are shown in the first and second rows, and the pressure solution is presented in the third row. The three columns contain the fine-scale, coarse-scale offline and coarse-scale online solutions. In both cases, we observe that the offline velocity solution is not able to capture the low values at the corners of the domain. Some features between inclusions also do not appear correctly in the offline solution. For example, in Figure 3.4, the low values in the upper left and lower right corner of the domain are missing in the offline velocity solu-

DOF	$\|\|\varepsilon_u\|\|_{L^2(\Omega)}(\%)$	$\|\|\varepsilon_u\|\|_{H^1(\Omega)}(\%)$	$\|\|\varepsilon_{\bar{p}}\|\|_{L^2(\Omega)}(\%)$
Standard snapshot (100%)			
534	12.49	36.91	21.46
1018	0.28	4.67	0.86
1986	0.031	1.64	0.0029
Randomized snapshot: $\omega^{+,\varepsilon} = \omega^{\varepsilon} + 4$, 18.1%			
534	4.99	23.95	13.4
1018	0.54	7.05	0.53
1986	0.04	1.77	0.02
Randomized snapshot: $\omega^{+,\varepsilon} = \omega^{\varepsilon} + 4$, 24.1%			
534	4.54	22.69	8.28
1018	0.47	6.6	0.52
1986	0.036	1.72	0.009

Table 3.3: Stokes problem in perforated domain with small inclusions (Figure 3.1 (a)) using standard snapshots and randomized snapshots.

DOF	$\|\|\varepsilon_u\|\|_{L^2(\Omega)}(\%)$	$\|\|\varepsilon_u\|\|_{H^1(\Omega)}(\%)$	$\|\|\varepsilon_{\bar{p}}\|\|_{L^2(\Omega)}(\%)$
Whole snapshot (100%)			
534	11.34	34.49	16.18
1018	0.17	3.62	1.09
1986	0.07	2.44	0.006
Randomized snapshot: $\omega^{+,\varepsilon} = \omega^{\varepsilon} + 4$, 13.8%			
534	6.04	24.84	9.37
1018	0.66	7.27	0.95
1986	0.07	2.53	0.02
Randomized snapshot: $\omega^{+,\varepsilon} = \omega^{\varepsilon} + 4$, 20.7%			
534	5.3	23.39	14.95
1018	0.56	6.87	0.73
1986	0.07	2.51	0.015

Table 3.4: Stokes pronlem in perforated domain with various sizes of inclusions (Figure 3.1 (b)) using standard snapshots and randomized snapshots.

tion. However, it was recovered very well in the online solution. Also, compared to the fine-scale solution, the features between the first hole on the left and the other inclusions are not captured in the offline solution. However, the online solutions get these features

well and outputs almost same profiles as the fine solution. In Figure 3.5, for the domain has various sized of inclusions with some extremely small inclusions around, we see even worse behavior of the offline solution compared to that in Figure 3.4, where the domain has several small inclusions. The low values of the velocity solution in the x_2-component along the right boundary are almost missing in the offline solution. The offline velocity solutions in both components around inclusions are still very poor. These observations highlights the advantage of the online method. We performed other tests for different perforated domains, and the results also suggest that online method is quite necessary.

Now, we turn our attention to velocity $L^2(\Omega^\varepsilon)$, $H^1(\Omega^\varepsilon)$ errors and pressure $L^2(\Omega^\varepsilon)$ error presented in Table 3.5 and Table 3.6. We consider different numbers of initial basis on each coarse neighborhood. For the perforated domain with small inclusions in Figure 3.4, we observe from Table 3.5 that both the velocity and pressure error decrease faster as we choose more initial bases. For example, the velocity has large H^1 error 66.28% using one initial basis. After adding one online basis, it reduces to 22.3%. When two initial bases are selected, the velocity H^1 error reduces from 23.4% to 3.2% after one step enrichment. Fixing the number of initial basis, we can compare the error behavior for the online method with or without adaptivity. It appears that online adaptive method reduces the errors more effectively. For instance, when one initial basis is selected, the velocity H^1 error is 22.302% for DOF 488 using non-adaptive online algorithm, while it is only 3.067% for a similar DOF 499 using adaptive online method with indicator 1 (see (3.5)). Comparing two error indicators for adaptive online method, we see that the indicator 1 is preferred when choosing one initial basis. Since the velocity error is 8.758% for DOF 504 using indicator 2 (see (3.6)), which is much larger than 3.067%. Also, the pressure error is 16.559% in this case when using indicator 2, which is almost 5 times larger compared with 3.575% when using indicator 1. However, both indicator works well when selecting more initial bases. We see very similar errors for both velocity and pressure fields using

different indicators when the number of initial basis is two or three.

For the second example in Figure 3.5, results are shown in Table 3.6. In this case, we observe that the online approach works better if we start with more initial basis. For example, the velocity H^1 error is 71.823% with one initial velocity basis, and reduces to 24.460% after adding one online basis. However it's only 20.430% with two initial basis without online enrichment. This implies that it is better to start with two or more initial basis in order to see that the more the online basis are used, the smaller the errors become. Similarly as before, the online approach with the adaptivity reduces the errors faster. Compared the two indicators, we see that the first error indicator (see (3.5)) for the adaptive online method gives slightly better results for any number of initial basis. One can also find that the pressure error also reduces significantly when we only enrich the velocity space.

3.2.2.3 Application

Digital rock physics has emerged as a powerful technology that images the rock microstructure and simulates fluids flow directly on the digital representation of the rock images. One of its major challenges lies in the significant computational demands of direct pore scale modeling of fluids flow through the real pore system. We apply our proposed online algorithm on this aspplication, and the data comes from [42] posted on the digital rock portal [43].

The numerical results show that multiscale reduced order model can significantly speed up the computation process. Solving the flow velocity and pressure in the multiscale space helps to improve the computational efficiency while obtaining good accuracy compared with the solution using standard finite element method, see Figure 3.7 for illustration.

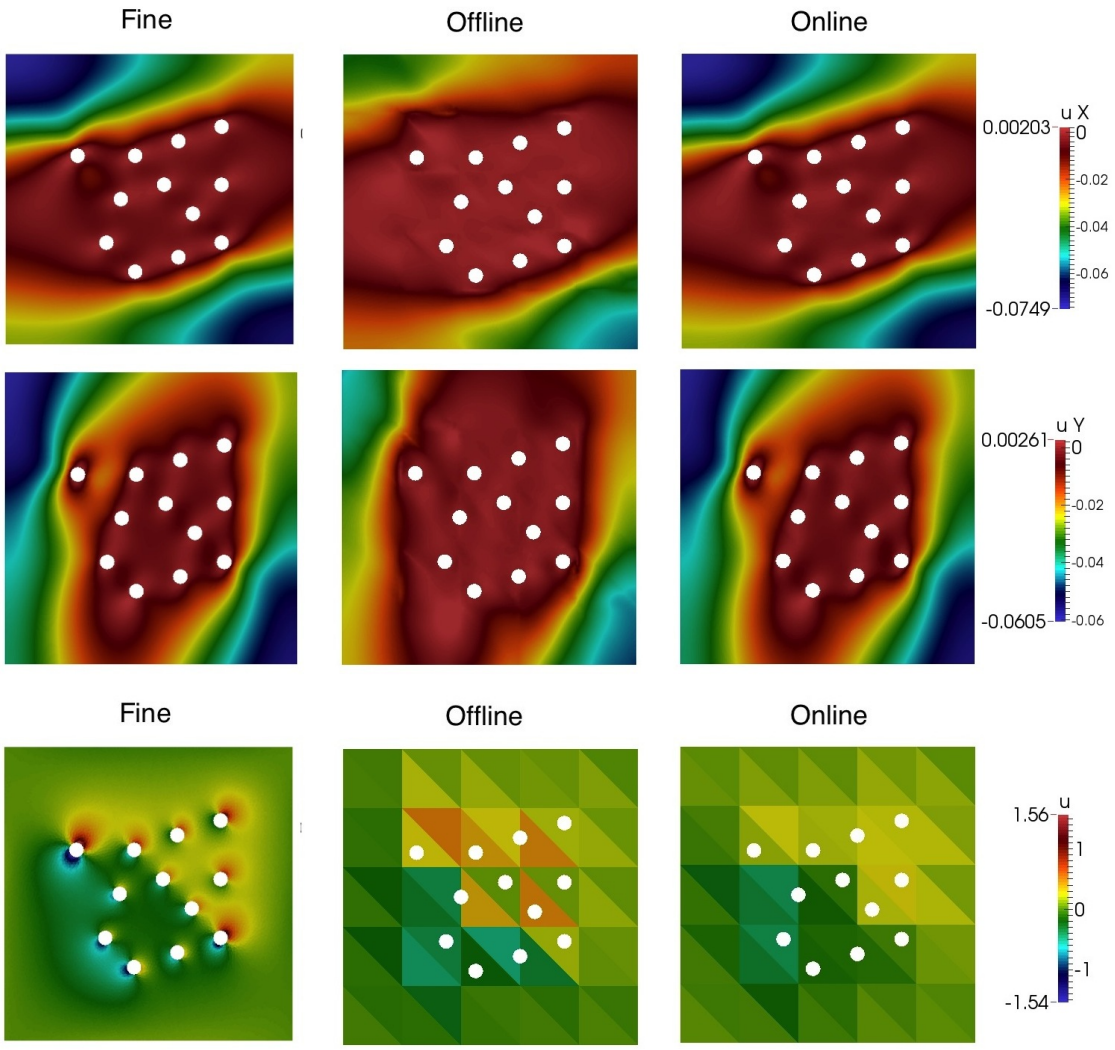

Figure 3.4: Stokes problem in perforated domain with small inclusions(Figure 3.1 (a)). Fine-scale and multiscale solutions for velocity and pressure (u_1 (Top), u_2 (Middle) and p (Bottom)). Left: fine-scale solution, $DOF = 77524$. Middle: multiscale solutions using 1 multiscale basis function for velocity, $DOF = 452$, velocity L^2 error is 42.439 %. Right: multiscale solutions after 2 online iteration without adaptivity, $DOF = 524$, velocity L^2 error is 1.688 %.

3.3 Convergence analysis

The result in [27] has shown the convergence for online adaptive method applied to elliptic problems, and the same results can be applied for elasticity problem. In this section,

DOF (# iter)	$\|\|e_u\|\|_{L^2}(\%)$	$\|\|e_u\|\|_{H^1}(\%)$	$\|\|e_{\bar{p}}\|\|_{L^2}(\%)$
452	42.4	66.3	81.9
without adaptivity			
488 (1)	6.3	22.3	41.8
524 (2)	1.7	7.2	10.4
596 (4)	0.1	0.7	0.8
740 (8)	0.04	0.5	0.04
with adaptivity, $\eta_i^2 = r_i^2$			
499 (4)	0.6	3.1	3.6
532 (6)	0.07	0.8	0.3
596 (10)	0.04	0.5	0.1
723 (20)	0.03	0.4	0.04
with adaptivity, $\eta_i^2 = r_i^2\lambda_{i+1}^{-1}$			
504 (3)	1.4	8.8	16.6
546 (5)	0.4	2.6	3.6
611 (8)	0.09	0.7	0.5
750 (15)	0.04	0.5	0.04

DOF (# iter)	$\|\|e_u\|\|_{L^2}(\%)$	$\|\|e_u\|\|_{H^1}(\%)$	$\|\|e_{\bar{p}}\|\|_{L^2}(\%)$
694	5.5	23.3	13.8
without adaptivity			
730 (1)	0.4	3.2	1.2
766 (2)	0.07	1.1	0.1
838 (4)	0.03	0.6	0.05
982 (8)	0.01	0.2	0.02
with adaptivity, $\eta_i^2 = r_i^2$			
732 (3)	0.09	1.3	0.2
781 (6)	0.04	0.7	0.08
844 (10)	0.02	0.4	0.02
992 (20)	0.004	0.1	0.003
with adaptivity, $\eta_i^2 = r_i^2\lambda_{i+1}^{-1}$			
745 (2)	0.09	1.4	0.3
769 (3)	0.06	1.0	0.1
841 (6)	0.03	0.6	0.03
988 (12)	0.01	0.2	0.02

DOF (# iter)	$\|\|e_u\|\|_{L^2}(\%)$	$\|\|e_u\|\|_{H^1}(\%)$	$\|\|e_{\bar{p}}\|\|_{L^2}(\%)$
936	0.9	8.8	8.5
without adaptivity			
972 (1)	0.03	0.8	0.1
1008 (2)	0.01	0.4	0.02
1080 (4)	0.007	0.3	0.005
1224 (8)	0.003	0.1	0.001
with adaptivity, $\eta_i^2 = r_i^2$			
975 (3)	0.02	0.5	0.03
1011 (6)	0.009	0.3	0.007
1082 (10)	0.005	0.2	0.003
1227 (20)	0.002	0.08	0.001
with adaptivity, $\eta_i^2 = r_i^2\lambda_{i+1}^{-1}$			
1003 (2)	0.013	0.4	0.02
1037 (3)	0.010	0.3	0.007
1105 (5)	0.006	0.2	0.004
1241 (9)	0.002	0.09	0.001

Table 3.5: Stokes problem for perforated domain with small inclusions(Figure 3.1 (a)). One (Upper left), two (Upper right) and three e(Bottom) offline basis functions ($\theta = 0.7$).

we will prove the convergence of adaptive online GMsFEM for Stokes problem.

First, we will prove the following inf-sup condition for the approximation of Stokes problem using offline GMsFEM. This ensures that the method, with both offline and online basis functions, is well-posed. We will assume the continuous inf-sup condition holds. In

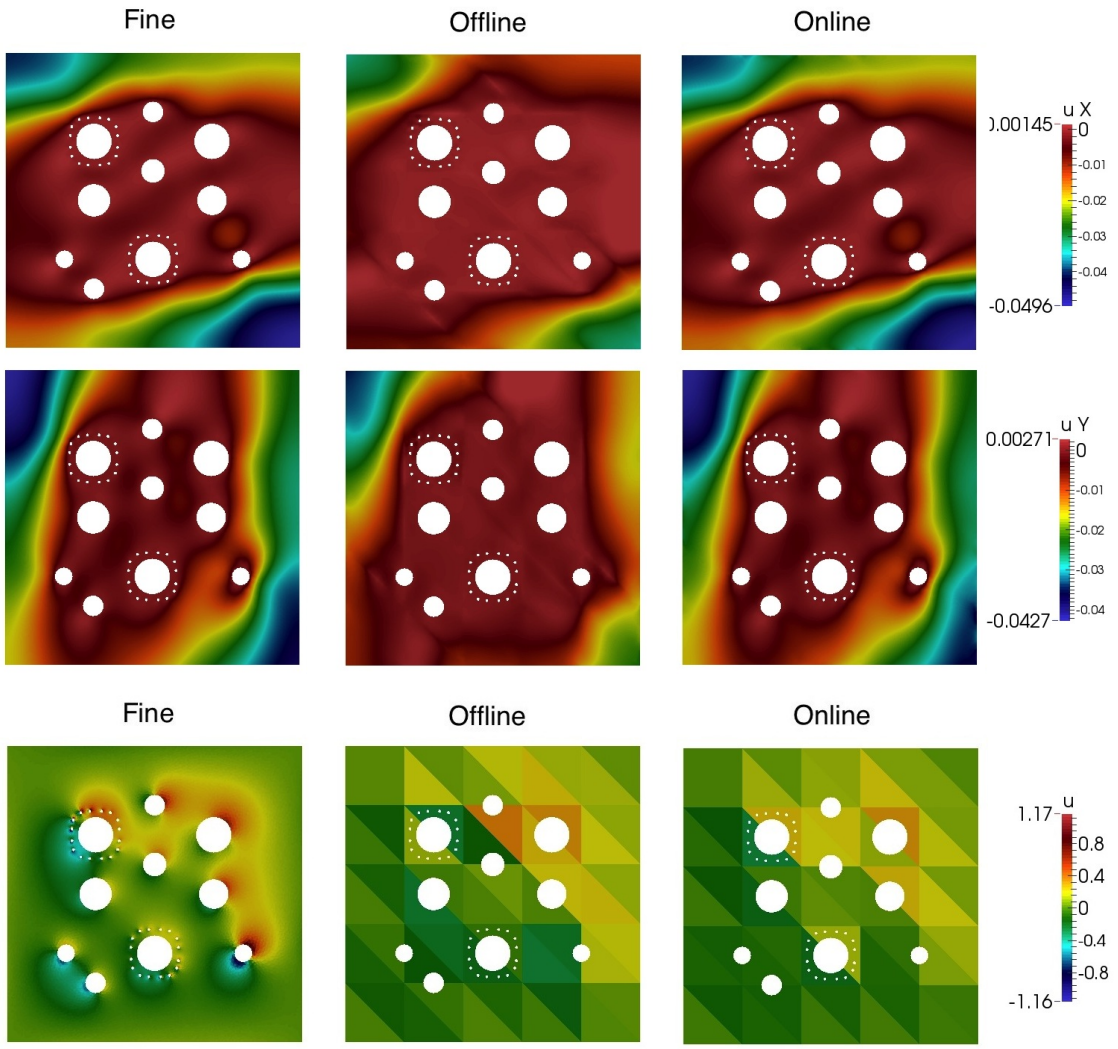

Figure 3.5: Stokes problem in perforated domain with various sizes of inclusions(Figure 3.1 (b)). Fine-scale and multiscale solutions for velocity and pressure (u_1 (Top), u_2 (Middle) and p (Bottom)). Left: fine-scale solution, $DOF = 101386$. Middle: multiscale solutions using 1 multiscale basis function for velocity, $DOF = 452$, velocity L^2 error is 47.943 %. Right: multiscale solutions after 2 online iteration without adaptivity, $DOF = 524$, velocity L^2 error is 2.266 %.

particular, there is a constant $C_{\text{cont}} > 0$ such that for any $p \in L^2(\Omega^\varepsilon)$ with zero mean, we

DOF (# iter)	$\|\|e_u\|\|_{L^2}(\%)$	$\|\|e_u\|\|_{H^1}(\%)$	$\|\|e_{\bar{p}}\|\|_{L^2}(\%)$
452	47.9	71.8	88.4
without adaptivity			
488 (1)	8.0	24.5	21.2
524 (2)	2.3	12.3	11.1
596 (4)	0.4	2.5	1.4
740 (8)	0.05	0.7	0.04
with adaptivity, $\eta_i^2 = r_i^2$			
492 (3)	2.4	13.5	11.4
534 (6)	0.5	4.3	3.2
593 (10)	0.09	0.9	0.3
718 (20)	0.04	0.5	0.03
with adaptivity, $\eta_i^2 = r_i^2 \lambda_{i+1}^{-1}$			
511 (2)	2.3	12.4	10.9
543 (3)	1.3	7.9	3.8
605 (5)	0.2	1.2	0.4
768 (11)	0.04	0.5	0.07

DOF (# iter)	$\|\|e_u\|\|_{L^2}(\%)$	$\|\|e_u\|\|_{H^1}(\%)$	$\|\|e_{\bar{p}}\|\|_{L^2}(\%)$
694	4.1	20.4	13.6
without adaptivity			
730 (1)	0.3	2.3	1.4
766 (2)	0.08	1.0	0.06
838 (4)	0.03	0.5	0.03
982 (8)	0.008	0.2	0.005
with adaptivity, $\eta_i^2 = r_i^2$			
735 (3)	0.08	1.1	0.07
766 (5)	0.05	0.7	0.03
842 (10)	0.02	0.3	0.02
981 (20)	0.006	0.1	0.002
with adaptivity, $\eta_i^2 = r_i^2 \lambda_{i+1}^{-1}$			
762 (2)	0.08	1.0	0.057
796 (3)	0.06	0.8	0.056
864 (5)	0.02	0.4	0.01
1000 (9)	0.007	0.1	0.004

DOF (# iter)	$\|\|e_u\|\|_{L^2}(\%)$	$\|\|e_u\|\|_{H^1}(\%)$	$\|\|e_{\bar{p}}\|\|_{L^2}(\%)$
936	0.4	5.6	2.1
without adaptivity			
972 (1)	0.03	0.7	0.06
1008 (2)	0.02	0.5	0.01
1080 (4)	0.007	0.2	0.004
1224 (8)	0.004	0.1	0.002
with adaptivity, $\eta_i^2 = r_i^2$			
977 (3)	0.02	0.6	0.03
1023 (6)	0.01	0.3	0.01
1085 (10)	0.006	0.2	0.003
1226 (19)	0.003	0.09	0.001
with adaptivity, $\eta_i^2 = r_i^2 \lambda_{i+1}^{-1}$			
972 (1)	0.03	0.7	0.06
1040 (3)	0.01	0.3	0.009
1108 (5)	0.006	0.2	0.003
1244 (9)	0.003	0.09	0.002

Table 3.6: Stokes problem for perforated domain with various sizes of inclusions(Figure 3.1 (b)). One (Upper left), two (Upper right) and three (Bottom) offline basis functions ($\theta = 0.7$).

have

$$\sup_{v \in (H_0^1(\Omega^\varepsilon))^2} \frac{\int_{\Omega^\epsilon} \text{div}(v) p}{\|v\|_{H^1(\Omega^\epsilon)}} \geq C_{\text{cont}} \|p\|_{L^2(\Omega^\epsilon)} . \tag{3.15}$$

Equivalently, there exists $v \in (H_0^1(\Omega^\varepsilon))^2$ such that $\text{div} v = p$ and $\|v\|_{H^1(\Omega^\varepsilon)} \leq C_{\text{cont}}^{-1} \|p\|_{L^2(\Omega^\varepsilon)}$.

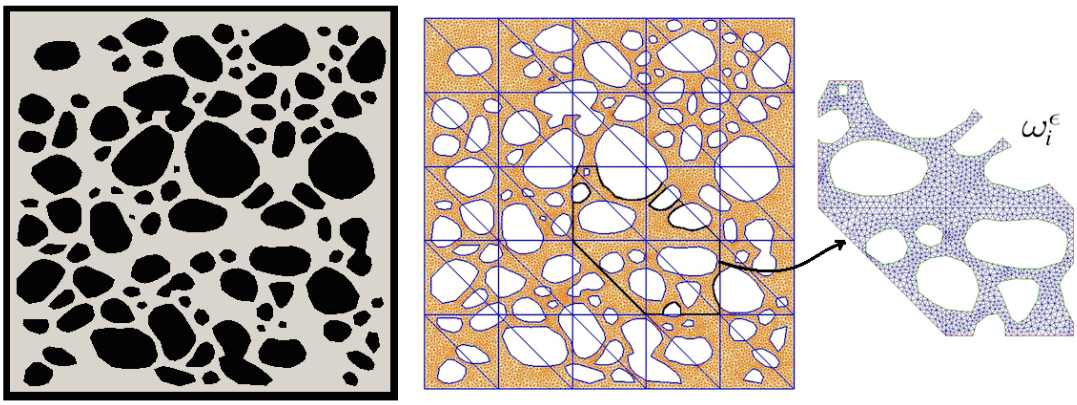

Figure 3.6: Application of the adaptive online method. Left: rock image, adapted from [42]. Right: fine and coarse grid on the image.

Let N_e^0 be the number of interior coarse edges. We remark that, for each interior coarse edge E_i, there exists a basis function Φ_i^{off} such that $\int_{E_i} \Phi_i^{\text{off}} \cdot n_i \neq 0$.

Lemma 3.3.1. *For all $p \in Q_{\text{off}}$, there is a constant $C_{\text{infsup}} > 0$ such that*

$$\sup_{u \in V_{\text{off}}} \frac{\int_{\Omega^\epsilon} div(u)p}{\|u\|_{H^1(\Omega^\epsilon)}} \geq C_{\text{infsup}} \|p\|_{L^2(\Omega^\epsilon)}. \tag{3.16}$$

Proof. Let $p \in Q_{\text{off}}$ with zero mean. Using the continuous inf-sup condition (3.15), there exists $v \in H_0^1(\Omega^\varepsilon)$ such that div$v = p$ and $\|v\|_{H^1(\Omega^\varepsilon)} \leq C_{\text{cont}}^{-1} \|p\|_{L^2(\Omega^\varepsilon)}$. Since, for each interior coarse edge E_i, there exists a basis function Φ_i^{off} such that $\int_{E_i} \Phi_i^{\text{off}} \cdot n_i \neq 0$. We can then define $u \in V_{\text{off}}$ by the following

$$u = \sum_{i=1}^{N_e^0} c_i \Phi_i^{\text{off}}, \quad c_i = \int_{E_i} v \cdot n_i$$

where we assume that the basis function are normalized so that $\int_{E_i} \Phi_i^{\text{off}} \cdot n_i = 1$. So, by

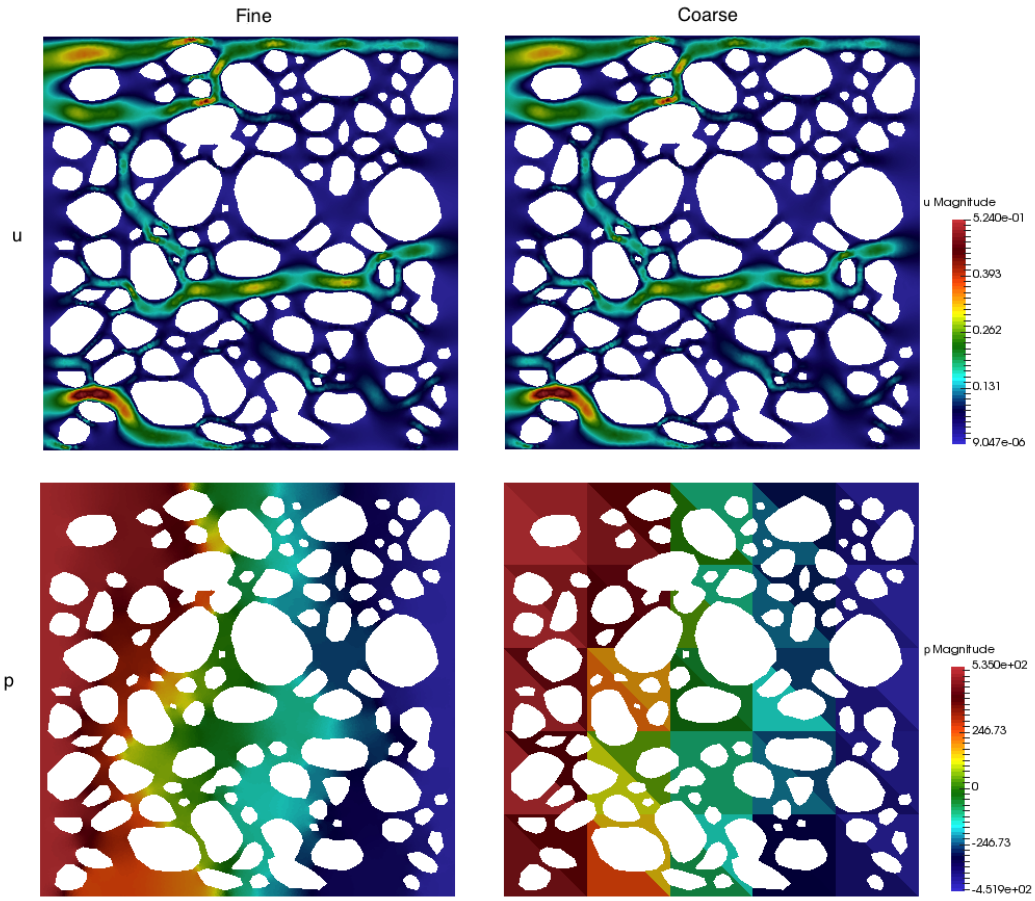

Figure 3.7: Application of the adaptive online method. First row: velocity magnitude. Second row: pressure. Left column: fine scale solution, $DOF = 127208$. Right column: coarse scale solution using the proposed multiscale method, $DOF = 1662$, velocity L^2 error is 4.8 %, average of the pressure error is 0.58 %.

the Green's identity, we have

$$\int_{\Omega^\epsilon} p^2 = \int_{\Omega^\epsilon} \text{div}(v)p = \sum_{i=1}^{N_e^0} \int_{E_i} (v \cdot n_i)[p] = \sum_{i=1}^{N_e^0} \int_{E_i} c_i(\Phi_i^{\text{off}} \cdot n_i)[p] = \int_{\Omega^\epsilon} \text{div}(u)p$$

where $[p]$ is the jump of p. We will next show that there is a constant $C_{\text{infsup}} > 0$ such that $\|u\|_{H^1(\Omega^\epsilon)} \leq C_{\text{infsup}}^{-1} \|p\|_{L^2(\Omega^\epsilon)}$.

Since $c_i^2 \leq H \int_{E_i} (v \cdot n_i)^2$, we have

$$\|\nabla u\|^2_{L^2(\Omega^\epsilon)} \leq \sum_{i=1}^{N_e^0} \int_{\omega_i^\epsilon} c_i^2 \, \nabla \Phi_i^{\text{off}} : \nabla \Phi_i^{\text{off}} \leq C_{\text{max}} H \sum_{K \in \mathcal{T}^H} \int_{\partial K} (v \cdot n)^2$$

where $C_{\text{max}} = \max_{1 \leq i \leq N_e^0} C_i$ and $C_i = \min \int_{\omega_i^\epsilon} \nabla \Phi_i^{\text{off}} : \nabla \Phi_i^{\text{off}}$ with the minimum taken over all basis functions Φ_i^{off} such that $\int_{E_i} \Phi_i^{\text{off}} \cdot n_i \neq 0$. Notice that the constant C_i are independent of the mesh size. Using the trace theorem on the coarse element K, we have $H \int_{\partial K} (v \cdot n)^2 \preceq \|v\|^2_{H^1(K)}$. So, by the continuous inf-sup condition, we obtain

$$\sum_{K \in \mathcal{T}^H} H \int_{\partial K} (v \cdot n)^2 \preceq \|v\|_{H^1(\Omega^\varepsilon)} \preceq \|p\|^2_{L^2(\Omega^\varepsilon)}.$$

This completes the proof.

□

Now, we will show the convergence of our online adaptive enrichment scheme for the Stokes problem. First, we define a reference solution by $(u, p) \in (H_0^1(\Omega^\varepsilon))^2 \times Q_{\text{off}}$ which solves

$$\langle \mathcal{L}^\varepsilon(u, p), (v, q) \rangle_{\Omega^\varepsilon} = ((f, 0), (v, q))_{\Omega^\varepsilon}, \qquad \text{for all } (v, q) \in H_0^1(\Omega^\varepsilon)^2 \times Q_{\text{off}}. \tag{3.17}$$

Notice that the solution of (3.17) and the solution of (2.12) have a difference proportional to the coarse mesh size H. We also define a snapshot solution by $(\hat{u}, \hat{p}) \in V_{\text{snap}} \times Q_{\text{off}}$ which solves

$$\langle \mathcal{L}^\varepsilon(\hat{u}, \hat{p}), (v, q) \rangle_{\Omega^\varepsilon} = ((f, 0), (v, q))_{\Omega^\varepsilon}, \qquad \text{for all } (v, q) \in V_{\text{snap}} \times Q_{\text{off}}. \tag{3.18}$$

We notice that the difference $\|u - \hat{u}\|_{H^1(\Omega^\varepsilon)}$ represents an irreducible error. Furthermore,

standard finite element analysis shows that

$$\|u - u_{\text{ms}}\|_{H^1(\Omega^\varepsilon)} \leq \|u - \widetilde{u}_{\text{ms}}\|_{H^1(\Omega^\varepsilon)} \tag{3.19}$$

for any $\widetilde{u}_{\text{ms}} \in V_{\text{off}}$. Next, we prove the following a-posteriori error bound for the offline GMsFEM (2.13). The notation $a \preceq b$ means that there is a generic constant $C > 0$ such that $a \leq Cb$.

Theorem 3.3.2. *Let u be the reference solution defined in (3.17), $\hat{u}$ be the snapshot solution defined in (3.18) and u_{ms} be the multiscale solution satisfying (2.13). Then, we have*

$$\|\hat{u} - u_{\text{ms}}\|^2_{H^1(\Omega^\epsilon)} \leq C_s \sum_{i=1}^{N_u} \left(1 + \frac{1}{\lambda^{i,\text{off}}_{l_i+1}}\right) \|R_i\|^2_{V^*} \tag{3.20}$$

where l_i is the number of offline basis functions used for the coarse neighborhood ω_i^ε, and $\lambda_j^{i,\text{off}}$ is the j-th eigenvalue for the coarse neighborhood ω_i^ε. The constant C_s is the maximum number of coarse neighborhoods corresponding to coarse blocks. Moreover, we have

$$\|u - u_{\text{ms}}\|^2_{H^1(\Omega^\epsilon)} \leq 2C_s \sum_{i=1}^{N_u} \left(1 + \frac{1}{\lambda^{i,\text{off}}_{l_i+1}}\right) \|R_i\|^2_{V^*} + 2\|u - \hat{u}\|^2_{H^1(\Omega^\epsilon)}. \tag{3.21}$$

Proof. For any $\phi \in V_{\text{snap}}$ such that $\int_{K_i^\epsilon} \text{div}\phi = 0$ and $\phi = \mathcal{H}(\phi)$, we have

$$\int_{\Omega^\epsilon} \nabla(\hat{u} - u_{\text{ms}}) : \nabla\phi = \int_{\Omega^\epsilon} \nabla(\hat{u} - u_{\text{ms}}) : \nabla\phi - \int_{\Omega^\epsilon} (\hat{p} - p_{\text{ms}})\text{div}\phi \tag{3.22}$$

where we use the fact that $\int_{K_i^\epsilon} (\hat{p} - p_{\text{ms}})\text{div}\phi = 0$ since $\hat{p} - p_{\text{ms}}$ is constant in K_i^ϵ. We can write (3.22) as

$$\int_{\Omega^\epsilon} \nabla(\hat{u} - u_{\text{ms}}) : \nabla\phi = R(\phi) \tag{3.23}$$

where $R(\phi)$ is the global residual defined by $R(\phi) = \int_{\Omega^\epsilon} \nabla(u - u_{\text{ms}}) : \nabla\phi - \int_{\Omega^\epsilon}(p - p_{\text{ms}})\text{div}\phi$ for all ϕ. Let ϕ^{off} be an arbitrary function in the space V_{off}. We can write $\phi^{\text{off}} = \sum_{i=1}^{N_u} \phi_i^{\text{off}}$ where ϕ_i^{off} is the component of ϕ^{off} in the local offline space corresponding to the coarse neighborhood ω_i^ε. Using the facts that $V_{\text{off}} \subset V_{\text{snap}}$ and $R(\phi^{\text{off}}) = 0$, we can write $R(\phi)$ as

$$R(\phi) = R(\mathcal{H}(\phi) - \phi^{\text{off}}) = R\Big(\sum_{i=1}^{N_u}(\mathcal{H}(\chi_i\phi) - \phi_i^{\text{off}})\Big) = \sum_{i=1}^{N_u} R_i\Big(\mathcal{H}(\chi_i\phi) - \phi_i^{\text{off}}\Big) \quad (3.24)$$

where R_i is the local residual defined in (3.12). We will define ϕ^{off} as follows. Notice that $\mathcal{H}(\chi_i\phi)$ belongs to the local snapshot space V_{snap}^i. We can take ϕ_i^{off} as the component of $\mathcal{H}(\chi_i\phi)$ in the offline space V_{off}^i. We write $\phi_i^{\text{off}} = \mathcal{H}(\chi_i\phi_i)$.

Then from (3.24), we have

$$R(\phi) \leq \sum_{i=1}^{N_u} \|R_i\|_{(V^i)^*} \, \|\mathcal{H}(\chi_i\phi) - \mathcal{H}(\chi_i\phi_i)\|_{H^1(\omega_i^\varepsilon)}.$$

Using the minimum energy property, we have

$$R(\phi) \leq \sum_{i=1}^{N_u} \|R_i\|_{(V^i)^*} \, \|\chi_i(\phi - \phi_i)\|_{H^1(\omega_i^\varepsilon)}.$$

By the spectral problem (3.8), we obtain

$$\begin{aligned} R(\phi) &\leq \sum_{i=1}^{N_u} \big(1 + \frac{1}{\lambda_{l_i+1}^{i,\text{off}}}\big)^{\frac{1}{2}} \|R_i\|_{(V^i)^*} \, \|\phi - \phi_i\|_{H^1(\omega_i^\varepsilon)} \\ &\leq \sum_{i=1}^{N_u} \big(1 + \frac{1}{\lambda_{l_i+1}^{i,\text{off}}}\big)^{\frac{1}{2}} \|R_i\|_{(V^i)^*} \, \|\phi\|_{H^1(\omega_i^\varepsilon)} \end{aligned} \quad (3.25)$$

where we used the orthogonality of eigenfunctions from the spectral problem (3.8). Fi-

nally, we take $\phi = \hat{u} - u_{\text{ms}}$. Notice that, by (3.18) and (2.13), we have

$$\int_{K_i^\varepsilon} \text{div}(\hat{u} - u_{\text{ms}}) = 0.$$

In addition, for this choice of ϕ, we have $\phi = \mathcal{H}(\phi)$ since $\hat{u}, u_{\text{ms}} \in V_{\text{snap}}$. Hence (3.23) and (3.25) imply that

$$\|\hat{u} - u_{\text{ms}}\|^2_{H^1(\Omega^\varepsilon)} \leq \sum_{i=1}^{N_u} \big(1 + \frac{1}{\lambda^{i,\text{off}}_{l_i+1}}\big)^{\frac{1}{2}} \|R_i\|_{(V^i)^*} \, \|\hat{u} - u_{\text{ms}}\|_{H^1(\omega_i^\varepsilon)},$$

which shows (3.20). The proof for (3.21) follows from $\|u - u_{\text{ms}}\|_{H^1(\Omega^\varepsilon)} \leq \|u - \hat{u}\|_{H^1(\Omega^\varepsilon)} + \|\hat{u} - u_{\text{ms}}\|_{H^1(\Omega^\varepsilon)}$.

□

We recall that the norm of the local residual R_i is defined in (3.13). We define a modified norm as

$$||R_i||_{(V_0^i)^*} = \sup_{v \in V_0^i} \frac{|R_i(v)|}{\|v\|_{H^1(\omega_i^\varepsilon)}} \tag{3.26}$$

where $V_0^i \subset V^i$ and the vectors $v \in V_0^i$ satisfies $\int_{\Omega^\varepsilon} \text{div}(v)\, q = 0$ for all $q \in Q_{\text{off}}$. It is easy to show that $||R_i||_{(V_0^i)^*} \leq ||R_i||_{(V^i)^*}$. In the next theorem, we will show the convergence of the online adaptive GMsFEM for the Stokes problem. The theorem states that our method is convergent up to an irreducible error $\|u - \hat{u}\|_{H^1(\Omega^\varepsilon)}$ with enough number of offline basis functions.

Theorem 3.3.3. *Let u be the reference solution defined in (3.17), $\hat{u}$ be the snapshot solution defined in (3.18) and u_{ms}^m be the multiscale solution of (2.13) in the enrichment level m. Assume that l_i offline basis functions for the coarse neighborhood ω_i^ε are used as initial basis in the online procedure. Suppose that one online basis is added to a single coarse*

neighborhood ω_i^ε. Then, there is a constant D such that

$$\begin{aligned}&\|u - u_{\text{ms}}^{m+1}\|^2_{H^1(\Omega^\varepsilon)}\\ &\leq (1+\delta_3)(1+\delta_2)\Big(1+\delta_1-\theta C_s^{-1}\frac{\lambda^{i,\text{off}}_{l_i+1}}{\lambda^{i,\text{off}}_{l_i+1}+1}\Big)\|\hat{u}-u_{\text{ms}}^m\|^2_{H^1(\Omega^\varepsilon)} + D\|u-\hat{u}\|^2_{H^1(\Omega^\varepsilon)}\end{aligned} \tag{3.27}$$

where $\delta_1, \delta_2, \delta_3 > 0$ are arbitrary and D depends only on $\delta_i, i = 1, 2, 3$. In addition, θ is the relative residual defined by

$$\theta = ||R_i||^2_{(V_0^i)^*} \Big/ \sum_{i=1}^{N_u} \|R_i\|^2_{(V^i)^*}\,.$$

Proof. We will first consider the addition of only one online basis function ϕ_i^{on} to the space V_{off}^m. For any function $\widetilde{u}_{\text{ms}} \in V_{\text{off}}^{m+1}$, by (3.19), we have

$$\|u - u_{\text{ms}}^{m+1}\|_{H^1(\Omega^\varepsilon)} \leq \|u - \widetilde{u}_{\text{ms}}\|_{H^1(\Omega^\varepsilon)} \leq \|\hat{u} - \widetilde{u}_{\text{ms}}\|_{H^1(\Omega^\varepsilon)} + \|u - \hat{u}\|_{H^1(\Omega^\varepsilon)}. \tag{3.28}$$

We will derive an estimate for $\|\hat{u} - \widetilde{u}_{\text{ms}}\|_{H^1(\Omega^\varepsilon)}$. We take $\widetilde{u}_{\text{ms}} = u_{\text{ms}}^m + \alpha\phi_i^{\text{on}}$ where α is a scalar to be determined. Then we have

$$\|\hat{u} - \widetilde{u}_{\text{ms}}\|^2_{H^1(\Omega^\varepsilon)} = \|\hat{u} - u_{\text{ms}}^m\|^2_{H^1(\Omega^\varepsilon)} - 2\alpha\int_{\omega_i^\varepsilon} \nabla(\hat{u} - u_{\text{ms}}^m) : \nabla\phi_i^{\text{on}} + \alpha^2\|\phi_i^{\text{on}}\|^2_{H^1(\Omega^\varepsilon)}.$$

Using the definition of the residual R_i and the fact that $\int_{\omega_i^\varepsilon} \text{div}(\phi_i^{\text{on}})\, q = 0$ for all $q \in Q_{\text{off}}$, we have

$$\|\hat{u}-\widetilde{u}_{\text{ms}}\|^2_{H^1(\Omega^\varepsilon)} = \|\hat{u}-u_{\text{ms}}^m\|^2_{H^1(\Omega^\varepsilon)} - 2\alpha R_i(\phi_i^{\text{on}}) + \alpha^2\|\phi_i^{\text{on}}\|^2_{H^1(\Omega^\varepsilon)} + 2\alpha\int_{\omega_i^\varepsilon}\nabla(u-\hat{u}) : \nabla\phi_i^{\text{on}}.$$

Taking $\alpha = R_i(\phi_i^{\text{on}})/\|\phi_i^{\text{on}}\|^2_{H^1(\omega_i^\varepsilon)}$, we have

$$\|\hat{u} - \widetilde{u}_{\text{ms}}\|^2_{H^1(\Omega^\varepsilon)} = \|\hat{u} - u^m_{\text{ms}}\|^2_{H^1(\Omega^\varepsilon)} - \frac{R_i(\phi_i^{\text{on}})^2}{\|\phi_i^{\text{on}}\|^2_{H^1(\omega_i^\varepsilon)}} + 2\alpha \int_{\omega_i^\varepsilon} \nabla(u - \hat{u}) : \nabla\phi_i^{\text{on}}. \quad (3.29)$$

Using (3.14), we have

$$R_i(v) = \int_{\omega_i^\varepsilon} \nabla\phi_i^{\text{on}} : \nabla v, \quad \forall v \in V_0^i. \quad (3.30)$$

By (3.26) and (3.30), we have $||R_i||_{(V_0^i)^*} \leq \|\phi_i^{\text{on}}\|_{H^1(\omega_i^\varepsilon)}$. Taking $v = \phi_i^{\text{on}}$ in (3.30), we have $R_i(\phi_i^{\text{on}}) = \|\phi_i^{\text{on}}\|^2_{H^1(\omega_i^\varepsilon)}$. Thus, (3.29) becomes

$$\|\hat{u} - \widetilde{u}_{\text{ms}}\|^2_{H^1(\Omega^\varepsilon)} = \|\hat{u} - u^m_{\text{ms}}\|^2_{H^1(\Omega^\varepsilon)} - ||R_i||^2_{(V_0^i)^*} + 2\alpha \int_{\omega_i^\varepsilon} \nabla(u - \hat{u}) : \nabla\phi_i^{\text{on}}. \quad (3.31)$$

Using the definition of θ and (3.20), we have

$$\|\hat{u} - \widetilde{u}_{\text{ms}}\|^2_{H^1(\Omega^\varepsilon)} \leq \Big(1 - \theta C_s^{-1} \frac{\lambda^{i,\text{off}}_{l_i+1}}{\lambda^{i,\text{off}}_{l_i+1} + 1}\Big)\|\hat{u} - u^m_{\text{ms}}\|^2_{H^1(\Omega^\varepsilon)} + 2\alpha \int_{\omega_i^\varepsilon} \nabla(u - \hat{u}) : \nabla\phi_i^{\text{on}}. \quad (3.32)$$

The last term in (3.32) can be estimated as

$$2\alpha \int_{\omega_i^\varepsilon} \nabla(u - \hat{u}) : \nabla\phi_i^{\text{on}} \leq 2\|u - \hat{u}\|_{H^1(\Omega^\varepsilon)} \frac{R_i(\phi_i^{\text{on}})}{\|\phi_i^{\text{on}}\|_{H^1(\omega_i^\varepsilon)}}$$

Using the definition of R_i, we have $R_i(\phi_i^{\text{on}}) = \int_{\omega_i^\varepsilon} \nabla(u - u^m_{\text{ms}}) : \nabla\phi_i^{\text{on}}$. So,

$$2\alpha \int_{\omega_i^\varepsilon} \nabla(u - \hat{u}) : \nabla\phi_i^{\text{on}} \leq 2\|u - \hat{u}\|_{H^1(\Omega^\varepsilon)} \|u - u^m_{\text{ms}}\|_{H^1(\Omega^\varepsilon)}.$$

Notice that $2\|u - \hat{u}\|_{H^1(\Omega^\varepsilon)} \|\hat{u} - u^m_{\text{ms}}\|_{H^1(\Omega^\varepsilon)} \leq \delta_1^{-1}\|u - \hat{u}\|^2_{H^1(\Omega^\varepsilon)} + \delta_1\|\hat{u} - u^m_{\text{ms}}\|^2_{H^1(\Omega^\varepsilon)}$ for

any $\delta_1 > 0$. Therefore, (3.32) becomes

$$\|\hat{u} - \widetilde{u}_{\text{ms}}\|^2_{H^1(\Omega^\varepsilon)} \leq \Big(1 + \delta_1 - \theta C_s^{-1} \frac{\lambda^{i,\text{off}}_{l_i+1}}{\lambda^{i,\text{off}}_{l_i+1} + 1}\Big) \|\hat{u} - u^m_{\text{ms}}\|^2_{H^1(\Omega^\varepsilon)} + (2 + \delta_1^{-1}) \|u - \hat{u}\|^2_{H^1(\Omega^\varepsilon)}. \tag{3.33}$$

Finally, combining (3.28) and (3.33), we have

$$\begin{aligned} &\|u - u^{m+1}_{\text{ms}}\|^2_{H^1(\Omega^\varepsilon)} \\ &\leq (1 + \delta_2)\Big(1 + \delta_1 - \theta C_s^{-1} \frac{\lambda^{i,\text{off}}_{l_i+1}}{\lambda^{i,\text{off}}_{l_i+1} + 1}\Big) \|\hat{u} - u^m_{\text{ms}}\|^2_{H^1(\Omega^\varepsilon)} + (3 + \delta_1^{-1} + \delta_2^{-1}) \|u - \hat{u}\|^2_{H^1(\Omega^\varepsilon)}. \end{aligned} \tag{3.34}$$

We obtain the desired result by noting that

$$\|\hat{u} - u^m_{\text{ms}}\|^2_{H^1(\Omega^\varepsilon)} \leq (1 + \delta_3) \|u - u^m_{\text{ms}}\|^2_{H^1(\Omega^\varepsilon)} + (1 + \delta_3^{-1}) \|u - \hat{u}\|^2_{H^1(\Omega^\varepsilon)}$$

for any $\delta_3 > 0$.

□

We remark that, in order to obtain rapid convergence, one needs to choose l_i large enough so that $\lambda^{i,\text{off}}_{l_i+1}$ is large. In this case, the quantity $\lambda^{i,\text{off}}_{l_i+1}/(\lambda^{i,\text{off}}_{l_i+1} + 1)$ is close to one. Then, (3.27) shows that the resulting online adaptive enrichment procedure has a rapid convergence.

Theorem 3.3.3 gives the convergence of our online adaptive enrichment procedure when one online basis is added at a time. One can also add online basis in non-overlapping coarse neighborhoods. Using the same proof as Theorem 3.3.3, we obtain the following result.

Theorem 3.3.4. *Let u be the reference solution defined in (3.17), $\hat{u}$ be the snapshot solution defined in (3.18) and u^m_{ms} be the multiscale solution of (2.13) in the enrichment level*

m. Assume that l_i offline basis functions for the coarse neighborhood ω_i^ε are used as initial basis in the online procedure. Let S be the index set for the non-overlapping coarse neighborhoods where online basis functions are added. Then, there is a constant D such that

$$\begin{aligned}
&\|u - u_{\text{ms}}^{m+1}\|^2_{H^1(\Omega^\varepsilon)} \\
&\leq (1+\delta_3)(1+\delta_2)\Big(1+\delta_1 - \theta C_s^{-1} \min_{j\in S} \frac{\lambda^{i,\text{off}}_{l_j+1}}{\lambda^{i,\text{off}}_{l_j+1}+1}\Big)\|\hat{u} - u_{\text{ms}}^m\|^2_{H^1(\Omega^\varepsilon)} + D\|u-\hat{u}\|^2_{H^1(\Omega^\varepsilon)}
\end{aligned} \tag{3.35}$$

where $\delta_1, \delta_2, \delta_3 > 0$ are arbitrary and D depends only on $\delta_i, i = 1, 2, 3$. In addition, θ is the relative residual defined by

$$\theta = \sum_{i\in S} ||R_i||^2_{(V_0^i)^*} \Big/ \sum_{i=1}^{N_u} \|R_i\|^2_{(V^i)^*}\,.$$

The above result suggests that adding more online basis functions at each iteration will speed up the convergence. Lastly, we remark that the convergence for the pressure can be obtained using the inf-sup condition (3.16).

4. A CONSERVATIVE LOCAL MULTISCALE MODEL REDUCTION METHOD FOR STOKES FLOWS *

In this chapter, we discuss a new multiscale model reduction technique for the Stokes flows in heterogeneous perforated domains. To obtain a reduced model, we apply the generalized multiscale finite element approach. Different from the approach in the previous chapter, here our basis functions are constructed locally with non-overlapping supports, which enhances the sparsity of the resulting linear system. The detailed constructions of the snapshot space and the offline space are presented in Section 4.2. In order to enforce the mass conservation, we propose a hybridized technique, and uses a Lagrange multiplier to achieve mass conservation. A mathematical analysis for the stability and the convergence of the proposed method is presented in Section 4.4. In addition, we show some numerical examples in Section 4.3 to illustrate the performance of the scheme.

4.1 Introduction to discontinuous Galerkin method

In this section, we consider the Stokes flow in perforated domain Ω^ϵ and introduce some notations in the discontinuous Galerkin framework. Given the source function f and two boundary functions g_D, g_N, we consider the same equation (2.6) as in chapter 2 subject to boundary condition $u = g_D$ on Γ_D, and $(\nabla u - pI)n = g_N$ on Γ_N, where $\Gamma_D \cup \Gamma_N = \partial\Omega^\epsilon$, n is the unit outward normal vector on $\partial\Omega^\epsilon$ and I is the $n \times n$ identity matrix. The unknown variable u denotes the fluid velocity and p denotes the fluid pressure. Since p is uniquely defined up to a constant, we assume that $\int_{\Omega^\epsilon} p = 0$, so that the problem (2.6) has a unique solution.

*Reprinted with permission from "A conservative local multiscale model reduction technique for Stokes flows in heterogeneous perforated domains" by Eric T Chung, Maria Vasilyeva and Yating Wang, 2017. Journal of Computational and Applied Mathematics, Volume 321, Pages 389-405, Copyright [2017] by Elsevier.

The weak formulation of the Stokes equation is (2.7) in chapter 2. It is well known that there is a unique weak solution to (2.7) (see for example [44]).

For the numerical approximation of the above problem, recall that we use the notations K and E to denote a coarse element and a coarse edge in the coarse grid $\mathcal{T}^H$. Moreover, we let $\mathcal{E}^H$ be the set of edges in $\mathcal{T}^H$. We write $\mathcal{E}^H = \mathcal{E}^H_{int} \cup \mathcal{E}^H_{out}$, where $\mathcal{E}^H_{int}$ is the set of interior edges and $\mathcal{E}^H_{out}$ is the set of boundary edges.

For each interior edge $E \in \mathcal{E}^H_{int}$, we define the jump $[u]$ and the average $\{u\}$ of a function u by

$$[u]_E = u|_{K^+} - u|_{K^-}, \quad \{u\}_E = \frac{u|_{K^+} + u|_{K^-}}{2},$$

where K^+ and K^- are the two coarse elements sharing the edge E, and the unit normal vector n on E is defined so that n points from K^+ to K^-. For $E \in \mathcal{E}^H_{out}$, we define

$$[u]_E = u|_E, \quad \{u\}_E = u|_E.$$

Next we introduce our DG scheme. Similar to the standard derivation of DG formulations [45, 46, 47, 48], the main idea is to consider the problem in each element K in the coarse mesh, and impose boundary conditions weakly on ∂K using the value of the velocity function in the neighboring elements. In addition, a penalizing term which penalize the jump of velocity will be introduced. After obtaining the local problems in each element, one can sum over all elements to get the global DG scheme. Remark that, in our approach, we will only assume discontinuity across the coarse edges, but use the standard continuous element inside coarse blocks. In this work, we also add an additional Lagrange multiplier in order to impose local mass conservation on the coarse elements. The details are given as follows.

We start with the definitions of the approximation spaces. We let Q_H be the piecewise

constant function space for the approximation of the pressure p. That is, the restriction of the functions of Q_H in each coarse element is a constant. In addition, we will define a piecewise constant space $\widehat{Q}_H$ for the approximation of the pressure $\widehat{p}$, which is defined on the set of coarse edges $\mathcal{E}^H$. That is, the functions in $\widehat{Q}_H$ are defined only in $\mathcal{E}^H$ and the restriction of the functions of $\widehat{Q}_H$ in each coarse edge is a constant. We remark that this additional pressure space is used to enforce local mass conservation in the coarse grid level. Moreover, we define V_H as the multiscale velocity space, which contains a set of basis functions supported in each coarse block K. To obtain these basis functions, we will solve some local problems in each coarse block with various Dirichlet boundary conditions to form a snapshot space and use a spectral problem to perform a dimension reduction. The details for the construction of this space will be presented in the next section.

For our GMsFEM using a DG approach, we define the bilinear forms

$$a_{\text{DG}}(u,v) = \int_{\Omega^\epsilon} \nabla u : \nabla v - \sum_{E\in\mathcal{E}^H} \Big(\int_E \{(\nabla u)\, n\}\cdot[v] + \{(\nabla v) n\}\cdot[u]\Big) + \frac{\gamma}{h} \sum_{E\in\mathcal{E}^H} \int_E [u]\cdot[v], \tag{4.1}$$

$$b_{\text{DG}}(v,q,\widehat{q}) = -\sum_{K\in\mathcal{T}^H} \int_K q\, \text{div} v + \sum_{E\in\mathcal{E}^H} \int_E \widehat{q}\,([v]\cdot n). \tag{4.2}$$

Then, we will find the multiscale solution $(u_H, p_H, \widehat{p}_H) \in V_H \times Q_H \times \widehat{Q}_H$ such that

$$\begin{aligned} a_{\text{DG}}(u_H,v) + b_{\text{DG}}(v,p_H,\widehat{p}_H) &= (f,v) + \int_{\Gamma_D} \Big(\frac{\gamma}{h} g_D\cdot v - ((\nabla v)\, n)\cdot g_D\Big) + \int_{\Gamma_N} g_N\cdot v, \\ b_{\text{DG}}(u_H,q,\widehat{q}) &= \int_{\Gamma_D} (g_D\cdot n)\,\widehat{q}, \end{aligned} \tag{4.3}$$

for all $v \in V_H$, $q \in Q_H$, $\widehat{q} \in \widehat{Q}_H$. The derivation of the above scheme follows the standard DG derivation procedures [45, 46, 47, 48]. We notice that the role of the variable $\widehat{p}_H$ is to enforce mass conservation on coarse elements. In particular, taking $q = 0$ in (4.3), we

have

$$\int_E \widehat{q}\,[u_H]\cdot n = 0, \quad \forall E \in \mathcal{E}_{int}^H, \quad \forall\, \widehat{q} \in \widehat{Q}_H.$$

This relation implies that

$$\int_K q\,\mathrm{div} u_H = 0, \quad \forall K \in \mathcal{T}^H, \quad \forall q \in Q_H.$$

The above is the key to the mass conservation, and we will discuss more in the numerical results section.

We will show the accuracy of our method by comparing the multiscale solution to a reference solution, which is computed on the fine mesh. To find the reference solution $(u_h, p_h, \widehat{p}_h)$, we will solve the following system

$$\begin{aligned} a_{\mathrm{DG}}(u_h, v) + b_{\mathrm{DG}}(v, p_h, \widehat{p}_h) &= (f, v) + \int_{\Gamma_D} \Big(\frac{\gamma}{h} g_D \cdot v - ((\nabla v)\, n)\cdot g_D\Big) + \int_{\Gamma_N} g_N \cdot v, \\ b_{\mathrm{DG}}(u_h, q, \widehat{q}) &= \int_{\Gamma_D} (g_D \cdot n)\, \widehat{q}, \end{aligned} \tag{4.4}$$

for all $v \in V_h^{\mathrm{DG}}, q \in Q_H, \widehat{q} \in \widehat{Q}_H$. We note that the reference velocity u_h belongs to the fine scale velocity space $V_h^{\mathrm{DG}} = \{v \in L^2(\Omega^\epsilon) | \quad v|_K \in C^0(K)^2$ for every $K \in \mathcal{T}^H,\ v|_K \in (\mathbb{P}_1(T))^2$ for every $K \in \mathcal{T}^h\}$. The space V_h^{DG} contains functions which are piecewise linear in each fine-grid element K and are continuous along the fine-grid edges, but are discontinuous across coarse grid edges. Moreover, the reference pressure p_h and $\widehat{p}_h$ belongs to the coarse scale pressure space Q_H and $\widehat{Q}_H$ respectively. Notice that the pressure p_h is determined up to a constant, we will achieve the uniqueness by requiring the averaging value of pressure over whole domain is zero. We remark that this reference solution $(u_h, p_h, \widehat{p}_h)$ is obtained using the coarse scale pressure spaces Q_H and $\widehat{Q}_H$ since we only consider multiscale solutions and reduced spaces for the velocity. The true fine

scale solution $(u_{\text{fine}}, p_{\text{fine}}, \widehat{p}_{\text{fine}})$ can be defined by

$$a_{\text{DG}}(u_{\text{fine}}, v) + b_{\text{DG}}(v, p_{\text{fine}}, \widehat{p}_{\text{fine}}) = (f, v) + \int_{\Gamma_D} \Big(\frac{\gamma}{h} g_D \cdot v - ((\nabla v)\, n) \cdot g_D \Big) + \int_{\Gamma_N} g_N \cdot v,$$
$$b_{\text{DG}}(u_{\text{fine}}, q, \widehat{q}) = \int_{\Gamma_D} (g_D \cdot n)\, \widehat{q},$$

for all $v \in V_h^{\text{DG}}, q \in Q_h, \widehat{q} \in \widehat{Q}_h$, where Q_h and $\widehat{Q}_h$ are suitable fine scale spaces. One can see that $(u_{\text{fine}}, p_{\text{fine}})$ will converge to the exact solution (u, p) in the energy norm as the fine mesh size $h \to 0$.

Now we define the energy norm as

$$\|u\|_A^2 = \int_\Omega |\nabla u|^2 + \frac{1}{h} \sum_{E \in \mathcal{E}^H} \int_E |[u]|^2. \tag{4.5}$$

Moreover, we also define the following L^2 norm

$$\|(q, \widehat{q})\|_Q^2 = \|q\|_{L^2(\Omega^\epsilon)}^2 + \sum_{E \in \mathcal{E}^H} h \|\widehat{q}\|_{L^2(E)}^2. \tag{4.6}$$

The notation $\alpha \lesssim \beta$ means that $\alpha \leq C\beta$ for a constant C independent of the mesh size.

One can show that

$$\|u_{\text{fine}} - u_h\|_A^2 \leq C \inf_{q \in Q_H, \widehat{q} \in \widehat{Q}_H} \|(p_{\text{fine}} - q, \widehat{p}_{\text{fine}} - \widehat{q})\|_Q^2.$$

Thus, the reference solution defined in (4.4) can be considered as the exact solution up to a coarse scale approximation error.

4.2 Construction of multiscale velocity space

In this section, we will present the construction of the multiscale space V_H for the coarse scale approximation of velocity. To construct the coarse scale velocity space, we

will follow the general idea of GMsFEM [49, 50], which contains two stages: (1) the construction of snapshot space, and (2) the construction of offline space. In the first stage, we will obtain the snapshot space, which contains a rich set of functions containing possible features in the solution. These snapshot functions are solutions of some local problems subject to all possible boundary conditions up to the fine grid resolution. Notice that for the generalized multiscale DG scheme proposed in [35, 51], one solves the local problems in each coarse block. Thus the resulting system is much smaller compared with that of the CG approach [30, 36, 25], where the local problems are solved in each overlapping coarse neighborhood. Next, in order to reduce the dimension of the solution space, we will use a space reduction technique to choose the dominated modes in the snapshot space. This procedure is achieved by defining proper local spectral problems. The resulting reduced order space is called the offline space and will be used for coarse scale velocity approximation. Note that for approximating pressure on the coarse grid, we will use piecewise constant functions as defined before. In Section 4.2.1, we will present the construction of the snapshot space, and in Section 4.2.2, we will present the construction of the offline space.

4.2.1 Snapshot space

We will construct local snapshot basis in each coarse block $K_i, (i = 1, \cdots, N)$, where N is the number of coarse blocks in Ω^ϵ. The local snapshot space consists of functions which are solutions $u \in V_h(K_i)$ of

$$\begin{aligned} -\Delta u + \nabla p &= 0, \qquad \text{in } K_i \\ \text{div} u &= c, \qquad \text{in } K_i \end{aligned} \tag{4.7}$$

with $u = \delta_i^k$ on ∂K_i, $(k = 1, \cdots, M_i)$, where M_i is the number of fine grid nodes on the boundary of K_i, and δ_i^k is the discrete delta function defined on ∂K_i. The above

problem (4.7) is solved on the fine mesh using some appropriate approximation spaces. For instances, we take the space $V_h(K_i)$ to be the standard conforming piecewise linear finite element space with respect to the fine grid on K_i. Note that the constant c in (4.7) is chosen by the compatibility condition, that is, $c = \frac{1}{|K_i|}\int_{\partial K_i} \delta_i^k \cdot nds$.

Take these M_i velocity solutions of (4.7) and denote them by $\psi_k^{i,\text{snap}}(k = 1, \cdots, M_i)$, we get the local snapshot space

$$V_{\text{snap}}^i = \text{span}\{\psi_1^{i,\text{snap}}, \cdots, \psi_{M_i}^{i,\text{snap}}\}.$$

Combining all the local snapshots, we can form the global snapshot space, that is

$$V_{\text{snap}} = \text{span}\{\psi_k^{i,\text{snap}}, \quad , 1 \leq k \leq M_i, 1 \leq i \leq N\}.$$

In the above construction, the local problems are solved for every fine grid node on ∂K_i. One can also apply the oversampling strategy [52, 50] in order to reduce the boundary effects. Applying this strategy, one can solve the local problem for each fine node on the boundary of the oversampled domain. An illustration of the original local domain K and the oversampled local domain K^+ are shown in Figure 4.1. Notice that in Figure 4.1, we present the triangular coarse grid in perforated domain with small inclusions on the left, and rectangular coarse grid perforated domain with multiple sizes of inclusions on the right. We will solve the local problem in an enlarged domain K_i^+ of K_i,

$$\begin{aligned} -\Delta u + \nabla p &= 0, \qquad \text{in } K_i^+ \\ \text{div} u &= c, \qquad \text{in } K_i^+ \end{aligned}$$

with $u = \delta_i^k$ on ∂K_i^+, where $k = 1, \cdots, M_i^+$, where M_i^+ is the number of fine nodes on the boundary of K_i^+. After removing linear dependence among these basis by POD, we

denote the linearly independent functions by $\psi_k^{+,i},\ (i = 1, \cdots, \tilde{M}_i)$. Note that the velocity solutions of these local problems are supported in the larger domain K_i^+. There are usually several following choices for identification of basis. One of the straight forward way is that, we can restrict the basis $\psi_k^{+,i}$ on K_i to form the snapshot basis, i.e. $\psi_k^{i,\text{snap}} = \psi_k^{+,i}|_{K_i}$. Then the span of these basis function $\psi_k^{i,\text{snap}}$ will form our new snapshot space. In this case, the local reduction will be performed in K_i. Another choice is that, one can keep the snapshot basis $\psi_k^{+,i}$ without restricting on K_i. But in this case, one needs to solve the offline basis also in the oversampled domain K_i^+ and finally restrict the offline basis on the original local domain K_i. It is known that these oversampling methods can improve the accuracy of our multiscale methods ([50]).

We remark that one can also use the idea of randomized snapshots (as in [31]) and reduce the computational cost substantially. In randomized snapshots approach, instead of solving the local problem for each fine node on the boundary of oversampled local domain, one only computes a few snapshots in each oversampled domain K_i^+ with several random boundary conditions. These random boundary functions are constructed by independent identically distributed (i.i.d.) standard Gaussian random vectors defined on the fine degrees of freedoms on the boundary. The randomized snapshot requires much fewer calculations to achieve a good accuracy compared with the standard snapshot space.

4.2.2 Offline space

In this section, we will perform local model reduction on the snapshot space by solving some local spectral problems. The reduced space consists of the important modes in the snapshot space, and is called the offline space. The coarse scale approximation of velocity solution will be obtained in this space. We have multiple choices of local spectral problems given the various constructions of snapshot space presented in the previous section.

First of all, if the snapshot basis obtained in the previous section is supported in each

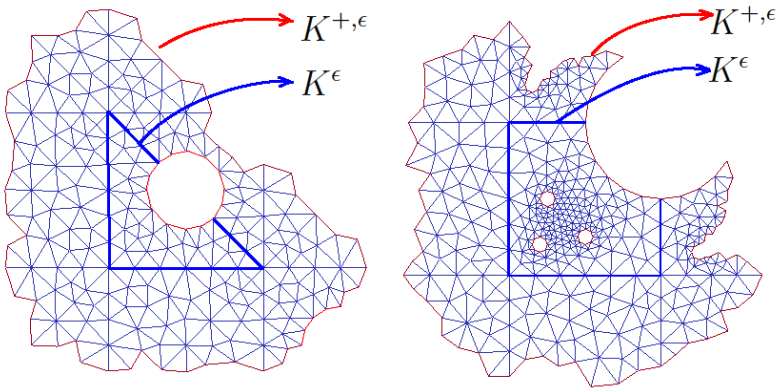

Figure 4.1: Illustration of oversampling domains. Left: Oversampling of a triangular coarse block for perforated domain with small inclusions. Right: Oversampling of a rectangular coarse block for perforated domain with multiple sizes of inclusions.

coarse element K_i, we will solve for (λ, Φ) from the generalized eigenvalue problem in the snapshot space

$$A\Phi = \lambda S\Phi \tag{4.8}$$

where A is the matrix representation of the bilinear form $a_i(u, v)$ and S is the matrix representation of the bilinear form $s_i(u, v)$. The choices for a_i and s_i are based on the analysis. In particular, we take

$$a_i(u, v) = \int_{K_i} \nabla u : \nabla v,$$
$$s_i(u, v) = \frac{\lambda}{H} \int_{\partial K_i} u \cdot v,$$

where we remark that the integral in $s_i(u, v)$ is defined on the boundary of the coarse block. In this case, the number of the spectral problem equals the number of coarse blocks.

We arrange the eigenvalues of (4.8) in increasing order. We will choose the first few eigenvectors corresponding to the first few small eigenvalues. Using these eigenvectors

as the coefficients, we can form our offline basis. More precisely, assume we arrange the eigenvalues in increasing order

$$\lambda_1^{(i)} \leq \lambda_2^{(i)} \leq \cdots \leq \lambda_{M_i}^{(i)}.$$

The corresponding eigenvectors are denoted by $\Phi_k^{(i)} = (\Phi_{kj}^{(i)})_{j=1}^{M_i}$, where $\Phi_{kj}^{(i)}$ is the j-th component of the eigenvector. We will take the first $L_i \leq M_i$ eigenvectors to form the offline space, that is, the offline basis functions can be constructed as

$$\phi_k^{i,\text{off}} = \sum_{j=1}^{M_i} \Phi_{kj}^{(i)} \psi_k^{i,\text{snap}}, \quad k = 1, \cdots, L_i.$$

On the other hand, one can use the snapshot basis $\psi_k^{+,i}$ (using oversampling strategy) without restricting on K_i in the space reduction process. To be more specific, since the snapshot basis are supported in the oversampled domain K_i^+, we will need another set of spectral problems, namely

$$A^+ \Phi^+ = \lambda S^+ \Phi^+ \tag{4.9}$$

where A^+ and S^+ are the matrix representations of the bilinear forms $a_{+,i}(u, v)$ and $s_{+,i}(u, v)$ respectively. Similar as before, we can choose $a_{+,i}, s_{+,i}$ as follows

$$a_{+,i}(u, v) = \int_{K_i^+} \nabla u : \nabla v,$$
$$s_{+,i}(u, v) = \frac{\lambda}{H} \int_{\partial K_i^+} u \cdot v.$$

We then arrange the eigenvalues in increasing order

$$\lambda_1^{(i)} < \lambda_2^{(i)} < \cdots < \lambda_{M_i^+}^{(i)}.$$

The corresponding eigenvectors are denoted by $\Phi_k^{+,(i)}$. We will take the first $L_i \leq M_i^+$ eigenvectors to form a basis supported in K_i^+

$$\phi_k^{+,i} = \sum_{j=1}^{M_i^+} \Phi_{kj}^{+,(i)} \psi_k^{+,i}, \quad k = 1, \cdots, L_i.$$

Then we will obtain our offline basis by restricting $\phi_k^{+,i}$ on K_i, namely

$$\phi_k^{i,\text{off}} = \phi_k^{+,i}|_{K_i}.$$

Now we can finally form the local offline space, which is the span of these basis functions

$$V_{\text{off}}^i = \text{span}\{\phi_1^{i,\text{off}}, \cdots, \phi_{L_i}^{i,\text{off}}\}.$$

The global offline space V_{off} is the combination of the local ones, i.e.

$$V_{\text{off}} = \text{span}\{\phi_k^{i,\text{off}}, \quad , 1 \leq k \leq L_i, 1 \leq i \leq N\}.$$

This space will be used as the coarse scale approximation space for velocity $V_H := V_{\text{off}}$.

4.3 Numerical results

In this section we will present numerical results of our method for various types of perforations, boundary conditions and sources. We will illustrate the performance of our method using two kinds of perforated domains: (1) perforated domain with small inclusions and (2) perforated domain with big inclusions as well as some extremely small inclusions, see Figure 4.2. We will also illustrate the performance of the oversampling strategy.

We set $\Omega = [0, 1] \times [0, 1]$. The computational domain is discretized coarsely using uniform triangulation for domain with small inclusions (Figure 4.2 (a)), and uniform rect-

angle coarse partition for domain with big inclusions (Figure 4.2 (b)). The coarse mesh size $H = \frac{1}{10}$. For the fine scale discretization, the size of the system is 69146 for domain with small inclusions (Figure 4.2 (a)) and 91588 for domain with multiple size of inclusions (Figure 4.2 (b)).

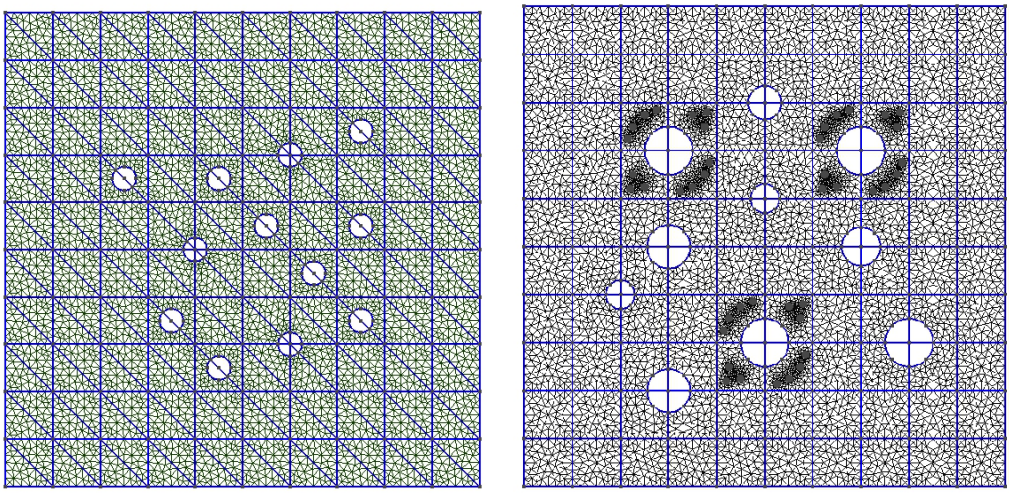

(a) (b)

Figure 4.2: llustration of the perforated domain with fine and coarse mesh. (a) perforated domain with small inclusions. (b) perforated domain with multiple sizes of inclusions.

We will consider two different boundary conditions and force terms:

- *Example 1*: Source term $f = (0, 0)$, boundary condition $u = (1, 0)$ on $\partial\Omega$ and $u = (0, 0)$ on $\partial\mathcal{B}^\epsilon$.

- *Example 2*: Source term $f = (1, 1)$, boundary condition $\frac{\partial u}{\partial n} - pn = (0, 0)$ on $\partial\Omega$ and $u = (0, 0)$ on $\partial\mathcal{B}^\epsilon$.

The errors will be measured in relative L^2, H^1 and DG norms for velocity, and L^2

norm for pressure

$$
\begin{aligned}
||e_u||_{L^2} &= \frac{\|u_h - u_H\|_{L^2(\Omega^\epsilon)}}{\|u_h\|_{L^2(\Omega^\epsilon)}}, \\
||e_u||_{H^1} &= \frac{\|u_h - u_H\|_{H^1(\Omega^\epsilon)}}{\|u_h\|_{H^1(\Omega^\epsilon)}}, \quad ||e_u||_{DG} = \frac{\sqrt{a_{\text{DG}}(u_h - u_H, u_h - u_H)}}{\sqrt{a_{\text{DG}}(u_h, u_h)}}, \\
||e_p||_{L^2} &= \frac{\|\bar{p}_{\text{fine}} - p_H\|_{L^2(\Omega^\epsilon)}}{\|\bar{p}_{\text{fine}}\|_{L^2(\Omega^\epsilon)}}.
\end{aligned}
$$

where $\bar{p}_{\text{fine}}$ is the cell average of the fine scale pressure, that is, $\bar{p}_{\text{fine}} = \frac{1}{|K_i|}\int_{K_i} p_{\text{fine}}$ for all $K_i \in \mathcal{T}^H$.

4.3.1 Perforated domain with small inclusions

In this section, we show the numerical results for the Stokes problem in perforated domain with small inclusions (Figure 4.2 (a)), see Table 4.1 for Example 1 and Table 4.2 for Example 2. Remark that the fine scale system has size 69146, while our coarse scale systems only have size $1280 - 6880$ when we take 4 to 32 basis, which are much smaller. We will first take a look at the numerical behavior for the first example, where we take Dirichlet boundary conditions $u = (1, 0)$ on the global boundary, and $u = (0, 0)$ on the boundary of inclusions. The force term $f = (0, 0)$. In Table 4.1, we observe that the errors reduce substantially when we add more than 4 basis in each coarse block. For example, when we construct basis without oversampling, the L^2 velocity error reduce from 33.2% to 6.5% when the number of basis increase from 4 to 8. Moreover, the energy error for velocity is 28% and the L^2 error for pressure is 12% as we take 32 offline basis for non-oversampling case. To get a faster convergence, we employ oversampling strategy when calculating the basis, that is, we solve the local problems in an oversampled coarse domain and then restrict the local velocity solution to the original coarse block to form our snapshot basis. In our numerical example, the oversampled domain is the original

coarse block plus four fine cells layers neighboring the original domain. We can see that, the oversampling case gives us better accuracy with respect to velocity energy error and pressure error. For instance, the velocity energy error reduces from 25% to 18% and the pressure error decreased from 12% to 2% when the number of offline basis is 32 comparing the non-oversampling with oversampling case.

For the second example in perforated domain with small inclusions, we take Neumann boundary condition $\frac{\partial u}{\partial n} - pn = (0,0)$ on the global boundary and Dirichlet condition $u = (0,0)$ on the boundary of inclusions. The convergence history is shown in Table 4.2. From this table, we find that the velocity L^2 error reduce from 39.9% to 7.6%, and the pressure error reduce from 69.8% to 5.0% when the basis number increase from 4 to 8 for the non-oversampling case. Moreover, the velocity L^2 error reduces to 4.9% when we take 32 basis. We also observe that the oversampling strategy works efficiently to speed up the convergence rate for both the L^2 error and the energy error for velocity. For example, the velocity L^2 error is 7.6% when we take 8 basis in non-oversampling case, however, it is only 2.6% when we take the same number of basis in oversampling case. The velocity H^1 error reduce from 30.5%(for non-oversampling case) to 17.4%(for oversampling case) when we take 32 basis. In addition, we check the local mass conservation and present the numerically computed constants $\int_{\partial K_i} u \cdot n \, ds$ in Table 4.3. From the table, we see that the maximum of the values $\int_{\partial K_i} u \cdot n \, ds$ is almost zero for all cases. This shows that we have exact mass conservation in the coarse grid level. We remark that we also have fine grid mass conservation by the construction of the basis functions.

Figure 4.3 and Figure 4.4 shows the corresponding solution plots for Example 1 and Example 2 in perforated domain with small inclusions, where we compare the fine scale velocity solution with different coarse scale velocity solution. In Figure 4.3, we take 8 and 16 basis functions per coarse element for coarse scale computations. We observe that some fine scale features are lost in the solution when we take 8 basis, and the frame of the

coarse edges can be seen in the figure. However, when we take 16 basis, we can observe a much smoother solution which capture the fine features well. Similar behavior can be found in Figure 4.4, where we observe higher contrast between 4 basis per element and 16 basis per element coarse scale solutions.

M_{off}	DOF	$\|\|e_u\|\|_{L^2}$	$\|\|e_u\|\|_{DG}$	$\|\|e_u\|\|_{H^1}$	$\|\|e_p\|\|_{L^2}$
Non-oversampling					
4	1280	33.2	96.8	76.8	–
8	2080	6.5	48.8	43.7	38.1
16	3680	2.6	31.9	28.9	12
32	6880	1.9	28.3	25.3	12
Oversampling, $K^+ = K + 4$					
4	1280	32.6	85.7	69.9	–
8	2080	6.6	39.6	36.7	23.4
16	3680	1.9	21.7	19.4	2.7
32	6880	1.8	20.3	18.5	2.7

Table 4.1: Stokes problem in perforated domain with small inclusions. Numerical results for *Example 1*. Non-oversampling and oversampling with 4 fine layers.

M_{off}	DOF	$\|\|e_u\|\|_{L^2}$	$\|\|e_u\|\|_{DG}$	$\|\|e_u\|\|_{H^1}$	$\|\|e_p\|\|_{L^2}$
Non-oversampling					
4	1280	39.9	87.6	71.2	69.8
8	2080	7.6	49.4	39.5	5.0
16	3680	6.7	36.7	31.8	2.6
32	6880	4.9	35.9	30.5	2.9
Oversampling, $K^+ = K + 4$					
4	1280	31.7	69.6	52.6	–
8	2080	2.6	36.7	27.8	16.8
16	3680	1.8	25.5	20.7	3.6
32	6880	1.5	20.3	17.4	3.5

Table 4.2: Stokes problem in perforated domain with small inclusions. Numerical results for *Example 2*. Non-oversampling and oversampling with 4 fine layers.

Example 1			
M_{off}	DOF	Non-oversampling	Oversampling
4	1280	2.9e-20	-4.4e-22
8	2080	6.6e-18	-4.2e-18
16	3680	5.7e-19	-9.5e-18
32	6880	-4.0e-18	1.2e-15
32	6880	-4.0e-18	1.2e-15
Example 2			
M_{off}	DOF	Non-oversampling	Oversampling
4	1280	-8.4e-22	4.1e-22
8	2080	-1.3e-19	-1.9e-20
16	3680	1.9e-19	-5.8e-22
32	6880	9.7e-20	-5.1e-18

Table 4.3: Stokes problem in perforated domain with small inclusions. Verification of local mass conservation by computing the maximum of $\int_{\partial K_i} u \cdot n \, ds$ over all coarse blocks. Top: Example 1. Bottom: Example 2.

4.3.2 Perforated domain with some extremely small inclusions

In this section, we show the numerical results for the Stokes problem in perforated domain with various size of inclusions (Figure 4.2 (b)), see Table 4.4 for Example 1 and Table 4.5 for Example 2. The fine degrees of freedoms for this domain is 91588, and the coarse degrees of freedoms range only from 680 for 4 basis per element to 3480 for 32 basis per coarse element. Note that, in this domain we use the coarse mesh where each block is a rectangle, thus the coarse degrees of freedom is less than that in the previous section where we used triangular blocks for coarse mesh. From the tables, we can see that for Example 1, the velocity L^2 errors can be less than 10% when we take more than 8 basis. Moreover, for Example 2, the velocity L^2 errors are already 6.1% (or 3.5%) for non-oversampling case (or oversampling case) when we take exactly 8 basis. The convergence results in Table 4.4 indicate that oversampling helps to reduce the energy errors for velocity. For example, we take 32 basis, the velocity H^1 error become 12.9% in

the oversampling case, which is much smaller than 20.1% in the non-oversampling case. The oversampling strategy works even better to improve the velocity results for Example 2. Table 4.5 shows that the velocity L^2, H^1 and DG errors are almost reduced by half when we take 8, 16 or 32 basis applying the oversampling strategy. The local mass conservation is also verified by the data presented in Table 4.6. Figure 4.5 and Figure 4.6 demonstrate the velocity solution plots for Example 1 and Example 2 respectively. In Figure 4.5, we compare the fine scale velocity solution with 8 basis coarse scale solution and 16 basis coarse scale solution. It is clear to see that when we take 8 basis, the higher value regions in the solution shrinks, and some properties of the solution between two inclusions are not captured well. These drawbacks are recovered better when we take 16 basis, and the solution is more comparable with fine scale solution. The solution is reported in Figure 4.6 for Example 2, where we compare 4 basis and 16 basis coarse scale solution with fine scale solution. The behavior is similar as before.

In addition, in Figure 4.7, we present the comparison the solutions for Example 2 in perforated domain with small inclusions (Figure 4.2 (a)) in oversampling and non-oversampling case respectively. The x-component of velocity is shown on the top, and the y-component is on the bottom, the results for non-oversampling are on the left (L^2 error 6.7%, H^1 error 31.8%), and results using oversampling is on the right (L^2 error 1.8%, H^1 error 20.7%). Here, we take 16 basis as an example. It can be observed that when we use the oversampling strategy, the transitions from lower values to the higher values in the solution are smoother compared with the one without oversampling. This helps us to understand the advantage of oversampling visually.

M_{off}	DOF	$\|\|e_u\|\|_{L^2}$	$\|\|e_u\|\|_{DG}$	$\|\|e_u\|\|_{H^1}$	$\|\|e_p\|\|_{L^2}$
Non-oversampling					
4	680	46.6	93.4	79.7	–
8	1080	11.5	55.0	52.1	39.6
16	1880	2.9	27.9	25.9	9.1
32	3480	1.9	22.3	20.1	5.6
Oversampling, $K^+ = K + 4$					
4	680	50.8	83.3	76.3	–
8	1080	10.8	48.1	45.3	31.6
16	1880	4.5	23.4	21.6	2.5
32	3480	1.6	14.5	12.9	2.1

Table 4.4: Stokes problem in perforated domain with additional small inclusions. Numerical results for *Example 1*. Non-oversampling and oversampling with 4 fine layers.

M_{off}	DOF	$\|\|e_u\|\|_{L^2}$	$\|\|e_u\|\|_{DG}$	$\|\|e_u\|\|_{H^1}$	$\|\|e_p\|\|_{L^2}$
Non-oversampling					
4	680	63.1	96.6	82.1	33.6
8	1080	6.1	47.7	36.5	3.7
16	1880	3.8	28.4	24.2	1.5
32	3480	2.9	26.6	22.3	1.4
Oversampling, $K^+ = K + 4$					
4	680	41.6	65.6	54.3	–
8	1080	3.5	29.3	23.1	11.8
16	1880	1.7	15.5	13.0	4.3
32	3480	1.3	12.9	11.0	2.8

Table 4.5: Stokes problem in perforated domain with additional small inclusions. Numerical results for *Example 2*. Non-oversampling and oversampling with 4 fine layers.

4.4 Convergence results

In this section, we will present the analysis of our multiscale method (4.3). First, we will prove the existence and uniqueness of the problem (4.3) by showing the coercivity and continuity of a_{DG}, the continuity of b_{DG} and the discrete inf-sup condition for b_{DG}. Next, we will derive a convergence result for our method. For our analysis, we use the definition

Example 1			
M_{off}	DOF	Non-oversampling	Oversampling
4	680	2.3e-20	2.6e-20
8	1080	1.8e-20	-5.5e-20
16	1880	-8.2e-18	5.5e-18
32	2480	3.9e-20	3.5e-17
Example 2			
M_{off}	DOF	Non-oversampling	Oversampling
4	680	1.8e-23	1.0e-22
8	1080	-5.1e-22	-1.8e-22
16	1880	4.7e-19	1.2e-19
32	2480	1.4e-20	-5.2e-21

Table 4.6: Stokes problem in perforated domain with small inclusions. Verification of local mass conservation on coarse edges by computing the maximum value of $\int_{\partial K_i} u \cdot n \, ds$ over all coarse blocks. Top: Example 1. Bottom: Example 2.

for the energy norm as in (4.5) and Q-norm in (4.6). We notice that the Q-norm in (4.6) is a weaker norm compared with the more usual choice $\|q\|^2_{L^2(\Omega^\epsilon)} + \sum_{E\in\mathcal{E}^H} H\|\widehat{q}\|^2_{L^2(E)}$.

First, we consider the continuity and coercivity of the bilinear form a_{DG}, as well as the continuity of the bilinear form b_{DG}. These properties are summarized in the following lemma.

Lemma 4.4.1. *Assume that $\gamma = O(1)$ is large enough. The bilinear form a_{DG} is continuous and coercive, that is*

$$|a_{DG}(u,v)| \leq a_1\|u\|_A\|v\|_A \tag{4.10}$$

$$a_{DG}(u,u) \geq a_0\|u\|^2_A \tag{4.11}$$

and the bilinear form b_{DG} is also continuous:

$$|b_{DG}(v,q,\widehat{q})| \leq b_1\|v\|_A\|(q,\widehat{q})\|_Q. \tag{4.12}$$

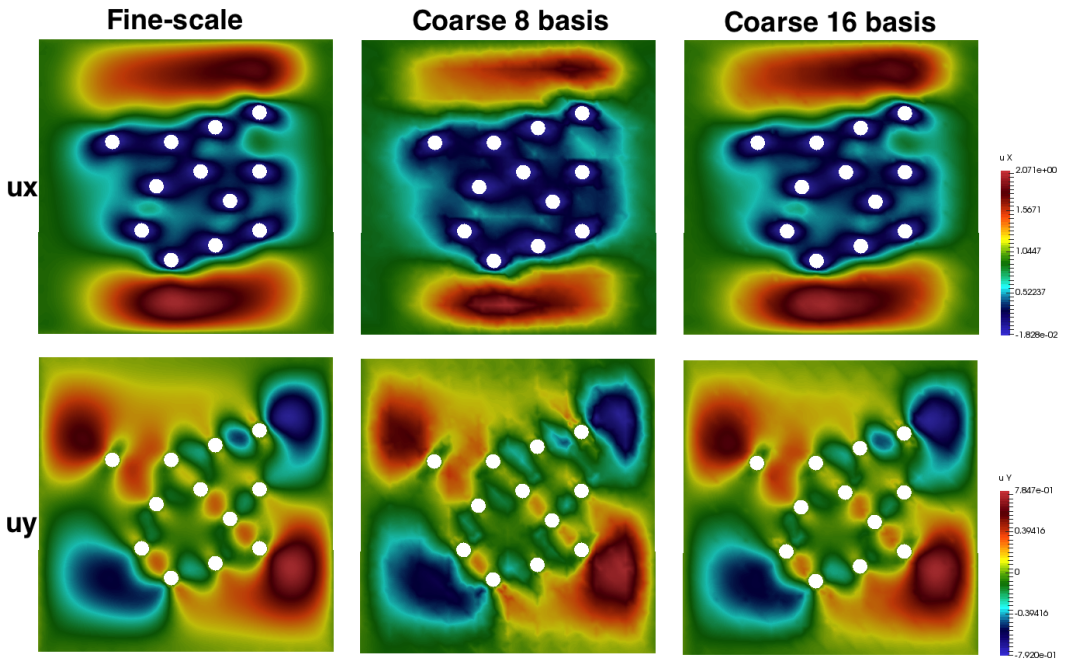

Figure 4.3: Stokes problem for perforated domain with small inclusions. Numerical solution for Example 1. Top: x-component of velocity. Bottom: y-component of velocity. Left: Fine-scale solution. Middle: Coarse-scale solution with 8 basis, non-oversampling. Right: Coarse-scale solution with 16 basis, non-oversampling.

Proof. The proof for continuity and coercivity of a_{DG} is classical [47, 35], and will be omitted here. For the continuity of b_{DG}, it follows from the Cauchy-Schwarz inequality. □

4.4.1 Inf-sup condition

In this section, we will prove an inf-sup condition for the bilinear form $b_{\mathrm{DG}}(v, q, \widehat{q})$. We will assume the continuous inf-sup condition holds for $b(v, q)$. That is, for any $q \in L_0^2(\Omega^\epsilon)$, we have

$$\sup_{u \in H_0^1(\Omega^\epsilon)} \frac{b(u, q)}{\|u\|_{H^1(\Omega^\epsilon)}} \geq \beta \|q\|_{L^2(\Omega^\epsilon)}. \tag{4.13}$$

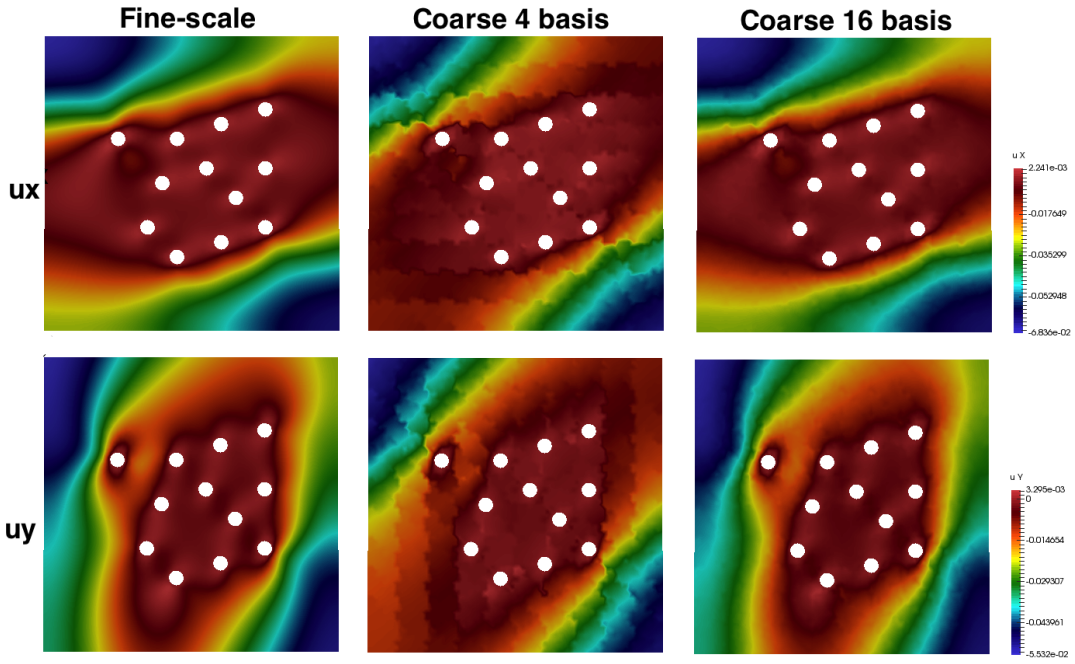

Figure 4.4: Stokes problem for perforated domain with small inclusions. Numerical solution for Example 2. Top: x-component of velocity. Bottom: y-component of velocity. Left: Fine-scale solution. Middle: Coarse-scale solution with 4 basis, non-oversampling. Right: Coarse-scale solution with 16 basis, non-oversampling.

This can be shown by a simple calculation. For any $q \in L_0^2(\Omega^\epsilon)$, one can choose u such that $(u, p) \in (H^1(\Omega^\epsilon))^2 \times L_0^2(\Omega^\epsilon)$ is the solution of

$$-\Delta u + \nabla p = 0, \quad \text{div} u = q, \quad \text{in } \Omega^\epsilon$$

with $u = 0$ on $\partial\Omega^\epsilon$.

We will also assume the following independence condition for the multiscale basis. For every coarse block $K_i \in \mathcal{T}^H$, there are at least 4 basis functions, denoted by $\phi_j^{i,\text{off}}$,

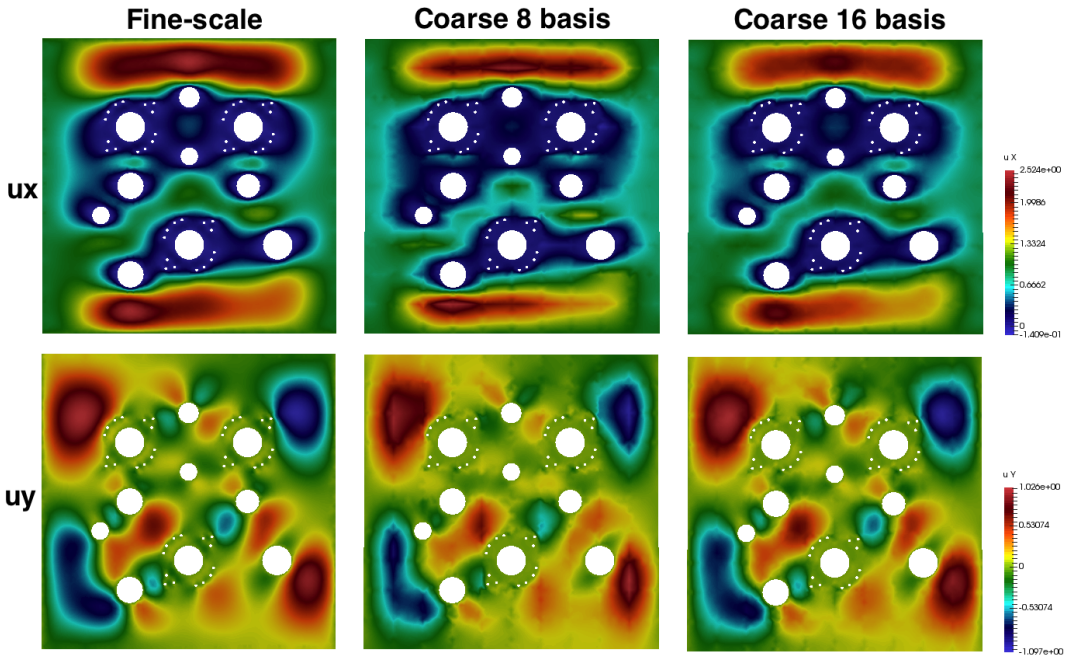

Figure 4.5: Stokes problem for perforated domain with multiple sizes of inclusions. Numerical solution for Example 1. Top: x-component of velocity. Bottom: y-component of velocity. Left: Fine-scale solution. Middle: Coarse-scale solution with 8 basis, non-oversampling. Right: Coarse-scale solution with 16 basis, non-oversampling.

$j = 1, 2, 3, 4$, in the local offline space V^i_{off} such that there are coefficients d_{jk} such that

$$\int_{E_l} \Big(\sum_{j=1}^{4} d_{jk} \phi_j^{i,\text{off}} \Big) \cdot n = \delta_{kl}, \quad k, l = 1, 2, 3, 4, \tag{4.14}$$

for all coarse edges E_l on the boundary of K_i. We remark that the above independence condition says that we can construct a function in V^i_{off} with normal component having mean value one on one coarse edge and mean value zero on the other coarse edges. In particular, for each coarse element K_i, and for every edge $E_j \in \partial K_i$, there is a basis function Ψ_j such that $\int_{E_j} \Psi_j \cdot n = 1$ and $\int_{E_k} \Psi_j \cdot n = 0$ for other coarse edges $E_k \in \partial K_i$.

The next lemma is the main result of this section.

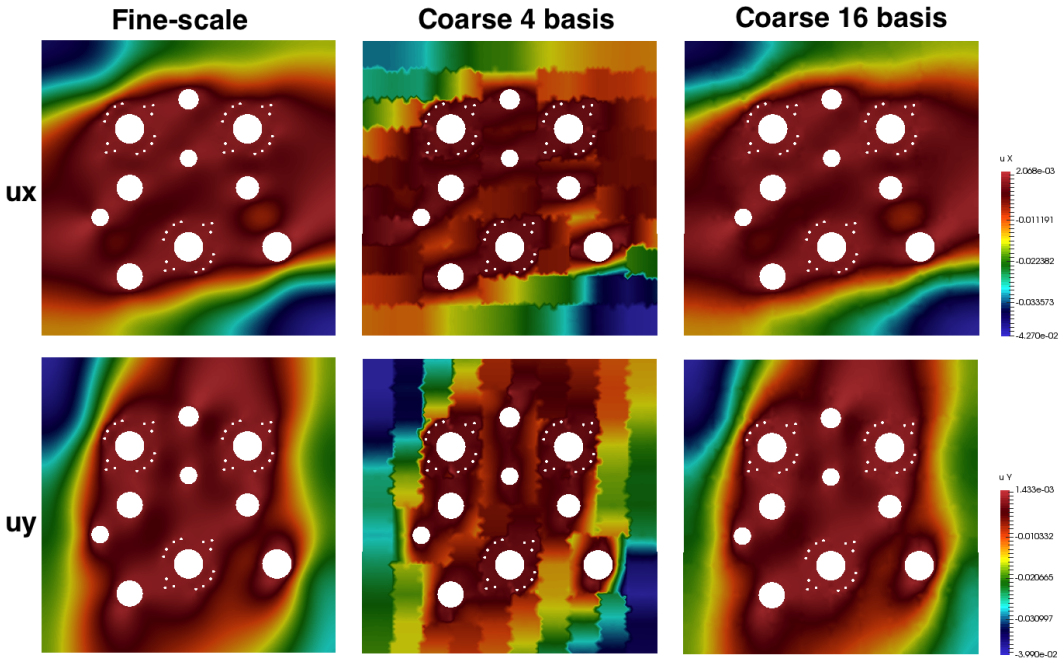

Figure 4.6: Stokes problem for perforated domain with multiple sizes of inclusions. Numerical solution for Example 2. Top: x-component of velocity. Bottom: y-component of velocity. Left: Fine-scale solution. Middle: Coarse-scale solution with 4 basis, non-oversampling. Right: Coarse-scale solution with 16 basis, non-oversampling.

Lemma 4.4.2. *For all $q \in Q_H$ and $\widehat{q} \in \widehat{Q}_H$, we have*

$$\|(q, \widehat{q})\|_Q \leq C_{\text{infsup}} \sup_{v \in V_H} \frac{b_{DG}(v, q, \widehat{q})}{\|v\|_A} \tag{4.15}$$

where $C_{\text{infsup}} > 0$ is a constant independent of the mesh size, provided the fine mesh size h is small enough.

Proof. Let $q \in Q_H$ and $\widehat{q} \in \widehat{Q}_H$ be arbitrary. By the continuous inf-sup condition (4.13), there is $u \in H_0^1(\Omega^\epsilon)^2$ such that div$u = q$ and $\|u\|_{H^1(\Omega^\epsilon)} \leq \beta^{-1}\|q\|_{L^2(\Omega^\epsilon)}$. By the assumption (4.14), for each coarse element K_i, and for every edge $E_j \in \partial K_i$, there is a basis function Ψ_j such that $\int_{E_j} \Psi_j \cdot n = 1$, and $\int_{E_k} \Psi_j \cdot n = 0$ for other coarse edges $E_k \in \partial K_i$.

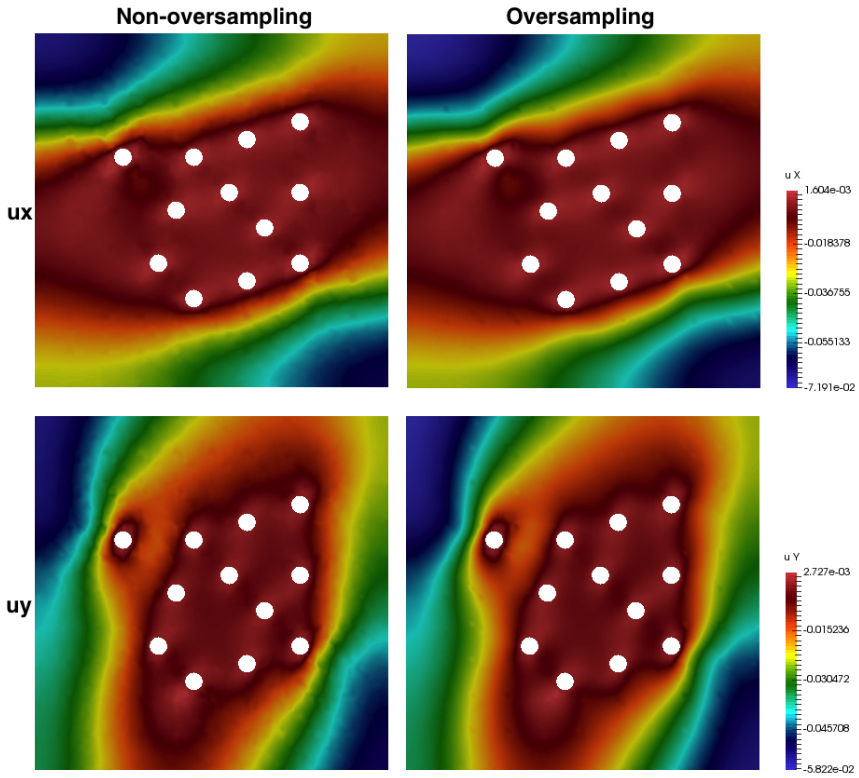

Figure 4.7: Stokes problem for perforated domain with small inclusions, comparison between oversampling and non-oversampling. Numerical solution for Example 2. Top: x-component of velocity. Bottom: y-component of velocity. Left: Coarse-scale solution with 16 basis, non-oversampling. Right: Coarse-scale solution with 16 basis, oversampling with 4 fine layers.

Note that we suppress the dependence of Ψ_j on i to simplify the notations. Then we define $v_1 \in V^{\text{off}}$ by

$$v_1 = \sum_{K_i \in \mathcal{T}^H} \sum_{E_j \in \partial K_i} c_{j,i} \Psi_j, \quad \text{with} \quad c_{j,i} = \int_{E_j} u \cdot n. \tag{4.16}$$

It is clear that

$$\int_{E_j} v_1 \cdot n = \int_{E_j} u \cdot n, \quad \text{and} \quad \int_{E_k} v_1 \cdot n = 0.$$

In addition, we define v_1 so that $\int_E v_1 \cdot n = 0$ for all boundary edges $E \in \partial\Omega^\epsilon$. We also

choose the normal vectors in (4.16) so that the average jumps of $v_1 \cdot n$ across all interior coarse edges are zero. This condition can be achieved by choosing a fixed normal direction for each coarse edge in the definition (4.16). By the definition of b_{DG}, integration by parts and using the definition of v_1, we have

$$b_{\mathrm{DG}}(v_1, q, \widehat{q}) = b(u, q) = \|q\|^2_{L^2(\Omega^\epsilon)}.$$

Next, we will show that $\|v_1\|_A \leq \alpha \|q\|_{L^2(\Omega^\epsilon)}$ for some positive constant α. We define the energy D_j of the basis function Ψ_j by

$$D_j := \int_{K_i} |\nabla \Psi_j|^2 + \frac{1}{h} \int_{\partial K_i} |\Psi_j|^2.$$

So, by the definition of $\|\cdot\|_A$, the trace inequality and the continuous inf-sup condition,

$$\|v_1\|^2_A \leq \sum_{K_i \in \mathcal{T}^H} \sum_{E_j \in \partial K_i} c^2_{j,i} D_j \lesssim \alpha \|q\|^2_{L^2(\Omega^\epsilon)},$$

where we define

$$\alpha = \max_{K_i \in \mathcal{T}^H} \max_{E_j \in \partial E_i} D_j.$$

On the other hand, we can choose $v_2 \in V^{\mathrm{off}}$ such that

$$\int_{E_j} v_2 \cdot n = \frac{1}{2}(hH)\widehat{q}, \quad \text{and} \quad \int_{E_k} v_2 \cdot n = 0$$

if E_j is an interior edge, or

$$\int_{E_j} v_2 \cdot n = (hH)\widehat{q}, \quad \text{and} \quad \int_{E_k} v_2 \cdot n = 0$$

if E_j is a boundary edge, where n is the outward normal vector on the boundary of K_i.

This can be achieved by defining

$$v_2 = \sum_{K_i \in \mathcal{T}^H} \sum_{E_j \in \partial K_i} d_{j,i} \Psi_j, \quad \text{with} \quad d_{j,i} = \sigma(hH)\widehat{q} \tag{4.17}$$

where $\sigma = 1$ or $\sigma = 1/2$ depending on the location of the coarse edge E_j. Thus, we have

$$\int_{E_j} [v_2] \cdot n = (hH)\widehat{q}$$

on all interior coarse edges. By the definition of b_{DG},

$$b_{\text{DG}}(v_2, q, \widehat{q}) = -\sum_{K \in \mathcal{T}^H} \int_K q \text{div} v_2 + h \sum_{E \in \mathcal{E}^H} \|\widehat{q}\|^2_{L^2(E)}.$$

We can show that $\|v_2\|^2_A \leq C_1 \alpha(hH) h \sum_{E \in \mathcal{E}^H} \|\widehat{q}\|^2_{L^2(E)}$ using arguments similar as above, where the constant C_1 is independent of the mesh size.

Finally, we let $v = \alpha_1 v_1 + v_2 \in V^{\text{off}}$. Then

$$b_{\text{DG}}(v, q, \widehat{q}) = \alpha_1 \|q\|^2_{L^2(\Omega^\epsilon)} - \sum_{K \in \mathcal{T}^H} \int_K q \text{div} v_2 + h \sum_{E \in \mathcal{E}^H} \|\widehat{q}\|^2_{L^2(E)}.$$

Using the Young's inequality, we have

$$b_{\text{DG}}(v, q, \widehat{q}) \geq$$
$$\alpha_1 \|q\|^2_{L^2(\Omega^\epsilon)} - \frac{1}{2C_1\alpha(hH)} \sum_{K \in \mathcal{T}^H} \int_K \text{div} v_2^2 - \frac{C_1 \alpha(hH)}{2} \sum_{K \in \mathcal{T}^H} \int_K q^2 + h \sum_{E \in \mathcal{E}^H} \|\widehat{q}\|^2_{L^2(E)}$$

which implies

$$b_{\text{DG}}(v, q, \widehat{q}) \geq (\alpha_1 - \frac{C_1 \alpha(hH)}{2}) \|q\|^2_{L^2(\Omega^\epsilon)} + \frac{1}{2} h \sum_{E \in \mathcal{E}^H} \|\widehat{q}\|^2_{L^2(E)}.$$

Taking $\alpha_1 = C_1\alpha(hH)$ and assuming that the fine mesh size h is small enough so that $C_1\alpha(hH) = O(1)$, we obtain

$$b_{\text{DG}}(v, q, \widehat{q}) \geq C\|(q, \widehat{q})\|_Q^2$$

where C is a constant independent of the mesh size. Moreover,

$$\|v\|_A^2 \lesssim \alpha_1^2\|v_1\|_A^2 + \|v_2\|_A^2 \lesssim \alpha_1^2\alpha\|q\|_{L^2(\Omega^\epsilon)}^2 + \alpha_1 h \sum_{E\in\mathcal{E}^H} \|\widehat{q}\|_{L^2(E)}^2.$$

Thus, choosing h small enough, we have $\|v\|_A^2 \lesssim \|(q, \widehat{q})\|_Q^2$. □

4.4.2 Convergence results

In this section, we will derive an error estimate between the fine scale solution u_h and coarse scale solution u_H. First, we construct a projection of the fine grid velocity in the snapshot space, and estimate the error for this projection. Second, we will estimate the difference between this projection and coarse scale velocity. Combine these two errors, we obtain the results as desired.

Theorem 4.4.3. *Let u_h be the fine scale velocity solution in* (4.4)*, and u_H be the coarse scale velocity solution of* (4.3)*. The following estimate holds*

$$\|u_h - u_H\|_A^2 \lesssim \sum_{i=1}^{N} \frac{H}{\lambda_{L_i+1}^{(i)}}(1 + \frac{H}{h\lambda_{L_i+1}^{(i)}}) \int_{\partial K_i} |(\nabla u_{\textit{snap}})\, n|^2 + H^2\|f\|_{L^2(\Omega^\epsilon)}^2,$$

where u_{snap} is the snapshot solution defined in (4.18)*.*

Proof. Let $(u_h, p_h) \in V_h^{\text{DG}} \times Q_H$ be the fine scale solution satisfying (4.4). We will next define a projection, denoted u_{snap}, of u_h in the snapshot space V_{snap}. For each coarse

element K, the restriction of u_{snap} on K is defined by solving

$$\begin{aligned} -\Delta u_{\text{snap}} + \nabla p_{\text{snap}} &= 0, && \text{in } K \\ \text{div} u_{\text{snap}} &= c, && \text{in } K \\ u_{\text{snap}} &= u_h, && \text{on } \partial K \end{aligned} \tag{4.18}$$

where p_{snap} is a constant, and c is chosen by the compatibility condition, $c = \frac{1}{|K|}\int_{\partial K} u_h \cdot n\, ds$. We remark that u_{snap} is obtained on the fine grid, and we therefore have $u_{\text{snap}} \in V_{\text{snap}}$. We define u_{off} as the projection of u_{snap} in the offline space V_H. Using [35], we obtain

$$\|u_{\text{snap}} - u_{\text{off}}\|_A^2 \leq \sum_{i=1}^{N} \frac{H}{\lambda_{L_i+1}^{(i)}}(1 + \frac{H}{h\lambda_{L_i+1}^{(i)}}) \int_{\partial K_i} |(\nabla u_{\text{snap}})\, n|^2. \tag{4.19}$$

Next, by comparing (4.3) and (4.4), we have

$$\begin{aligned} a_{\text{DG}}(u_h - u_H, v) + b_{\text{DG}}(v, p_h - p_H, \widehat{p}_h - \widehat{p}_H) &= 0, \\ b_{\text{DG}}(u_h - u_H, q, \widehat{q}) &= 0, \end{aligned} \tag{4.20}$$

for all $v \in V_H$, $q \in Q_H$, $\widehat{q} \in \widehat{Q}_H$. Then, using the inf-sup condition (4.15) and standard arguments, we have

$$\|u_h - u_H\|_A \lesssim \|u_h - u_{\text{off}}\|_A. \tag{4.21}$$

Finally, we define $u_h = u_{\text{snap}} + u_0$, where $u_0 = u_h - u_{\text{snap}}$. Then (4.20) and (4.19) imply that

$$\|u_h - u_H\|_A^2 \lesssim \sum_{i=1}^{N} \frac{H}{\lambda_{L_i+1}^{(i)}}(1 + \frac{H}{h\lambda_{L_i+1}^{(i)}}) \int_{\partial K_i} |(\nabla u_{\text{snap}})\, n|^2 + \|u_0\|_A^2. \tag{4.22}$$

By (4.4), we have

$$a_{\text{DG}}(u_0, v) = -a_{\text{DG}}(u_{\text{snap}}, v) + (f, v) + \int_{\Gamma_D} \left(\frac{\gamma}{h} g_D \cdot v - ((\nabla v)\, n) \cdot g_D \right) - b_{\text{DG}}(v, p_h, \widehat{p}_h) \tag{4.23}$$

for all $v \in V_h^{\text{DG}}$. By the definition of u_0, we see that $u_0 = 0$ on ∂K for all coarse element $K \in \mathcal{T}^H$. Thus, using (4.11) and taking $v = u_0$ in (4.23), we have

$$\|\nabla u_0\|_A^2 \lesssim -a_{\text{DG}}(u_{\text{snap}}, u_0) + (f, u_0). \tag{4.24}$$

Notice that

$$(f, u_0) = \sum_{K \in \mathcal{T}^H} \int_K f\, u_0 \leq \sum_{K \in \mathcal{T}^H} \|f\|_{L^2(K)}\, \|u_0\|_{L^2(K)} \lesssim H \sum_{K \in \mathcal{T}^H} \|f\|_{L^2(K)}\, \|\nabla u_0\|_{L^2(K)} \tag{4.25}$$

where the last inequality follows from the Poincare inequality. So, we obtain

$$(f, u_0) \lesssim H \|f\|_{L^2(\Omega^\epsilon)}\, \|u_0\|_A. \tag{4.26}$$

By the definition of a_{DG} and u_0, we have

$$a_{\text{DG}}(u_{\text{snap}}, u_0) = \int_{\Omega^\epsilon} \nabla u_{\text{snap}} : \nabla u_0 - \sum_{E \in \mathcal{E}^H} \int_E \{(\nabla u_0) n\} \cdot [u_{\text{snap}}].$$

Notice that $[u_{\text{snap}}] = [u_h]$ for all E. Thus, by the results in [35], we obtain

$$\sum_{E \in \mathcal{E}^H} \int_E \{(\nabla u_0) n\} \cdot [u_{\text{snap}}] \lesssim \|u_0\|_A \left(\frac{1}{h} \sum_{E \in \mathcal{E}^H} \int_E |[u_h]|^2 \right)^{\frac{1}{2}}. \tag{4.27}$$

By the variational form of (4.18), we have, for all coarse elements K

$$\int_K \nabla u_{\text{snap}} : \nabla u_0 = \int_K p_{\text{snap}} \,\text{div} u_0 = 0$$

since p_{snap} is a constant and $u_0 = 0$ on ∂K. Combining the above results, we have

$$\|u_0\|_A^2 \lesssim \sum_{i=1}^{N} \frac{H}{\lambda_{L_i+1}^{(i)}}(1 + \frac{H}{h\lambda_{L_i+1}^{(i)}}) \int_{\partial K_i} |(\nabla u_{\text{snap}})\, n|^2 + H^2 \|f\|_{L^2(\Omega^\epsilon)}^2. \tag{4.28}$$

This completes the proof.

□

5. MULTISCALE MODEL REDUCTION FOR TRANSPORT AND FLOW PROBLEMS *

Convection-dominated transport phenomena have wide applications. In these physical processes, the transport velocity is often a solution of a heterogeneous flow problem. In this work, we consider coupled flow (Stokes problem) and transport (unsteady convection-diffusion problem) in perforated domains. We propose a coarse-scale solver based on Generalized Multiscale Finite Element Method (GMsFEM). Multisclae spaces for the velocity in the mixed Stokes equations and the flux in the mixed transport equation are constructed. As for the pressure in the flow equation, we use piecewise constant functions. For the concentration in the transport equation, we first use piecewise constant functions for approximation and later enrich the space by adding interior basis functions. Due to the asymmetric of the transport equation, two different Petrov-Galerkin mixed formulations (see (5.2) for Formulation 1 and (5.3) for Formulation 2) are proposed to guarantee the stability of the global system. In order to employ the Petrov-Galerkin formulations, we also design the test functions for the mixed formulation of transport equation by taking the solutions of local adjoint problem.

Two different approaches for the coupling of flow and transport equation are discussed. In the first approach, called de-coupled GMsFEM, the flow equation is solved on a coarse grid using the GMsFEM and, furthermore, the approximate velocity solution is used in constructing offline spaces for the transport equations (both trial and test spaces). In the second approach, named coupled GMsFEM, the multiscale basis functions for flow and transport are constructed jointly. i.e., we do not solve global flow equation in this case.

*Reprinted with permission from "Multiscale model reduction for transport and flow problems in perforated domains" by Eric T Chung, Maria Vasilyeva and Yating Wang, 2018. Journal of Computational and Applied Mathematics, Volume 330, Pages 519-535, Copyright [2018] by Elsevier.

This is challenging because one does not know the global flow information and the basis functions for the transport nonlinearly depends on the coarse-grid components of the flow equations. Details of basis construction and numerical experiments are shown below.

5.1 Overview of the transport equation

The flow equation for the velocity field is described by a steady state Stokes problem (2.6). For the approximation on the fine grid, we use the standard Crouzeix-Raviart element for velocity and the piecewise constant element for pressure in this chapter. We can write approximation of the Stokes problem in the following matrix form

$$\begin{pmatrix} A_h & (B_h^u)^T \\ B_h^u & 0 \end{pmatrix} \begin{pmatrix} u_h \\ p_h \end{pmatrix} = \begin{pmatrix} F_h \\ 0 \end{pmatrix}, \tag{5.1}$$

where

$$v_h^T A_h u_h = a(u_h, v_h) \quad \text{and} \quad q_h^T B_h^u u_h = b(u_h, q_h).$$

.

The transport equation is described by a unsteady convection-diffusion equation for the concentration (2.8), and the velocity in the equaiton u can be calculated using the Stokes equation. We note that the velocity field describes an incompressible flow which implies that it is a divergence free field. We consider transport equation (2.8) with the homogeneous Neumann boundary conditions and the initial condition $c(x, 0) = 0$ in Ω^ε. The convection-diffusion equation describes how the rate of a scalar quantity in a differential control volume changes. It is actually calcluated by the diffusion and flow into and out of part of the system, taking into account the generation or consumption inside the control volume. It is common to write the transport equation in a mixed formulation. In this work, we write two different formulations associated to two different flux choices.

- **Formulation 1.** Let $q = -D\nabla c$ be the flux, namely diffusive flux which arises due to diffusion, then we have the following mixed formulation for flux and concentration (q, c)

$$\begin{aligned} D^{-1}q + \nabla c = 0, \quad &\text{in } \Omega^\varepsilon \\ \frac{\partial c}{\partial t} + \text{div} q - D^{-1}u \cdot q = f, \quad &\text{in } \Omega^\varepsilon. \end{aligned} \tag{5.2}$$

- **Formulation 2.** Let $q = -D\nabla c + uc$ be the flux, namely the toal flux, then we have the following mixed formulation for flux and concentration (q, c)

$$\begin{aligned} D^{-1}q + \nabla c - D^{-1}uc = 0, \quad &\text{in } \Omega^\varepsilon \\ \frac{\partial c}{\partial t} + \text{div} q = f, \quad &\text{in } \Omega^\varepsilon. \end{aligned} \tag{5.3}$$

To define the weak formulation for transport equation, we introduce the spaces

$$V^q = \{v \in L^2(\Omega^\varepsilon)^d : \text{div} v \in L^2(\Omega^\varepsilon)\},$$

and $Q^c = L^2(\Omega^\varepsilon)$. In addition, we define V_0^q as the subspace of V^q containing vector fields with zero normal component on $\partial\Omega^\varepsilon \cap \partial\mathcal{B}^\varepsilon$.

The weak formulation of the transport equation in the mixed formulation (5.2) (**Formulation 1**) reads: find $q \in V_0^q$ and $c \in Q^c$ such that

$$\begin{aligned} m^q(q, v) + b(v, c) = 0 \quad \forall v \in V_0^q \\ m^c(c, r) - b(q, r) + s(q, r) = l(r) \quad \forall r \in Q^c, \end{aligned} \tag{5.4}$$

where

$$m^q(q, v) = \int_{\Omega^\varepsilon} D^{-1}q \cdot v \quad b(v, c) = -\int_{\Omega^\varepsilon} \text{div} v \, c \quad m^c(c, r) = \int_{\Omega^\varepsilon} \tau^{-1} c \, r$$

$$s(v,c) = -\int_{\Omega^\varepsilon} D^{-1}\, u \cdot\, v\, c \quad l(r) = \int_{\Omega^\varepsilon} (f + \tau^{-1}\check{c})r$$

and $\check{c}$ is the concentration in the previous time step and τ is the time step. Remark that for the time discretization we used an implicit scheme.

We can write (5.4) as the following matrix form

$$\begin{pmatrix} M_h^q & B_h^T \\ -B_h + S_h & M_h^c \end{pmatrix} \begin{pmatrix} q_h \\ c_h \end{pmatrix} = \begin{pmatrix} 0 \\ F_h \end{pmatrix}, \tag{5.5}$$

where $q_h \in V_h^q \subset V_0^q$, $c_h \in Q_h^c \subset Q^c$ and

$$v_h^T M_h^q q_h = m^q(q_h, v_h), \quad c_h^T B_h q_h = b(q_h, c_h), \quad c_h^T S_h h_h = s(v_h, c_h), \quad r_h^T M_h^c c_h = m^c(c_h, r_h).$$

For the formulation (5.3) (**Formulation 2**), we have following weak forms

$$\begin{aligned} m^q(q,v) + b(v,c) + s(v,c) = 0 \quad \forall v \in V_0^q \\ m^c(c,r) - b(q,r) = l(r) \quad \forall r \in Q^c. \end{aligned} \tag{5.6}$$

or in matrix form

$$\begin{pmatrix} M_h^q & B_h^T + S_h^T \\ -B_h & M_h^c \end{pmatrix} \begin{pmatrix} q_h \\ c_h \end{pmatrix} = \begin{pmatrix} 0 \\ F_h \end{pmatrix}. \tag{5.7}$$

As for the fine scale discretization of the transport problem, we use the standard lowest-order Raviart-Thomas space (RT_0) for flux and the piecewise constant space for concentration.

5.2 Coarse-scale offline approximation using GMsFEM

Let $\mathcal{T}^H$, $\mathcal{T}^h$ and $\mathcal{E}^H$ be the mesh ingredients as discussed in chapter 2. We emphasize that we use ω_i to denote a coarse neighborhood, and use K to denote a coarse grid block.

For the Stokes problem, we define the neighborhood ω_i for every coarse node and midpoint of coarse edge, i.e, both coarse nodal-based and edge-based neighborhood.

For the transport problem, we use the neighborhood of the facet $E_i \in \mathcal{E}^H$ by

$$\omega_i = \bigcup_j \left\{ K_j \in \mathcal{T}^H \,|\, E_i \in \partial K_j \right\}.$$

Notice that ω_i is a union of two coarse grid blocks when E_i lies in the interior of the domain Ω, i.e., only the edge-based coarse neighborhood.

We will construct an offline solution space for the flux and concentration:

$$V_H^q := \text{span}\{\psi_i^q\}_{i=1}^{N_q}, \quad Q_H := \text{span}\{\psi_i^c\}_{i=1}^{N_c}.$$

where ψ_i^q are the multiscale basis functions and N_q is the number of basis functions for flux, and ψ_i^c are the multiscale basis functions and N_c is the number of basis functions for concentration. For the test spaces, we denote

$$\hat{V}_H^q := \text{span}\{\phi_i^q\}_{i=1}^{N_q}, \quad \hat{Q}_H := Q_H.$$

For global coupling in **Formulation 1**, we define the mixed GMsFEM as follows: find $q_{ms} \in V_H$ and $c_{ms} \in Q_H$ such that

$$\begin{aligned} m^q(q_{ms}, v) + b(v, c_{ms}) &= 0, \quad \forall v \in \hat{V}_H^q \\ m^c(c_{ms}, r) - b(q_{ms}, r) + s(q_{ms}, r) &= l(r), \quad \forall r \in \hat{Q}_H. \end{aligned} \tag{5.8}$$

We can write system (5.8) in matrix form

$$\begin{pmatrix} \hat{R}_q M_h^q R_q^T & \hat{R}_q B_h^T R_c^T \\ R_c(-B_h + S_h) R_q^T & R_c M_h^c R_c^T \end{pmatrix} \begin{pmatrix} q_{ms} \\ c_{ms} \end{pmatrix} = \begin{pmatrix} 0 \\ R_c F_h \end{pmatrix}, \tag{5.9}$$

where R_q, R_c and $\hat{R}_q^T$ are defined as:

$$R_q = \left[\psi_1^q, \ldots, \psi_{N_q}^q\right], \quad \hat{R}_q = \left[\phi_1^q, \ldots, \phi_{N_q}^q\right], \quad R_c = \left[\psi_1^c, \ldots, \psi_{N_c}^c\right].$$

For the **Formulation 2**, we define the mixed GMsFEM as follows: find $q_{ms} \in V_H$ and $c_{ms} \in Q_H$ such that

$$\begin{aligned} m^q(q_{ms}, v) + b(v, c_{ms}) + s(v, c_{ms}) = 0, \quad \forall v \in \hat{V}_H^q \\ m^c(c_{ms}, r) - b(q_{ms}, r) = l(r), \quad \forall r \in \hat{Q}_H. \end{aligned} \tag{5.10}$$

and for matrix form we have

$$\begin{pmatrix} \hat{R}_q M_h^q R_q^T & \hat{R}_q (B_h^T + S_h^T) R_c^T \\ -R_c B_h R_q^T & R_c M_h^c R_c^T \end{pmatrix} \begin{pmatrix} q_{ms} \\ c_{ms} \end{pmatrix} = \begin{pmatrix} 0 \\ R_c F_h \end{pmatrix}, \tag{5.11}$$

Next, we will present details of constructing multiscale trial basis and test basis. For the multiscale basis functions in trial space, we first use the primal problem to construct snapshot space that contains an extensive set of basis functions formed by the solution of local problems with all possible boundary conditions up to the fine grid resolution. Then we will apply a spectral decomposition to select dominant modes in the snapshot space. Then for the construction of test multiscale basis, we will use the adjoint problem and find corresponding multiscale test basis for every constructed multiscale trial basis.

5.2.1 Offline trial space for the transport equation

Let ω_i^q be the union of all coarse blocks sharing the coarse-grid edge $E_i \in \mathcal{E}^H$, we aim to find q_l^i and c_l^i on the coarse neighborhoodω_i^q such that:

$$\begin{aligned} m^q(q_l^i, v) + b(v, c_l^i) &= 0, \quad \forall v \in V_h^i \\ -b(q_l^i, r) + s(q_l^i, r) &= (g, r), \quad \forall r \in Q_h^i. \end{aligned} \tag{5.12}$$

with boundary condition $q_l^i \cdot n_i = 0$ on $\partial\omega_i^q$, where n_i is the outward unit normal vector on $\partial\omega_i^q$. The above local problem is solved numerically on the fine-grid defined in ω_i^q using the lowest-order Raviart-Thomas element. To be more specific, for an interior coarse edge E_i, we have $E_i = \cup_{l=1}^{J_i} e_l$, where e_l are the fine-grid facets on $E_i/\partial\mathcal{B}^\varepsilon$, and J_i is the number of these fine grid facets on $E_i/\partial\mathcal{B}^\varepsilon$. For each l, the local problem (5.12) is solved separately on each coarse-grid element $K_j^i \subset \omega_i^q$ which shares the edge E_i, with boundary condition $q_l^i \cdot n_i = \delta_l^i$ on E_i. The function δ_l^i is a piecewise constant function defined on $E_i/\partial\mathcal{B}^\varepsilon$ such that it has value 1 on e_l and value 0 on the other fine-grid edges. We remark that the function δ_l^i is always zero on the boundary of perforations intersecting with the edge E_i. The consnant g in (5.12) is chosen by compatibility condition, that is, $g = \frac{1}{|K_j^i|}\int_{E_i} q_l^i \cdot n_i \, ds$, $j = 1, 2$.

Let $\Psi_l^{i,\text{snap}} = q_l^i$, we can obtain the the local snapshot space on E_i defined by

$$V_{\text{snap}}^i = \text{span}\{\Psi_l^{i,\text{snap}}, 0 \le l \le J_i\}.$$

Next, we perform a dimension reduction on the snapshot space via a local spectral problem in ω_i^q. The following local eigenvalue problem is considered

$$A^{i,\text{off}}\Psi_k = \lambda_k^{i,\text{off}} S^{i,\text{off}}\Psi_k, \tag{5.13}$$

where

$$A^{i,\text{off}} = [a^{\text{off}}_{mn}] = a_i(\Psi^{i,\text{snap}}_m, \Psi^{i,\text{snap}}_n) = R_{i,\text{snap}} A^i_f R^T_{i,\text{snap}},$$

$$S^{i,\text{off}} = [m^{\text{off}}_{mn}] = s_i(\Psi^{i,\text{snap}}_m, \Psi^{i,\text{snap}}_n) = R_{i,\text{snap}} M_f R^T_{i,\text{snap}},$$

$$R_{i,\text{snap}} = \left[\Psi^{i,\text{snap}}_1, \ldots, \Psi^{i,\text{snap}}_{J_i}\right],$$

and

$$a_i(q,v) = \int_{E_i} D^{-1}(q \cdot n_i)(v \cdot n_i), \quad \text{and} \quad s_i(q,v) = \int_{\omega^q_i} D^{-1} q \cdot v.$$

We arrange the eigenvalues in an increasing order and choose the first M_i eigenvalues, the corresponding eigen-functions $\psi^q_{k,E_i} = R_{i,\text{snap}} \Psi_k$, for $k = 1, 2, ..., M_i$, are then selected to be the trial basis for the flux.

We can obtain the offline space using these eigenfunctions:

$$V^q_H = \text{span}\{\psi^q_{k,E_i} : \quad 1 \le i \le N_e \text{ and } 1 \le k \le M_i\}, \quad R_{i,\text{off}} = \left[\psi^q_{1,E_i}, \ldots, \psi^q_{M_i,E_i}\right].$$

Using a single index notation, we can write $V^q_H = \text{span}\{\psi^q_i\}_{i=1}^{N_q}$ where $N_q = \sum_{i=1}^{N_e} M_i$.

5.2.2 Offline test space for the transport equation

After construction of the multiscale trial basis functions, we solve the adjoint problem in order to find corresponding multiscale test basis functions

$$\begin{aligned} m^q(\phi^j, v) - b(v,c) + s(v,c) = 0, \quad \forall v \in V^i_h \\ b(\phi^j, r) = (g,r), \quad \forall r \in Q^i_h. \end{aligned} \tag{5.14}$$

with boundary condition $q^j \cdot n = \psi^{\text{off}}_j \cdot n$.

Then

$$\hat{V}^q_H = \text{span}\{\phi_i\}_{i=1}^{N_q}$$

where $N_q = \sum_{i=1}^{N_e} M_{i,\text{off}}$.

We note that, the above multiscale trial and test basis are constructed for Formulation 1 of transport equation.

Remark 5.2.1. *For construction of a offline basis functions of trial space for Formulation 2, we should use the following equations to construct snapshot space*

$$\begin{aligned} m^q(q_l^i, v) + b(v, c_l^i) + s(v, c_l^i) = 0, \quad \forall v \in V_h^i \\ -b(q_l^i, r) = (g, r), \quad \forall r \in Q_h^i. \end{aligned} \tag{5.15}$$

In an analogous manner, we solve an eigenvalue problem (5.13) *to select dominant modes in the snapshot space. As for construction of test space for Formulation 2, we will solve the following adjoint problem*

$$\begin{aligned} m^q(\phi^j, v) - b(v, c) = 0, \quad \forall v \in V_h^i \\ b(\phi^j, r) + s(\phi^j, r) = (g, r), \quad \forall r \in Q_h^i, \end{aligned} \tag{5.16}$$

Similarly as before, the multiscale test basis for every constructed multiscale trial basis.

It is worth to mention that, in this set of multiscale basis of the transport problem, we use piecewise constant basis for concentration in both trial and test space:

$$Q_H = \{q \in L^2(\Omega) : q|_K \in P^0(K), \forall K \in \mathcal{T}_H\}.$$

We will provide a method to enrich the multiscale space of concentration in later sections.

5.2.3 Multiscale space for velocity in the Stokes flow

In this section, we form the coarse-scale system for the flow problem. Recall that, we define the neighborhood ω_i for every coarse vertices and mid-points of coarse edges.We

construct an offline space for the velocity

$$V_H^u := \text{span}\{\psi_{i,x}^u, \psi_{i,y}^u\}_{i=1}^{N^u},$$

where $\psi_{i,x}^u, \psi_{i,y}^u$ are the multiscale basis functions for velocity, and N^u is the number of basis functions. Each ψ_i^u is supported in a coarse neighborhood ω_l. Basically, for the construction of the multiscale velocity space, we follow our previous work [33], and the details can be found in Chapter 3.

As for the pressure basis, we will use the space of piecewise constant functions, that is

$$Q_H^p = \{q \in L^2(\Omega) : q|_K \in P^0(K), \forall K \in \mathcal{T}_H\},$$

where the number of basis N_p is equal to the number of coarse blocks.

At this point of development, we define the global system of mixed GMsFEM as follows: find $u_{ms} \in V_H^u$ and $p_{ms} \in Q_{\text{off}}$ such that

$$\begin{aligned} a(u_{ms}, v) + b(v, p_{ms}) &= 0, \quad \forall v \in V_H^u \\ b(u_{ms}, q) &= 0, \quad \forall q \in Q_H^p. \end{aligned} \tag{5.17}$$

We can further denote the above system in matrix form

$$\begin{pmatrix} R_u A_h R_u^T & R_u (B_h^u)^T R_p^T \\ R_p B_h^u R_u^T & 0 \end{pmatrix} \begin{pmatrix} u_{ms} \\ p_{ms} \end{pmatrix} = \begin{pmatrix} R_u F_h \\ 0 \end{pmatrix}, \tag{5.18}$$

where R_u and R_p are

$$R_u = \left[\psi_{1,x}^u, \psi_{1,y}^u, \ldots, \psi_{N^u,x}^u, \psi_{N^u,x}\right], \quad R_p = [q_1, \ldots, q_{N^p}].$$

Here $\{\psi^u_{i,x}, \psi^u_{i,y}\}_{i=1}^{N^u}$ are the multiscale basis functions for velocity and $\{q_i\}_{i=1}^{N^p}$ are the piesewise constant basis functions for pressure.

5.2.4 Numerical results

In this section, we present numerical results for coupled transport and flow problems. We present examples corresponding to two different approaches.The first example is using the de-coupled GMsFEM, where we assume the velocity field are known and can be solved from the global Stokes system. In the second one, we do not solve a global flow equation. Instead, the coupled multiscale basis for flow and transport are constructed using several potential velocity fields.

Here are some basic information regarding the numerical tests. We set $\Omega = [0, 1] \times [0, 1]$. The computational domain is discretized coarsely using uniform triangulation as shown in the Figure 5.1, where the coarse mesh size $H = 1/10$. Nonuniform triangulation is used inside each coarse triangle element to obtain a finer discretization. The coarse grid consists of 200 cells, 320 edges and 121 vertices and the fine grid contains 44816 cells, 67616 edges and 22789 vertices.

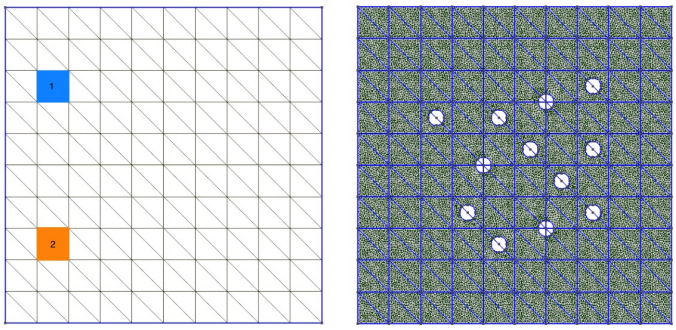

Figure 5.1: Coarse and fine grids for perforated domain.

The errors will be measured in the following

$$||\varepsilon_q||^2_{L^2(\Omega^\epsilon)} = \frac{\int_{\Omega^\epsilon} |q_f - q_{ms}|^2}{\int_\Omega^\epsilon |q_f|^2}, \quad ||\varepsilon_q||^2_{H(div)(\Omega^\epsilon)} = \frac{\int_{\Omega^\epsilon} |q_f - q_{ms}|^2 + (\text{div}(q_f - q_{ms}))^2}{\int_\Omega^\epsilon |q_f|^2 + (\text{div}(q_f))^2},$$

$$||\varepsilon_c||^2_{L^2(\Omega^\epsilon)} = \frac{\int_{\Omega^\epsilon} (c_f - c_{ms})^2}{\int_\Omega^\epsilon c_f^2},$$

where (q_f, c_f) and (q_{ms}, c_{ms}) are fine-scale and coarse-scale solution, respectively for flux and concentration. In addition, for the relative L^2 norm for concentration, $||c_f - c_{ms}||_{L^2(\Omega)}$, we also compare the numerical concentration with the cell average of the fine scale concentration, that is, $\bar{c}_f = \frac{1}{|K|}\int_K c_f$ for all $K \in \mathcal{T}_H$ ($||\varepsilon_{\bar{c}}||_{L^2(\Omega)}$). Similar norms will be used for velocity and pressure of the flow equation as in Chapter 3.

5.2.4.1 Example 1: De-coupled approach

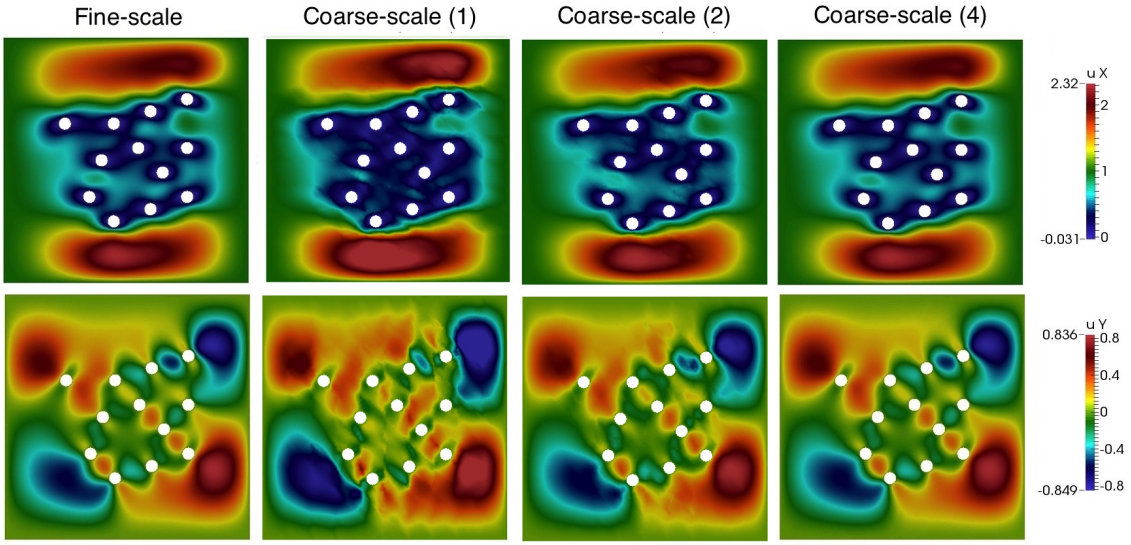

Figure 5.2: Stokes flow. Fine-scale and coarse-scale solutions for velocity u_x(top), u_y(bottom) in perforated domain with different number of basis functions (1, 2 and 4 mutiscale basis functions for velocity).

M^u_{off}	DOF^u_c	$\|\|\varepsilon_u\|\|_{L^2}(\%)$	$\|\varepsilon_u\|_{H^1}(\%)$	$\|\|\varepsilon_p\|\|_{L^2}(\%)$	$\|\|\varepsilon_{\bar{p}}\|\|_{L^2}(\%)$
1	1082	13.9	57.671	40.435	37.912
2	1964	2.766	23.645	16.373	6.174
3	2846	0.732	8.016	15.218	0.872
4	3728	0.158	3.018	15.194	0.120

Table 5.1: Decoupled approach. Stokes flow. Error history for velocity and pressure of Stokes flow in perforated domain.

In our first example, we consider the Stokes problem with zero velocity on the inclusions $\partial\Omega^\varepsilon \cap \partial\mathcal{B}^\varepsilon$, and $u = (1, 0)$ on the global outer boundary $\partial\Omega$. In Figure 5.2, we show fine-scale and coarse-scale solutions for velocity (u_x, u_y) in perforated domain with different number of velocity basis functions, $M^u_{\text{off}} = 1, 2$ and 4. The relative errors for velocity and pressure when taking different number of velocity basis are presented in Table 5.1. We observe that the velocity error decrease fast when the number of basis increase. For example, the velocity L^2 error is 13.9% when $DOF^u_c = 1082$ ($M^u_{\text{off}} = 1$), 2.7% when $DOF^u_c = 1964$ for $M^u_{\text{off}} = 2$ and 0.1% when $DOF^u_c = 3728$ ($M^u_{\text{off}} = 4$).

Next, we compare the results of transport equation when we take different resolutions of flow velocity solution. For instance, we will take the fine scale stokes velocity($DOF^u_f = 180048$), coarse scale stokes velocity with 1 basis($DOF^u_c = 1082$), 2 basis($DOF^u_c = 1964$) and 3 basis($DOF^u_c = 2846$). In this example, we take diffusion coefficient $D = 0.03$, time $T_{max} = 0.5$ with 15 time steps and use nonzero source terms (see left picture in Figure 5.1, where blue block corresponds to $f = -1$ and orange block corresponds to $f = 1$, and $f = 0$ elsewhere in the domain).

The convergence results for transport equation for two different formulations will both be investigated. In Tables 5.2 - 5.3, we present relative errors for flux and concentration using Formulation 1 and Formulation 2, respectively. It can be seen that, in general, Formulation 2 gives smaller $||\varepsilon_q||_{H(div)}$ errors compared with that of Formulation 1 for the

M^q_{off}	DOF	$\|\|\varepsilon_q\|\|_{L^2}(\%)$	$\|\|\varepsilon_q\|\|_{H(div)}(\%)$	$\|\|\varepsilon_c\|\|_{L^2}(\%)$	$\|\|\varepsilon_{\bar{c}}\|\|_{L^2}(\%)$
With fine scale velocity, $DOF^u_f = 180048$					
2	840	33.9	39.2	27.6	12.9
4	1480	7.0	8.7	24.7	1.5
6	2120	2.7	3.1	24.7	1.5
8	2760	2.3	2.7	24.7	1.5
With coarse scale velocity, 1 basis, $DOF^u_c = 1082$					
2	840	41.2	45.2	35.6	26.5
4	1480	16.6	21.0	24.8	3.7
6	2120	4.2	6.6	24.7	1.8
8	2760	3.9	6.4	24.7	1.8
With coarse scale velocity, 2 basis, $DOF^u_c = 1964$					
2	840	34.4	40.2	28.0	13.7
4	1480	7.5	9.3	24.7	1.9
6	2120	3.5	3.5	24.7	1.9
8	2760	3.1	3.1	24.7	1.9
With coarse scale velocity, 3 basis, $DOF^u_c = 2846$					
2	840	33.9	39.4	27.7	13.0
4	1480	7.1	8.8	24.7	1.5
6	2120	2.8	3.2	24.7	1.5
8	2760	2.3	2.8	24.7	1.5

Table 5.2: Decoupled approach. Relative errors for flux and concentration for transport problem in perforated domain with $D = 0.03$ using formulation 1, for different resolutions of the flow solution.

same degrees of freedom. As the number of flux basis increases, two formulations has similar convergence behavior for both concentration and flox. We also observe that with better resolution of multiscale flow velocity, especially when we take 3 velocity basis, the solutions of the transport equation are almost the same as the solutions using fine-scale velocity, especially for Formulation 2. This is acceptable, since we define the flux to be diffusive flux in Formulation 1 and total flux in Formulation 2.

In Figure 5.3, we show the fine-scale and coarse-scale solutions for concentration, where coarse-scale solution was computed using 4 multiscale flux basis functions. Note that we present the cell averaging fine-scale solution since piecewise constant basis func-

M^q_{off}	DOF	$\|\|\varepsilon_q\|\|_{L^2}(\%)$	$\|\|\varepsilon_q\|\|_{H(div)}(\%)$	$\|\|\varepsilon_c\|\|_{L^2}(\%)$	$\|\|\varepsilon_{\bar{c}}\|\|_{L^2}(\%)$
With fine scale velocity, $DOF_f^u = 180048$					
1	520	38.8	5.4	32.4	21.7
2	840	10.2	2.3	24.7	2.5
4	1480	6.0	2.0	24.7	1.6
6	2120	5.9	2.0	24.7	1.6
With coarse scale velocity, 1 basis, $DOF_c^u = 1082$					
1	520	39.0	5.4	32.4	21.7
2	840	10.7	2.3	24.8	2.6
4	1480	6.8	2.1	24.7	1.8
6	2120	6.7	2.1	24.7	1.8
With coarse scale velocity, 2 basis, $DOF_c^u = 1964$					
1	520	38.8	5.4	32.4	21.7
2	840	10.2	2.3	24.7	2.5
4	1480	6.2	2.0	24.7	1.6
6	2120	6.2	2.0	24.7	1.6
With coarse scale velocity, 3 basis, $DOF_c^u = 2846$					
1	520	38.8	5.4	32.4	21.7
2	840	10.2	2.3	24.7	2.5
4	1480	6.0	2.0	24.7	1.6
6	2120	5.9	2.0	24.7	1.6

Table 5.3: Decoupled approach. Relative errors for flux and concentration for transport problem in perforated domain with $D = 0.03$ using formulation 2, for different resolutions of the flow solution.

tions are used in the approximation of the concentration in coarse-scale system. The averaged fine-scale solution is depicted on the top of Figure 5.3 and coarse-scale solution using GMsFEM is shown on the bottom of Figure 5.3. From left to right in Figure 5.3, we present concentration solution when $T = 0.03, 0.17$ and 0.5 correspondingly. The concentration error at the last time step (right of Figure 5.3) is $||\varepsilon_{\bar{c}}||_{L^2} = 1.6\%$. The figures show that we obtain a good approximation of concentration in terms of cell averaging solutions.

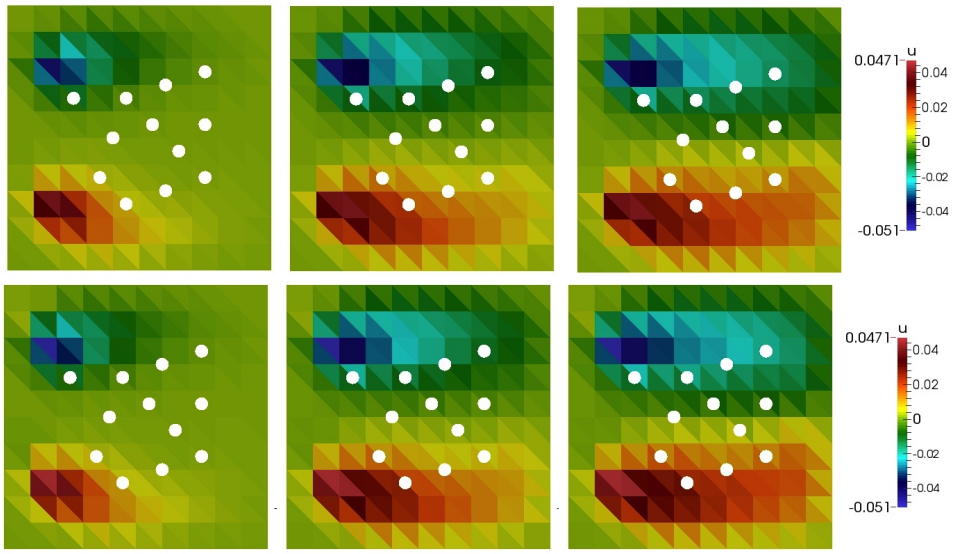

Figure 5.3: Fine-scale and coarse-scale solution for concentration (c_f and c_{ms}) in perforated domain with $D = 0.03$ using formulation 2 for $T = 0.03(1)$, $0.17(5)$ and $0.5(15)$ (from left to right). Top: averaged fine-scale solution. Bottom: multiscale solutions using 4 multiscale basis functions for flux.

M^q_{off}	DOF	$\|\|\varepsilon_q\|\|_{L^2}(\%)$	$\|\|\varepsilon_q\|\|_{H(div)}(\%)$	$\|\|\varepsilon_c\|\|_{L^2}(\%)$	$\|\|\varepsilon_{\bar{c}}\|\|_{L^2}(\%)$
With four possible velocities u_i					
2	840	81.0	17.5	85.4	84.5
4	1480	13.2	1.9	21.4	1.8
6	2120	11.8	1.7	21.4	1.5
8	2760	11.7	1.7	21.4	1.5
Without velocity, only diffusion D					
2	840	81.1	17.5	85.4	84.5
4	1480	13.6	1.9	21.4	1.5
6	2120	12.3	1.7	21.4	1.5
8	2760	12.2	1.7	21.4	1.5

Table 5.4: Coupled approach. Relative errors for flux and concentration for perforated domain with $D = 0.03$ using Formulation 2. easis are construced using 4 possible velocity fields shown in Figure 5.4.

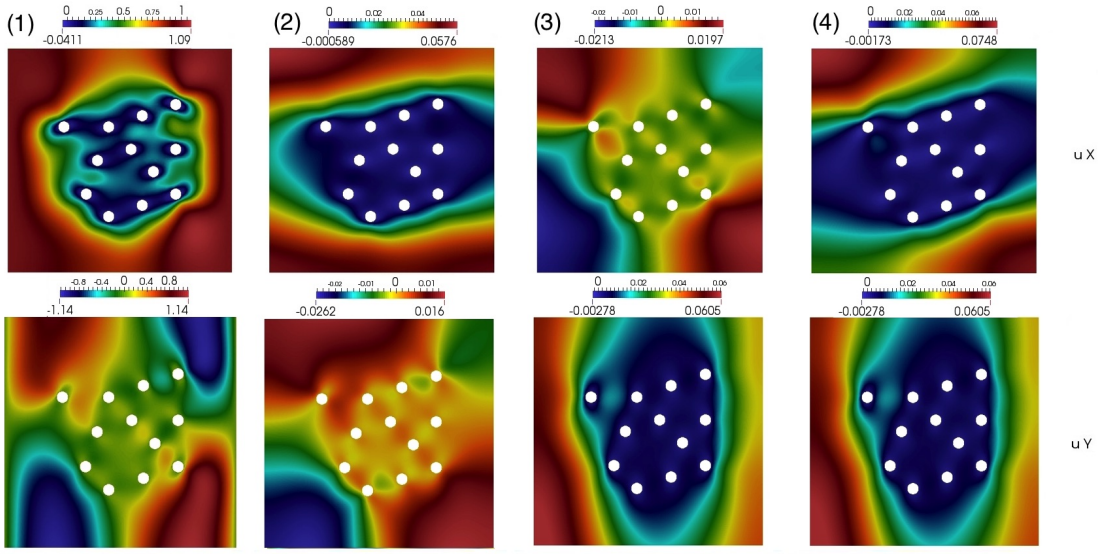

Figure 5.4: Velocities fields, u_1, u_2, u_3 and u_4 (from left to right).

5.2.4.2 Example 2: Coupled approach

In our second example, we present numerical experiments assuming we do not know exact velocity field or the velocity of the flow is time dependent when constructing flux multiscale basis. Basically, we want to provide a GMsFEM algorithm where we construct a universal precomputed flux trial space based on several potential velocity fields at first, and then use the constructed flux basis to solve the transport prolem for any given velocity field. It's worth to mention that, this basis construction process is performed in the offline stage. The algorithm is as follows:

- **Stage 1**. Local offline space generation for transport flux in every ω with several possible velocities u_i.
  - For each u_i, construct snapshot space by solving local problem defined in (5.12), denote by V^i_{snap} the snapshot space and R^i_{snap} $(i = 1, 2, ...)$the matrix containing all snapshot basis.The subscript i represents different potential

velocity fields.

– For each u_i, construct offline flux space V^i_{off} from corresponding snapshot space using following eigenvalue problem

$$A^i_{off}\Psi_i = \lambda S^i_{off}\Psi_i,$$

where

$$A^i_{off} = R^i_{snap}A^i_f(R^i_{snap})^T, \quad S^i_{off} = R^i_{snap}M^i_f(R^i_{snap})^T,$$

and

$$a_i(q,v) = \int_E D^{-1}(q\cdot n_i)(v\cdot n_i), \quad \text{and} \quad s_i(q,v) = \int_\omega D^{-1}q\cdot v,$$

We then collect the offline basis in the matrix R_{off} for future use.

- **Stage 2**. Offline multiscale space for flux for every ω. In this step, we reduce the size of local offline spaces V_{off} using POD:

$$R_{off}R^T_{off}\Psi = \lambda\mathcal{I}\Psi.$$

Keep eigenvectors related to the first largest eigenvelues as basis functons. This step guarentees the linear independence among the local offline spaces for different velocity fields u_i. The resulting offline space will be used for solving global problems for any given velocity.

Remark 5.2.2. *The above two stages are conducted offline and the resulting offline space can be used later for different velocity inputs.*

As for multiscale test basis functions for the flux, they are constructed using exact velocity and calculated for each trial multiscale basis function, following the same idea as shown in 5.2.2.

Possible velocitity fields u_i, $\forall i = 1, 2, 3, 4$ is presented in Figure 5.4. In Table 5.4, we present relative errors for flux and concentration when we use precomputed multiscale basis functions for flux without information about the real velocty field. We observe that, in the coupled approach, if we take enough basis, say more than 2 basis, we can obtain similar error behavior when we use or don't use exact velocity for basis calculation, comparing the data in Table 5.4 and Table 5.3. For example, taking 4 multiscale basis functions for flux, when we use some possible velocities, H^{div} error for flux is 1.9%; when we use exact velocity, we obtain 2.0% error. We can see that, this approach can be used when solving coupled transport and flow problems where velocity field may varies significantly by time. For comparison, in this table we also show the errors for another way of calculating the multiscale basis functions for flux, where we didn't use information about velocity but only use mixed elliptic problem for trial basis calculation. We note that for our test examples, we can also use this set of basis for a rough approximation.

5.3 Multicale interior basis functions for concentration of the transport equation

In this section, we present another type of basis functions that can help to improve coarse-scale solution for concentration. Let the multiscale basis functions presented above be the first set of offline basis functions (V_H^q and Q_H^q), which gives the enrichment of the normal component of velocity across coarse grid edges. The second set of basis functions can be considered as interior bases (V_H^c and Q_H^c), which can capture the standing modes within coarse elements with zero boundary conditions. We will construct interior basis functions for Formulation 1.

First we present construction of the trial space for interior basis functions. We solve

following spectral problem on the coarse element K_i^q : Find $\psi_q \in V_h(K_i^q), \psi_c \in Q_h(K_i^q)$ such that

$$\begin{aligned} m^q(\psi_q, v) + b(v, \psi_c) &= 0, \quad \forall v \in V_h(K_i^q) \\ -b(\psi_q, r) + s(\psi_q, r) &= \lambda(\psi_c, r), \quad \forall r \in Q_h(K_i^q). \end{aligned} \tag{5.19}$$

subject to $\int_{K_i^q} \psi_c = 0$. Then we arrange the eigenvalues in an ascending order, and take the first L_i eigenfunctions $(\psi_q^{k,K_i}, \psi_c^{k,K_i})$ as basis functions.

Let N_c be the number of coarse cells. We define $V_H^c = \text{span}\{\psi_q^{k,K_i} : 1 \leq i \leq N_c \text{ and } 1 \leq k \leq L_i\}$, $Q_H^c = \text{span}\{\psi_c^{k,K_i} : 1 \leq i \leq N_c \text{ and } 1 \leq k \leq L_i\}$ Using a single index notation, we can write

$$V_H^c = \text{span}\{\psi_{i,K}^q\}_{i=1}^{M_{\text{off}}^c} \quad Q_H^c = \text{span}\{\psi_{i,K}^c\}_{i=1}^{M_{\text{off}}^c}$$

where $M_{\text{off}}^c = \sum_{i=1}^{N_c} L_i$.

Next, we consider construction of the test space. After construction of the multiscale trial basis functions, we solve adjoint problem for construction of the interior test basis functions

$$\begin{aligned} m^q(\phi_c^{i,K}, v) + b(v, \phi_c^{i,K}) + s(v, \phi_c^{i,K}) &= 0, \quad \forall v \in V_h^i \\ b(\phi_q^{i,K}, r) &= (\psi_{i,K}^c, r), \quad \forall r \in Q_h^i. \end{aligned} \tag{5.20}$$

where $\psi_c^{i,K}$ is the concentration trial basis constructed using problem (5.19).

Then the test space $\hat{V}_H^c$ and $\hat{Q}_H^c$ can be denoted as:

$$\hat{V}_H^c = \text{span}\{\phi_q^{i,K}\}_{i=1}^{M_{\text{off}}^c}, \quad \hat{Q}_H^c = Q_H^c.$$

Finally, for offline trial space we take $V_H = V_H^q + V_H^c$, $Q_H = Q_H^q + Q_H^c$; for test space

we take $\hat{V}_H = \hat{V}_H^q + \hat{V}_H^c$.

$M_{\text{off}}^q + M_{\text{off}}^c$	DOF	$\|\|\varepsilon_q\|\|_{L^2}(\%)$	$\|\|\varepsilon_q\|\|_{H(div)}(\%)$	$\|\|\varepsilon_c\|\|_{L^2}(\%)$
$M_{\text{off}}^q = 2$				
2+0	840	33.8	39.2	27.6
2+1	1240	33.0	38.8	18.3
2+2	1640	33.0	38.8	16.0
2+4	2440	33.0	38.8	14.3
$M_{\text{off}}^q = 4$				
4+0	1480	7.0	10.1	24.7
4+1	1880	6.9	9.8	13.2
4+2	2280	6.9	9.8	9.3
4+4	3080	6.9	9.7	5.2
$M_{\text{off}}^q = 8$				
8+0	2760	2.3	2.7	24.7
8+1	3160	1.6	1.7	13.2
8+2	3560	1.5	1.4	9.2
8+4	4360	1.5	1.3	5.1

Table 5.5: Multiscale interior basis. Relative errors for flux and concentration for perforated domain with $D = 0.03$ using formulation 1 for different number of interior basis functions M_{off}^c.

In Figure 5.5, we present the fine scale and coarse-scale solutions for concentration. For coarse-scale solution we used $M_{\text{off}}^q = M_{\text{off}}^c = 4$ and observe a smooth solution for concentration with an error of 5.2%. In Tables 5.5 and 5.6, we present errors for different number of interior basis functions. We observe that the interior basis functions can only reduce concentration error and hardly impact the flux errors. For a larger diffusion coefficient $D = 0.3$, we obtain smaller errors in general (see Table 5.6).

5.4 Residual-based online basis functions for the coupled approach

In Section 5.2.4, we present the coupled approach to solve the transport equation without using the true velocity information. In this section, we consider the construction of the

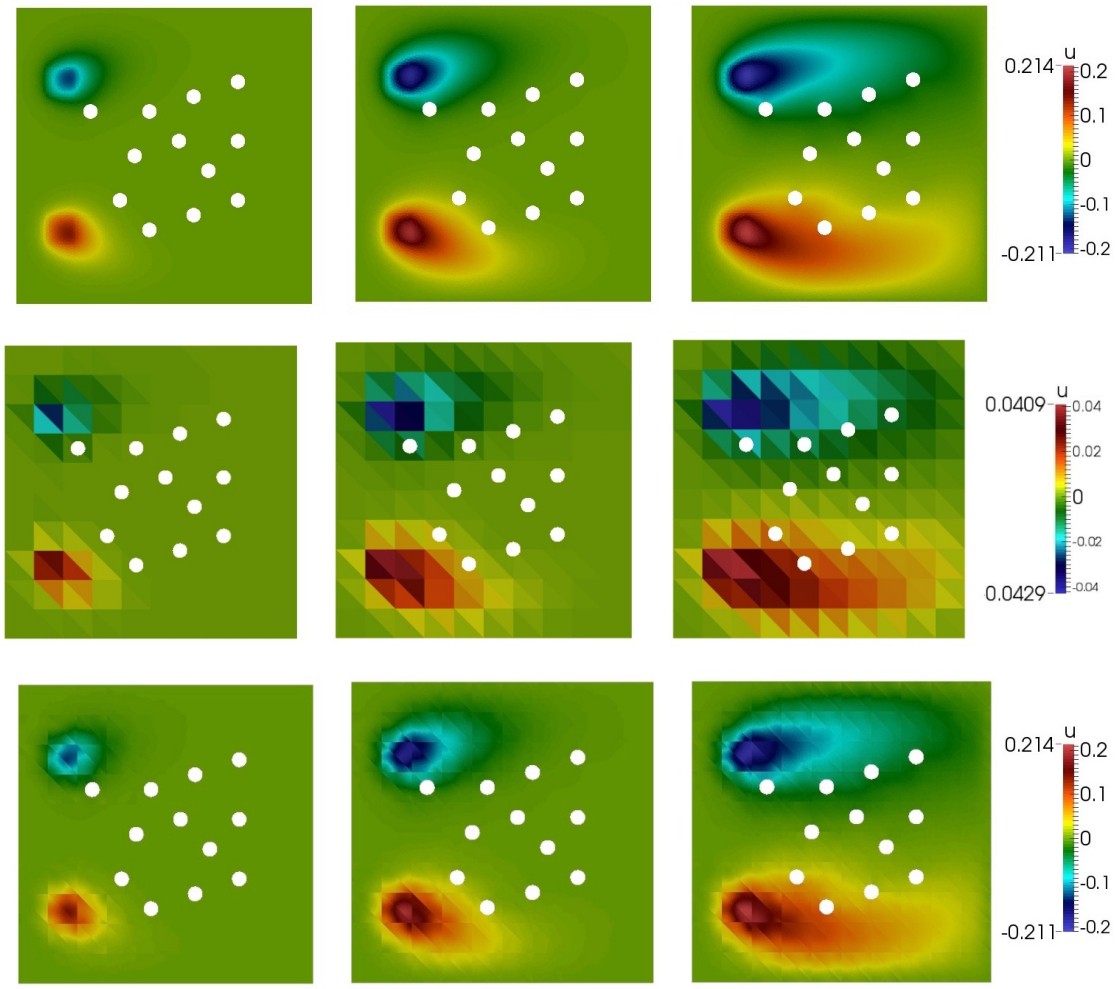

Figure 5.5: Using multiscale interior basis, formulation 1. Fine-scale and multiscale solutions for concentration (c) for $T = 0.03(1)$, $0.16(5)$ and $0.5(15)$ in perforated domain. Top: fine-scale solution, $DOF = 112432$. Middle: multiscale solutions using 4 multiscale boundary basis functions for flux, $DOF = 1480$, concentration L^2 error is 23.2 % and 1.26 % for average value. Bottom: multiscale solutions using 4 multiscale boundary basis functions for flux, 3 multiscale interior basis for flux and concentration, $DOF = 2680$, concentration L^2 error is 5.8 %.

$M^q_{\text{off}} + M^c_{\text{off}}$	DOF	$\|\|\varepsilon_q\|\|_{L^2}(\%)$	$\|\|\varepsilon_q\|\|_{H(div)}(\%)$	$\|\|\varepsilon_c\|\|_{L^2}(\%)$
$M^q_{\text{off}} = 1$				
2+0	840	14.5	2.2	22.2
2+2	1640	14.5	2.2	8.3
2+4	2440	14.5	2.2	5.2
2+8	4040	14.5	2.2	3.9
2+16	7240	14.5	2.2	3.2
$M^q_{\text{off}} = 4$				
4+0	1480	1.7	0.2	22.2
4+2	2280	1.7	0.2	7.9
4+4	3080	1.7	0.2	4.4
4+8	4680	1.7	0.2	2.6
4+16	7880	1.7	0.2	1.3
$M^q_{\text{off}} = 8$				
8+0	2760	0.5	0.06	22.2
8+2	3560	0.5	0.06	7.9
8+4	4360	0.5	0.06	4.4
8+8	5960	0.5	0.06	2.6
8+16	9160	0.5	0.06	1.3

Table 5.6: Multiscale interior basis. Relative errors for flux and concentration for perforated domain with $D = 0.3$ using formulation 1 for different number of interior basis functions M^c_{off}.

online basis functions ([28, 33, 27]) for transport equation which will take into the true velocity information at online stage. We use the index $m \geq 1$ to represent the enrichment level. The online basis functions are computed based on local residuals from the current multiscale solution $u^m_{\text{ms}} \in V^m_{\text{ms}}$, where we use V^m_{ms} to denote the corresponding solution space that can contain both offline and online basis functions.

The online basis function can be constructed using information based current residual in non-overlapping local regions ω:

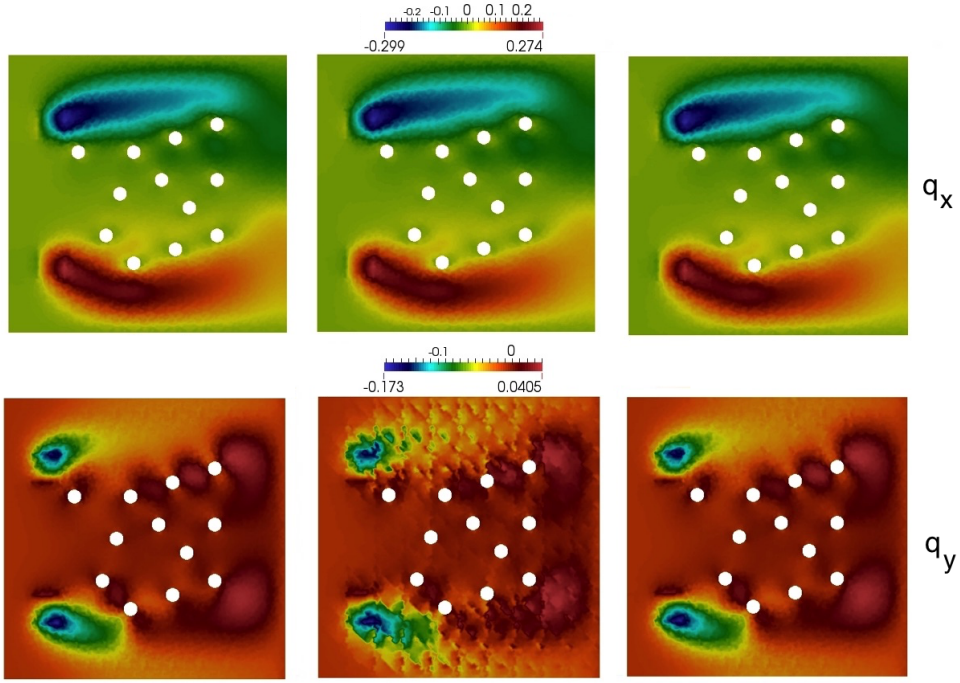

Figure 5.6: Fine-scale and coarse-scale solution for flux (q_f and q_{ms}) in perforated domain with $D = 0.03$ using formulation 2 (component q_x on the top of figure and q_y on the bottom). For offline basis calculations we used possible velocities $u_1 + u_2 + u_3 + u_4$. Left: fine-scale solution, $DOF = 112432$. Middle: multiscale solutions using 4 offline bases for flux, $DOF = 1480$. Right: multiscale solutions using 4 offline and one online basis functions for flux, $DOF = 1800$.

- Online trial basis functions ψ^{on} for flux (Formulation 2):

$$\begin{aligned} D^{-1}\psi^{on} + \nabla c - D^{-1}uc &= R_\omega, \text{ in } \omega \\ \text{div}\psi^{on} &= 0, \text{ in } \omega, \end{aligned} \tag{5.21}$$

where $R_\omega = -D^{-1}q^m - \nabla c^m + D^{-1}u\,c^m$ and we solve in fine-grid, V_h^ω.

M^q_{off}	DOF	$\|\|\varepsilon_q\|\|_{L^2}(\%)$	$\|\|\varepsilon_q\|\|_{H(div)}(\%)$	$\|\|\varepsilon_c\|\|_{L^2}(\%)$
With exact velocity, u				
4	1480	9.0	1.3	21.4
6	2120	7.6	1.1	21.4
8	2760	7.4	1.0	21.4
With exact velocity, u + one online bases				
4	1800	1.4	0.2	21.4
6	2440	0.6	0.09	21.4
8	3080	0.2	0.03	21.4
With four possible velocities u_i				
4	1480	13.2	1.9	21.4
6	2120	11.8	1.7	21.4
8	2760	11.7	1.7	21.4
With possoble velocities u_i + one online bases				
4	1800	1.4	0.2	21.4
6	2440	0.7	0.1	21.4
8	3080	0.5	0.07	21.4

Table 5.7: Multiscale online basis. Relative errors for flux and concentration for transport problem in perforated domain (Figure 5.1) with $D = 0.03$ using Formulation 1 with residual based online basis functions.

- Online test basis functions ψ for flux (Formulation 2):

$$\begin{aligned} D^{-1}\psi + \nabla c &= D^{-1}\psi^{on}, \text{ in } \omega \\ \text{div}\psi - D^{-1}u\psi &= 0, \text{ in } \omega, \end{aligned} \tag{5.22}$$

  where ψ^{on} is the residual based online trial basis function and we solve in fine-grid, V_h^ω.

We can apply the same algorithm to construct the online residual-based basis functions for Formulation 1.

In Figure 5.6 we present the fine scale and coarse-scale solutions for flux. We observe that the offline solution is close to the fine-scale solution; however, there are some missing features in the offline solution. On the other hand, the solution using the online procedure

with similar number of degrees of freedom compared with the offline solution has very good accuracy.

Next, we present results for the transport and flow problems in two complex geometries as shown in Figure 5.7 applying the online algorighm. We set $\Omega = [0, 1.2] \times [0, 1]$. The computational domain is discretized coarsely using uniform triangulation with the coarse mesh size $H = 1/10$ and consists of 240 cells and 382 edges. The fine grids for two geometries are presented in Figure 5.7. The mesh in the left of Figure 5.7 contains 31974 cells, 48453 edges and the mesh in the right of Figure 5.7 contains 33636 cells, 51378 edges.

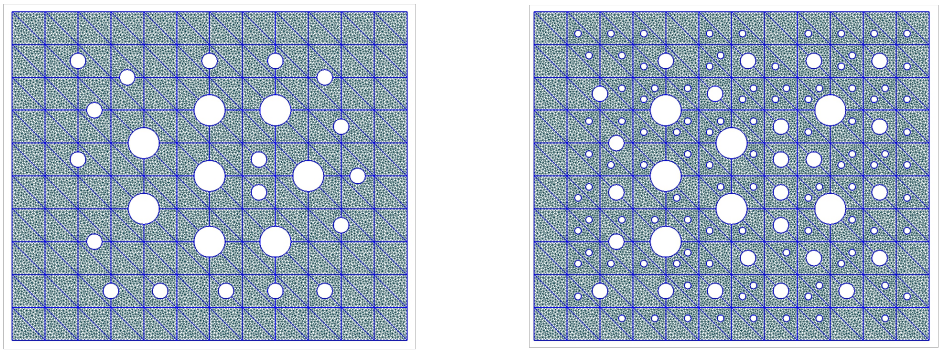

(a) (b)

Figure 5.7: Coarse and fine grids for two complex perforated domains. (a) geometry with big perforations. (b) extreme case with additional small inclusions.

We present results of the transport problem when we take different number of offline flux basis functions and add one residual based online basis function. In this example, we aim to discover the effect of online basis, so that the offline basis for flux are constructed in a standard way using exact velocity field. The fine-scale solution and coarse-scale solution corresponding to the two different perforated domains in Figure 5.7 are presented in Figures 5.8 and 5.9, respectively. Fine solutions for concentration and flux are shown

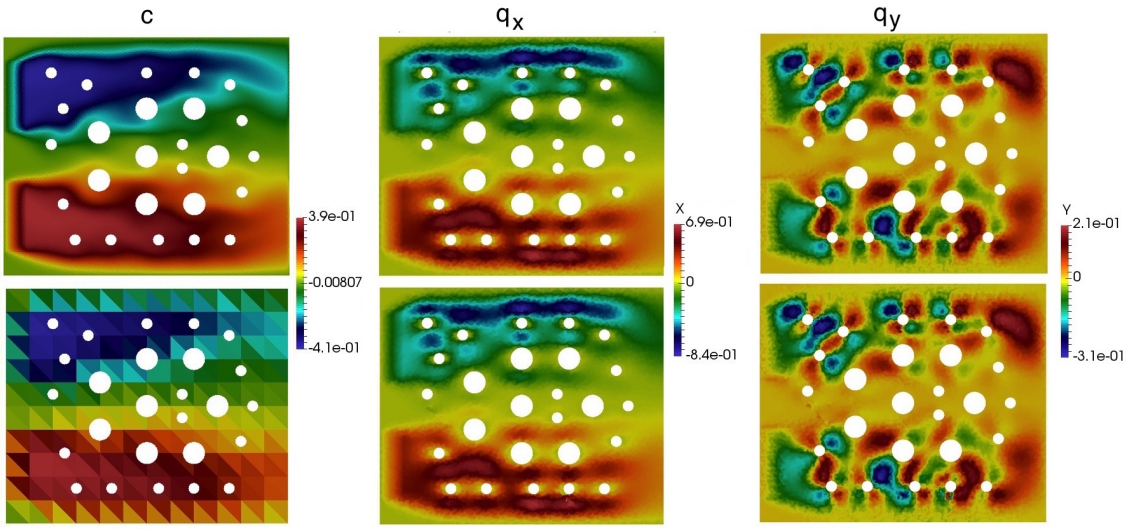

Figure 5.8: Fine-scale (top) and coarse-scale (bottom) solution for flux and concentration (c, q_x, q_y from left to right) for $T = 0.5$ in perforated domain with big inclusions (Figure 5.7) (a) with $D = 0.005$ using Formulation 2. Coarse-scale solution was computed using 4 multiscale boundary basis functions and one online basis.

M^q_{off}	DOF	$\|\|\varepsilon_q\|\|_{L^2}(\%)$	$\|\|\varepsilon_q\|\|_{H(div)}(\%)$	$\|\|\varepsilon_c\|\|_{L^2}(\%)$	$\|\|\varepsilon_{\bar{c}}\|\|_{L^2}(\%)$
Offline					
2	1004	21.9	6.9	22.5	9.5
4	1768	11.8	4.5	20.6	1.6
6	2532	11.3	4.4	20.6	1.5
8	3296	11.3	4.4	20.6	1.5
Offline + one online basis					
2	1386	18.1	5.1	22.5	9.5
4	2159	5.54	3.7	20.6	1.6
6	2914	2.8	3.1	20.6	1.5
8	3678	1.9	3.1	20.6	1.5

Table 5.8: Complicated geometry 1. Relative errors for flux and concentration in perforated domain with big inclutions (Figure 5.7 (a)) with $D = 0.005$ using Formulation 2 with online residual based basis functions.

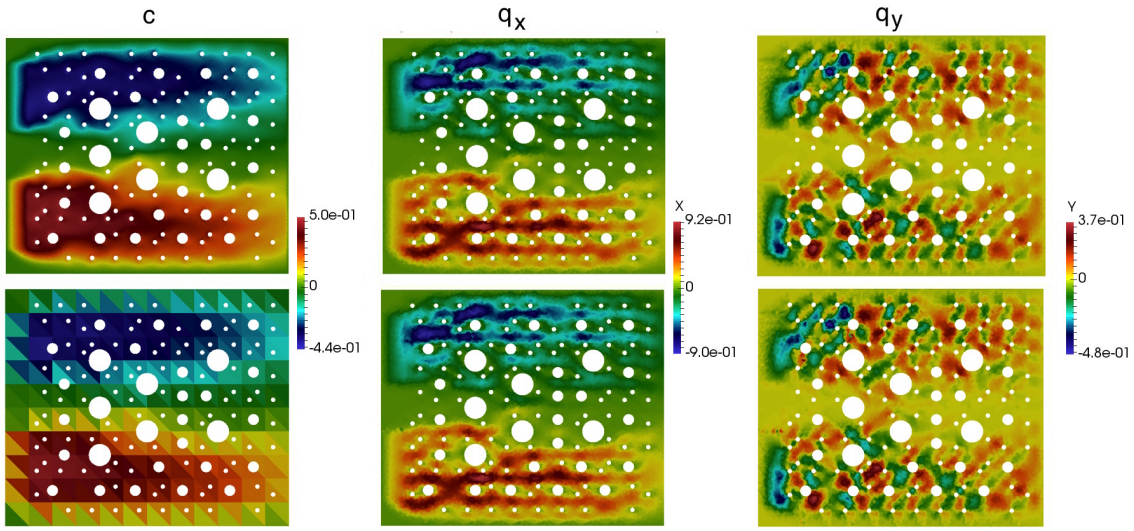

Figure 5.9: Fine-scale (top) and coarse-scale (bottom) solution for flux and concentration (c, q_x, q_y from left to right) for $T = 0.5$ in perforated domain for extreme case (Figure 5.7) (b) with $D = 0.005$ using Formulation 2. Coarse-scale solution was computed using 4 multiscale boundary basis functions and one online basis.

M^q_{off}	DOF	$\|\|\varepsilon_q\|\|_{L^2}(\%)$	$\|\|\varepsilon_q\|\|_{H(div)}(\%)$	$\|\|\varepsilon_c\|\|_{L^2}(\%)$	$\|\|\varepsilon_{\bar{c}}\|\|_{L^2}(\%)$
Offline					
2	1004	28.7	8.9	23.7	12.4
4	1768	13.4	5.0	20.5	2.2
6	2532	10.8	4.4	20.5	1.7
8	3296	10.8	4.4	20.5	1.7
Offline + one online basis					
2	1386	26.6	7.8	23.7	12.4
4	2159	5.3	4.3	20.5	2.0
6	2914	2.0	3.3	20.5	1.7
8	3678	2.0	3.3	20.5	1.7

Table 5.9: Complicated geometry 2. Relative errors for flux and concentration in perforated domain for extreme case (Figure 5.7 (b)) with $D = 0.005$ using Formulation 2 with online residual based basis functions.

on the top of the figure, coarse online solutions are on the bottom. We observe that after adding one online basis, the multiscale solution shows quite good accuracy.

In Tables 5.8 and 5.9, we first present the convergence history when the problem is solved in two different perforated domain with 2, 4, 6 and 8 initial offline bases. Then, on the bottom of table we present errors after adding one online residual-based basis functions. We observe that the coarse-scale calculations for two geometries give similar results. By enriching the solution space with online basis, we can speed up the convergence significantly. For example, when we use 4 initial offline basis, the L^2 and energy error reduce to 11.8% and 4.5% and after one online iteration we obtain 5.5% and 3.7% errors in domain with big inclusions. If we select 8 initial bases, the the L^2 and energy error can be reduced to 1.9% and 3.1% respectively after one online iteration.

6. SUMMARY AND CONCLUSIONS

In this section, we will give a summary of this dissertation. In Chapter 3, we present an efficient multiscale procedure for solving PDEs in perforated domains. We consider elliptic, elastic, and Stokes systems. We investigate that the convergence of multiscale methods can be significantly accelerated if appropriate online basis functions are constructed and appropriate number of offline basis functions are used. The construction of online basis functions relies on analysis and the choice of the offline basis functions. In this chapter, we develop analysis for GMsFEM in perforated domains, design procedures for constructing online multiscale basis functions, present analysis of online algorithm, develop adaptive procedures and show numerical results. By using a computable error indicator, we locate regions, where enrichment is necessary, and construct new online basis functions in order to improve the accuracy. Our numerical results for the elasticity equation and the Stokes system show that the method has an excellent performance and rapid convergence. In particular, only a few online basis functions in some selected regions improve the accuracy of the solution. Our analysis shows that the convergence rate depends on the number of offline basis functions, and one can obtain a fast convergence by including enough offline basis functions. This convergence theory can also be applied to the Laplace equation and the elasticity equation. One possible future direction is the goal-oriented adaptivity [53], in which basis functions are added in order to reduce the goal error.

In Chapter 4, we develop a new GMsFEM considering the discontinuous Galerkin method for global coupling for Stokes problems in perforated domains. The method constructs local basis functions for each non-overlapping coarse region. The construction of basis follows the general framework of GMsFEM by using local snapshots and local spectral problems. In addition, we use a hybridized technique in order to achieve mass

conservation. Our numerical results show that only a few basis functions per coarse region are needed in order to obtain a good accuracy. We also show numerically that the multiscale solution satisfies the mass conservation property. Furthermore, we prove the stability and the convergence of the scheme. In the future, we plan to develop adaptivity ideas for this method.

In Chapter 5, we develop a multiscale model reduction approach based on GMsFEM for the coupled flow and transport problem in perforated domains. The coarse scale discretization is based on a mixed formulation, which gives the crucial mass conservation property. For the construction of multiscale basis functions, we follow the general ideas of GMsFEM and define suitable snapshot spaces and spectral problems. Two types of basis are considered. The first type is decoupled basis, which are obtained from some local solutions of the flow problem. The second type is coupled basis, which are obtained from local solutions of the coupled flow and transport problem. We present and compare the performance of the two types of basis functions. Moreover, with the aim of further improving accuracy, we present the construction of interior basis as well as the online basis functions and show their performance. In summary, our results show that only a few of the proposed basis functions are able to give accurate solutions.

REFERENCES

[1] V. V. Jikov, S. M. Kozlov, and O. A. Oleinik, *Homogenization of Differential Operators and Integral Functionals*. Springer-Verlag, 1991.

[2] U. Hornung, *Homogenization and porous media*. Springer Science & Business Media, 2012.

[3] G. Allaire, "Homogenization of the navier-stokes equations in open sets perforated with tiny holes ii: Non-critical sizes of the holes for a volume distribution and a surface distribution of holes," *Archive for Rational Mechanics and Analysis*, vol. 113, no. 3, pp. 261–298, 1991.

[4] O. A. Oleinik and T. A. Shaposhnikova, "On the homogenization of the poisson equation in partially perforated domains with arbitrary density of cavities and mixed type conditions on their boundary," *Atti della Accademia Nazionale dei Lincei. Classe di Scienze Fisiche, Matematiche e Naturali. Rendiconti Lincei. Matematica e Applicazioni*, vol. 7, no. 3, pp. 129–146, 1996.

[5] T. Fratrović and E. Marušić-Paloka, "Nonlinear brinkman-type law as a critical case in the polymer fluid filtration," *Applicable Analysis*, pp. 1–22, 2015.

[6] I. Pankratova and K. Pettersson, "Spectral asymptotics for an elliptic operator in a locally periodic perforated domain," *Applicable Analysis*, vol. 94, no. 6, pp. 1207–1234, 2015.

[7] G. Allaire and H. Hutridurga, "Upscaling nonlinear adsorption in periodic porous media–homogenization approach," *Applicable Analysis*, pp. 1–36, 2015.

[8] Z. Bare, J. Orlik, and G. Panasenko, "Non homogeneous dirichlet conditions for an elastic beam: an asymptotic analysis," *Applicable Analysis*, pp. 1–12, 2015.

[9] R. P. Gilbert, A. Panchenko, and A. Vasilic, "Acoustic propagation in a random saturated medium: the biphasic case," *Applicable Analysis*, vol. 93, no. 4, pp. 676–697, 2014.

[10] A. Muntean, M. Ptashnyk, and R. E. Showalter, "Analysis and approximation of microstructure models," *Applicable Analysis*, vol. 91, no. 6, pp. 1053–1054, 2012.

[11] R. P. Gilbert, A. Panchenko, and X. Xie, "A prototype homogenization model for acoustics of granular materials," *International Journal for Multiscale Computational Engineering*, vol. 4, no. 5-6, 2006.

[12] R. P. Gilbert and M.-j. Ou, "Acoustic wave propagation in a composite of two different poroelastic materials with a very rough periodic interface: a homogenization approach," *International Journal for Multiscale Computational Engineering*, vol. 1, no. 4, 2003.

[13] W. E and B. Engquist, "Heterogeneous multiscale methods," *Comm. Math. Sci.*, vol. 1, no. 1, pp. 87–132, 2003.

[14] P. Henning and M. Ohlberger, "The heterogeneous multiscale finite element method for elliptic homogenization problems in perforated domains," *Numerische Mathematik*, vol. 113, no. 4, pp. 601–629, 2009.

[15] A. Y. Beliaev and S. Kozlov, "Darcy equation for random porous media," *Communications on pure and applied mathematics*, vol. 49, no. 1, pp. 1–34, 1996.

[16] L. Le Bris, F. Legoll, and A. Lozinski, "An MsFEM type approach for perforated domains," *SIAM J. Multiscale Modeling & Simulation*, vol. 12(3), pp. 1046–1077, 2014.

[17] T. Hou and X. Wu, "A multiscale finite element method for elliptic problems in composite materials and porous media," *J. Comput. Phys.*, vol. 134, pp. 169–189, 1997.

[18] Y. Efendiev and T. Hou, *Multiscale Finite Element Methods: Theory and Applications*, vol. 4 of *Surveys and Tutorials in the Applied Mathematical Sciences*. New York: Springer, 2009.

[19] Y. Efendiev, J. Galvis, and X. H. Wu, "Multiscale finite element methods for high-contrast problems using local spectral basis functions," *Journal of Computational Physics*, vol. 230, no. 4, pp. 937–955, 2011.

[20] Y. Efendiev, T. Hou, and X. Wu, "Convergence of a nonconforming multiscale finite element method," *SIAM J. Numer. Anal.*, vol. 37, pp. 888–910, 2000.

[21] O. Iliev, R. Lazarov, and J. Willems, "Variational multiscale finite element method for flows in highly porous media," *Multiscale Model. Simul.*, vol. 9, no. 4, pp. 1350–1372, 2011.

[22] C.-C. Chu, I. G. Graham, and T.-Y. Hou, "A new multiscale finite element method for high-contrast elliptic interface problems," *Math. Comp.*, vol. 79, no. 272, pp. 1915–1955, 2010.

[23] G. Allaire and R. Brizzi, "A multiscale finite element method for numerical homogenization," *SIAM J. Multiscale Modeling & Simulation*, vol. 4, no. 3, pp. 790–812, 2005.

[24] Y. Efendiev, J. Galvis, and T. Hou, "Generalized multiscale finite element methods (gmsfem)," *Journal of Computational Physics*, vol. 251, pp. 116–135, 2013.

[25] E. T. Chung, Y. Efendiev, and G. Li, "An adaptive GMsFEM for high contrast flow problems," *J. Comput. Phys.*, vol. 273, pp. 54–76, 2014.

[26] E. T. Chung, Y. Efendiev, and C. Lee, "Mixed generalized multiscale finite element methods and applications," *SIAM Multicale Model. Simul.*, vol. 13, pp. 338–366, 2014.

[27] E. T. Chung, Y. Efendiev, and W. T. Leung, "Residual-driven online generalized multiscale finite element methods," *Journal of Computational Physics*, vol. 302, pp. 176–190, 2015.

[28] H. Y. Chan, E. T. Chung, and Y. Efendiev, "Adaptive mixed GMsFEM for flows in heterogeneous media," *Numerical Mathematics: Theory, Methods and Applications*, vol. 9, no. 4, pp. 497–527, 2016.

[29] M. Ohlberger and F. Schindler, "Error control for the localized reduced basis multiscale method with adaptive on-line enrichment," *SIAM Journal on Scientific Computing*, vol. 37, no. 6, pp. A2865–A2895, 2015.

[30] E. T. Chung, Y. Efendiev, G. Li, and M. Vasilyeva, "Generalized multiscale finite element method for problems in perforated heterogeneous domains," *Applicable Analysis*, vol. 255, pp. 1–15, 2015.

[31] V. Calo, Y. Efendiev, J. Galvis, and G. Li, "Randomized oversampling for generalized multiscale finite element methods," *SIAM J. Multiscale Modeling & Simulation*, vol. 14, no. 1, pp. 482–501, 2016.

[32] Y. Efendiev, J. Galvis, G. Li, and M. Presho, "Generalized multiscale finite element methods. oversampling strategies," *International Journal for Multiscale Computational Engineering*, vol. 12(6), pp. 465–484, 2014.

[33] E. T. Chung, Y. Efendiev, W. Leung, M. Vasilyeva, and Y. Wang, "Online adaptive local multiscale model reduction for heterogeneous problems in perforated domains," *Applicable Analysis*, vol. 96, no. 12, pp. 2002–2031, 2017.

[34] E. T. Chung, M. Vasilyeva, and Y. Wang, "A conservative local multiscale model reduction technique for stokes flows in heterogeneous perforated domains," *Journal of Computational and Applied Mathematics*, vol. 321, pp. 389–405, 2017.

[35] E. T. Chung, Y. Efendiev, and W. T. Leung, "An online generalized multiscale discontinuous galerkin method (GMsDGM) for flows in heterogeneous media," *Communications in Computational Physics*, vol. 21, no. 2, pp. 401–422, 2017.

[36] E. T. Chung, Y. Efendiev, and S. Fu, "Generalized multiscale finite element method for elasticity equations," *International Journal on Geomathematics*, vol. 5(2), pp. 225–254, 2014.

[37] E. T. Chung, Y. Efendiev, and W. T. Leung, "Generalized multiscale finite element method for wave propagation in heterogeneous media," *SIAM Multicale Model. Simul.*, vol. 12, pp. 1691–1721, 2014.

[38] E. T. Chung, Y. Efendiev, R. L. Gibson Jr, and M. Vasilyeva, "A generalized multiscale finite element method for elastic wave propagation in fractured media," *GEM-International Journal on Geomathematics*, pp. 1–20, 2015.

[39] E. T. Chung, W. T. Leung, M. Vasilyeva, and Y. Wang, "Multiscale model reduction for transport and flow problems in perforated domains," *Journal of Computational and Applied Mathematics*, vol. 330, pp. 519–535, 2018.

[40] M. S. Alnæs, J. Blechta, J. Hake, A. Johansson, B. Kehlet, A. Logg, C. Richardson, J. Ring, M. E. Rognes, and G. N. Wells, "The fenics project version 1.5," *Archive of Numerical Software*, vol. 3, no. 100, 2015.

[41] M. S. Alnæs, A. Logg, K. B. Ølgaard, M. E. Rognes, and G. N. Wells, "Unified form language: A domain-specific language for weak formulations of partial differential equations," *ACM Transactions on Mathematical Software*, vol. 40, no. 2, 2014.

[42] P. Mohammadmoradi, "Fractional-wet medium (openfoam file)." `http://www.digitalrocksportal.org/projects/70`, 2016.

[43] M. Prodanovic, M. Esteva, M. Hanlon, G. Nanda, and P. Agarwa, "Digital rocks portal: a repository for porous media images," 2015.

[44] F. Brezzi and M. Fortin, *Mixed and hybrid finite element methods*, vol. 15 of *Springer Series in Computational Mathematics*. New York: Springer-Verlag, 1991.

[45] D. Arnold, F. Brezzi, B. Cockburn, and L. Marini, "Unified analysis of discontinuous Galerkin methods for elliptic problems," *SIAM J. Numer. Anal.*, vol. 39, no. 5, pp. 1749–1779, 2001.

[46] R. Ewing, J. Wang, and Y. Yang, "A stabilized discontinuous finite element method for elliptic problems," *Numer. Linear Algebra Appl.*, vol. 10, no. 1-2, pp. 83–104, 2003.

[47] R. Lazarov, J. Pasciak, J. Schöberl, and P. Vassilevski, "Almost optimal interior penalty discontinuous approximations of symmetric elliptic problems on non-matching grids," *Numer. Math.*, vol. 96, no. 2, pp. 295–315, 2003.

[48] R. Lazarov, S. Tomov, and P. Vassilevski, "Interior penalty discontinuous approximations of elliptic problems," *Comput. Methods Appl. Math.*, vol. 1, no. 4, pp. 367–382, 2001.

[49] Y. Efendiev, J. Galvis, and T. Hou, "Generalized multiscale finite element methods," *Journal of Computational Physics*, vol. 251, pp. 116–135, 2013.

[50] Y. Efendiev, J. Galvis, G. Li, and M. Presho, "Generalized multiscale finite element methods. oversampling strategies," *International Journal for Multiscale Computational Engineering, accepted*, vol. 12(6), 2013.

[51] E. T. Chung and W. T. Leung, "A sub-grid structure enhanced discontinuous galerkin method for multiscale diffusion and convection-diffusion problems," *Communications in Computational Physics*, vol. 14, pp. 370–392, 2013.

[52] I. Babuška, V. Nistor, and N. Tarfulea, "Generalized finite element method for second-order elliptic operators with Dirichlet boundary conditions," *J. Comput. Appl. Math.*, vol. 218, pp. 175–183, 2008.

[53] E. T. Chung, W. T. Leung, and S. Pollock, "Goal-oriented adaptivity for GMsFEM," *Journal of Computational and Applied Mathematics*, pp. 625–637, 2015.